11th World Conference on Applied Science, Engineering and Technology

(WCASET-2018)

Frankfurt, Germany

17th - 18th August'18

World Conference on Applied Science, Engineering and Technology

www.wcaset.com

Publisher: WCASET Explore

Editorial:

We cordially invite you to attend the 11th World Conference on Applied Science, Engineering and Technology (WCASET-18), which will be held in Holiday Inn, Frankfurt, Germany on 17th - 18th August 2018. The main objective of WCASET -18 is to provide a platform for researchers, engineers, academicians as well as industrial professionals from all over the world to present their research results and development activities in Applied Science, Engineering and Technology. This conference provides opportunities for the delegates to exchange new ideas and experience face to face, to establish business or research relations and to find global partners for future collaboration.

These proceedings collect the up-to-date, comprehensive and worldwide state-of-art knowledge on Applied Science, Engineering and Technology. All accepted papers were subjected to strict peer-reviewing by 2-4 expert referees. The papers have been selected for these proceedings because of their quality and the relevance to the conference. We hope these proceedings will not only provide the readers a broad overview of the latest research results on Applied Science, Engineering and Technology but also provide the readers a valuable summary and reference in these fields.

The conference is supported by many universities and research institutes. Many professors played an important role in the successful holding of the conference, so we would like to take this opportunity to express our sincere gratitude and highest respects to them. They have worked very hard in reviewing papers and making valuable suggestions for the authors to improve their work. We also would like to express our gratitude to the external reviewers, for providing extra help in the review process, and to the authors for contributing their research result to the conference.

Since June 2018, the Organizing Committees have received more than 60 manuscript papers, and the papers cover all the aspects in Applied Science, Engineering and Technology. Finally, after review, about 18 papers were included to the proceedings of WCASET - 18.

We would like to extend our appreciation to all participants in the conference for their great contribution to the success of World Conference 2018. We would like to thank the keynote and individual speakers and all participating authors for their hard work and time. We also sincerely appreciate the work by the technical program committee and all reviewers, whose contributions make this conference possible. We would like to extend our thanks to all the referees for their constructive comments on all papers; especially, we would like to thank to organizing committee for their hard work.

Editor-In-Chief
Dr. CHAO LIU,
Assistant Professor
University of Colorado Denver, Colorado.

Acknowledgement

WCASET is hosting the 11th World Conference on Applied Science, Engineering and Technology this year in month of August. Technical advantage is the backbone of development and Engineering & Technology has become the platform behind all the sustainable growth 11th World Conference on Applied Science, Engineering and Technology will provide a forum for students, professional engineers, academician, and scientist engaged in research and development to convene and present their latest scholarly work and application in the industry. The primary goal of the conference is to promote research and developmental activities in Applied Science, Engineering and Technology and to promote scientific information interchange between researchers, developers, engineers, students, and practitioners working in and around the world. The aim of the Conference is to provide a platform to the researchers and practitioners from both academia as well as industry to meet the share cutting-edge development in the field.

I express my hearty gratitude to all my Colleagues, staffs, Professors, reviewers and members of organizing committee for their hearty and dedicated support to make this conference successful. I am also thankful to all our delegates for their pain staking effort to travel such a long distance to attain this conference.

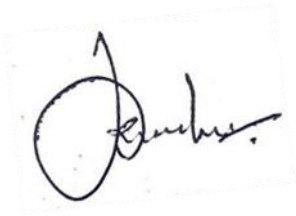

Mr. Kumar
Secretary
World Conference on Applied Science, Engineering and Technology (WCASET)

CONTENTS

S.NO	TITLES AND AUTHORS	PAGE NO
1.	Study of Solar, Biogas and Wind Micro-Grid at Sanjeevan Socio-Medical Foundation, Nagpur ➢ ***Nikhil Morey*** ➢ ***AkshayThombare*** ➢ ***Dr.S.S.Ambekar***	1-6
2.	Embedded Solution for Aircraft Fault Detection and Passenger Safety System Using Wireless Technology ➢ ***JayendraChavan*** ➢ ***AjitShinde*** ➢ ***Hrishikesh More*** ➢ ***RavindraPatil*** ➢ ***SachinGurav***	7-10
3.	Enhancement to CCTV Footage Technology using Keyframes and Background Substraction ➢ ***Shivam Bhatia*** ➢ ***Chethan S***	11-14
4.	Effect of Inorganic and Organic Fertilisers on Walnut Quality and Leaf Macro Nutrient Status ➢ ***Imtiyaz A. wani*** ➢ ***Rayees A. Ahanger***	15-18
5.	New Records of Bloodsucking Flies Associated with Wild Birds of Haftad-Gholleh Protected Area, Iran (Diptera: Hippoboscidae, Calliphoridae) ➢ ***Araghi MP*** ➢ ***Gilasian E*** ➢ ***Samaie A***	19-22
6.	Real Time Distribution Transformer Monitoring System with Data Logging ➢ ***SonaliPatil*** ➢ ***PriyankaPatil*** ➢ ***PallaviKhot*** ➢ ***SurajPatil***	23-25
7.	CO2 Purification using an Aqueous Amine Absorbent in the Syngas ➢ ***Jeong Ho Choi*** ➢ ***Soung Hee Yun*** ➢ ***Yeo Il Yoon*** ➢ ***Jung-Hyun Lee***	26-31
8.	An Approach to Measure Similarity of Software Projects at the Design Phase ➢ ***Asif imran***	32-37

CONTENTS

S.NO	TITLES AND AUTHORS	PAGE NO
9.	Effect of Ultrasonic stress in Semiconductor Materials and Devices ➢ ***Awadhesh Prasad***	38-41
10.	Mechanical Properties of A □□Ti -Xnb-3.5sn Alloy Synthesized by Mechanical Alloying and Cold Isostatic Pressure ➢ ***Abdel-Nasser Omran*** ➢ ***Mohammed Y. Abdellah*** ➢ ***Soltan Ghanim Al-Fadli***	42-48
11.	Smart Trolley for a Smart Shopping ➢ ***Renjini Jose*** ➢ ***saleh Musallam Abdullah Al Harthi*** ➢ ***Ahmed Abdullah Awadh Koofan*** ➢ ***Aida Khamis Ahmed Al Raiisi***	49-51
12.	Derivation of Probability Density Functions for Stress Concentration Factors In Uniplanar Tubular KT-Joints under In-Plane Bending Loads ➢ ***Hamid Ahmadi*** ➢ ***MirAmin MousaviNezhad Benam***	52-63
13.	Molecular Ordering in Poly (Aniline) through Controlled Cross-linking ➢ ***Mohammad Changez*** ➢ ***Zainab Ibrahim Mohammad Al-Baushi*** ➢ ***Mohammad Faiyaz Anwar***	64-66
14.	Employing Wind Energy as Aconveyance Mechanismfor India ➢ ***Yasin Yusuf Halai*** ➢ ***Naeesha Yusuf Halai***	67-71
15.	The Microstructures of Hydroxyapatite/Collagen Thin Films Coating on Ti6Al4V TitaniumAlloy Using Electrodeposit Method ➢ ***Supachai Surapunt*** ➢ ***Thanyalak Chumsud***	72-75
16.	Potential of Soya Beans Seasoning With Garlic and Ginger for Sustainable Health ➢ ***Aishatu Ibrahim*** ➢ ***Eldah Ephraim Buba***	76-81
17.	Identifying and Maintaining Overleaded Servers Through Dynamic Placement of Virtual Machines in Cloud ➢ ***Dr. Md. Mahbubul Alam Joarder*** ➢ ***Asif Imran*** ➢ ***Lamisha Rawshan***	82-87
18.	Online Shop: Influences of Online Shopping ➢ ***Larkai Jonathan***	88-90

ORGANIZATION COMMITTEE

International Advisory Committee

1. Dr. Isa Salman Hasan Qamber
University of Bahrain,Kingdom of Bahrain

2. Dr. Somasundaram Valliappan
UNSW Australia,Australia

3. Prof. Er Meng Joo
Nanyang Technological University,Singapore

4. Professor. Kabir SADEGHİ
Near East University,Turkey

5. Proff. Dr. Qing Quan Liang
College of Engineering and Science Victoria University,Australia

6. Proff. Dr. SAMREEN AMIR
Ziauddin University,Pakistan

7. Proff. Hamid Ullah
UniversitiTeknologi Brunei,Brunei Darussalam

8. Proff. SATYABRATA JIT
Indian Institute of Technology (BHU), INDIA

9. Dr. Sanath Alahakoon
CQUniversity,Australia

10. Dr. Chwastek Krzysztof
University of Technology,Poland

11. Dr. Garng M. Huang
Texas A&M University at Qatar,Qatar

12. Dr. Khursheed Aurangzeb
King Saud University,Saudi Arabia

Study of Solar, Biogas and Wind Micro-Grid at Sanjeevan Socio-Medical Foundation, Nagpur

[1] Nikhil Morey, [2] AkshayThombare, [3] Dr.S.S.Ambekar
[1][2] BE 8th Semester Electrical Engg, K.D.K. College of Engineering
[3] Head, Electrical Department, K.D.K. College of Engineering

***Abstract*: -- In India most of the electricity is produce by thermal power plant and many of them are located in central India. Thermal power plants use coal as a fuel, which will release sulphur dioxide in environment during combustion, also the land after extraction of coal will became infertile and of no use, hence in this region use of clean energy is require immediate attention. Power generated by the solar, biogas and wind which are renewable and cause zero pollution, from this renewable resources we can form a micro grid which will be able to generate enough power for the small regions with battery and loads. In central India the intensity of sunrays is good for generation of electricity by using solar panels. This paper presents study of such type of micro grid which is installed at Sanjeevan socio-medical foundation near Nagpur (central India) which consists of solar plant which generates 2KW, biogas plant which generates 12 KW and wind plant which generates 1 KW.This micro grid is connected to the main power grid and it is self dependent in almost every season. The area of foundation is also lit by using solar street lights. This type of micro grids should be installed in central India in more numbers because of the advantages like no fuel cost, predictable 24/7 power, no pollution and global warming effects.**

***Keywords:* - Micro grid, solar, photovoltaic, biogas, wind, battery, solar controller, wind controller.**

I. INTRODUCTION

In recent years, pollution situation increasingly worse in India, Red warning, as top level warning, has been triggered for serious air pollution in over 20 cities, including Delhi. Air quality index has been "exploded" in many cities. The coal extraction in central India is done at Nagpur, Umrer, chandrapur, Ballarpur, Manjri, Wani, Waninorth(Maharashtra), Pench, Kanhan(Madhya Pradesh), Pathakhera (Madhya Pradesh). The biggest coal consumer is thermal power plant. The thermal power plant is really the chief offender. Coal will release sulphur dioxide during combustion and due to which many people near the thermal power plant get diseases like asthma, skin allergy etc. The land after extraction of coal is of no use and also became infertile, So here loss of local people is observed. Hence, we should move towards use of clean energy. Use of clean energy is imperative. For large scale utilization and development of solar energy, biogas energy and wind energy which are regenerative, pollutant free, green and clean energy, the best way to generate power and connect to power grid for distributed energy is to develop micro-grid. Wind energy and solar energy generated amongst micro-grid will be stored in energy storage unit and the energy generated using Biogas will be directly distributed to the loads. This micro grids can be installed at any place and are very efficient and produce no pollution and gives pure electricity to the consumer. Application of such micro grids will definitely decrease the load on the main grid and also by some means reduce the nearby pollution level.

II. STUDY OF MICRO-GRID

MICRO-GRID:

A micro-grid is a group of interconnected loads and distributed energy resources (DERs) within clearly defined electrical boundaries that acts as a single controllable entity with respect to the grid. Micro-grid can be classified as grid connected or isolated. In isolated micro-grid it acts as a small power system with its all part (generation, transmission, and distribution). The main driver for isolated micro-grid is the availability of local energy resources. Hybrid Renewable energy system (HRES) is a combination of one or more renewable resources such as solar Photo Voltaic (PV) and wind turbine (WT) with other technologies such as batteries to supply electric power systems. Solar and wind are clean energy sources with enormous potential to alleviate grid dependence.

3.1.1 TYPES OF MICRO-GRID :-

There are several types of micro-grids for different applications. As markets, technology, and regulation changes, the types of micro-grids will continue to evolve. Military Micro-grids the ability to reliably incorporate solar PV and energy storage into military energy systems is a critical objective for the United States DOD. Reliance on diesel fuel in remote regions in the world is a weak point in military operations, and the results can be costly and deadly due to the challenge of transporting fuel through hostile regions. Additionally, the use DOD recognizes climate change as a driver of increasing instability, resulting in internal and

external pressure to reduce emissions. Campus Micro-grids could refer to corporate campuses, university campuses, and military campuses. They are often CHP / Combined Heat and Power. Community Micro-grids could be considered community solar 2.0. In the developing world, community micro-grids can be used to achieve electrification for the first time. In the developed world they are often used to help communities achieve renewable energy targets. Island Micro-grids are attractive due to the high cost of importing liquid fuels. While traditionally run off diesel, small and large islands around the world are incorporating renewables and energy storage into their energy systems. Examples of island micro-grids.

Remote Micro-grids create energy access beyond the grid. Like island micro-grids, remote micro-grids were traditionally dominated by diesel but are rapidly incorporating solar plus storage. Utility Micro-grids are done by incumbent electric utilities.

3.1.2 ON-GRID AND OFF-GRID MICRO-GRIDS :-

On-grid micro-grids means your system is tied to your local utility company's system. This is what most residential homes will use because you are covered if your system under or over-produces in regard to your varying energy needs. This entire means for you is that your utility system acts as your battery space. If you are producing more energy with your solar panels or wind mill than you are using, the excess energy is sent to your grid's power company, allowing you to build credit that you can cash out with at the end of the year, in a process called net metering. Being grid-tied is beneficial because you don't have to buy an expensive battery back-up system to store any excess energy. Off-Grid micro-grid:-Being off-grid means you are not connected in any way to your grid's power system or utility company. This is appealing because you are 100% self-sustaining your energy use.

3.2 SOLAR PANELS:-

3.2.1 DEFINITION:-

Solar panels absorb the sunlight as a source of energy to generate electricity or heat. A photovoltaic (PV) module is a packaged, connect assembly of typically 6x10 photovoltaic solar cells. Photovoltaic modules constitute the photovoltaic array of a photovoltaic system that generates and supplies solar electricity in commercial and residential applications. Each module is rated by its DC output power under standard test conditions (STC), and typically ranges from 100 to 365 Watts (W). The efficiency of a module determines the area of a module given the same rated output – an 8% efficient 230 W module will have twice the area of a 16% efficient 230 W module. There are a few commercially available solar modules that exceed efficiency of 22% and reportedly also exceeding 24%.A single solar module can produce only a limited amount of power; most installations contain multiple modules. A photovoltaic system typically includes an array of photovoltaic modules, an inverter, a battery pack for storage, interconnection wiring, and optionally a solar tracking mechanism.

3.2.2 TYPES OF SOLAR PANELS :-

MONO-CRYSTALLINE :-

To make solar cells for mono-crystalline solar panels, silicon is formed into bars and cut into wafers. These types of panels are called "mono-crystalline" to indicate that the silicon used is single-crystal silicon. Because the cell is composed of a single crystal, the electrons that generate a flow of electricity have more room to move. As a result, mono-crystalline panels are more efficient than their polycrystalline counterparts

POLYCRYSTALLINE:-

Polycrystalline solar panels are also made from silicon. However, instead of using a single crystal of silicon, manufacturers melt many fragments of silicon together to form the wafers for the panel. Polycrystalline solar panels are also referred to as "multi-crystalline," or many-crystal silicon. Because there are many crystals in each cell, there is to less freedom for the electrons to move. As a result, polycrystalline solar panels have lower efficiency ratings than mono-crystalline panels.

MONO VS. POLY SOLAR PANELS:- COMPARISON TABLE:-

	Mono-crystalline	Polycrystalline
Cost	More expensive	Less expensive
Efficiency	More efficient	Less efficient
Aesthetics	Solar cells are a black hue	Solar cells have a blue-ish hue
Longevity	25+ years	25+ years
Major manufacturers	Canadian Solar Sun power LG Hyundai Solar World	Hanwha Kyocera Hyundai Solar world Trina

Mono vs poly solar panels comparison table.

3.2.3 THEORY AND CONSTRUCTION:-

Photovoltaic modules use light energy (photons) from the Sun to generate electricity through the photovoltaic effect. The majority of modules use wafer-based crystalline silicon cells or thin-film cells. The structural (load carrying) member of a module can either be the top layer or the back layer. Cells

must also be protected from mechanical damage and moisture. Most modules are rigid, but semi-flexible ones are available, based on thin-film cells. The cells must be connected electrically in series, one to another. Externally, most of photovoltaic modules use MC4 connectors type to facilitate easy weatherproof connections to the rest of the system.
Modules electrical connections are made in series to achieve a desired output voltage and/or in parallel to provide a desired current capability. The conducting wires that take the current off the modules may contain silver, copper or other non-magnetic conductive transition metals. Bypass diodes may be incorporated or used externally, in case of partial module shading, to maximize the output of module sections still illuminated. Some special solar PV modules include concentrators in which light is focused by lenses or mirrors onto smaller cells. This enables the use of cells with a high cost per unit area (such as gallium arsenide) in a cost-effective way.

3.2.7 CHARGE CONTROLLERS:-

DEFINITION:-

A charge controller, charge regulator or battery regulator limits the rate at which electric current is added to or drawn from electric batteries. It prevents overcharging and may protect against overvoltage, which can reduce battery performance or lifespan, and may pose a safety risk.

SOLAR CHARGE CONTROLLER:-

A solar charge controller is fundamentally a voltage or current controller to charge the battery and keep electric cells from overcharging. It directs the voltage and current hailing from the solar panels setting off to the electric cell. Generally, 12V boards/panels put out in the ballpark of 16 to 20V, so if there is no regulation the electric cells will damaged from overcharging. Generally, electric storage devices require around 14 to 14.5V to get completely charged. The solar charge controllers are available in all features, costs and sizes. The range of charge controllers are from 4.5A and up to 60 to 80A.

TYPES OF SOLAR CHARGER CONTROLLER:-

There are three different types of solar charge controllers, they are:
1) Simple 1 or 2 stage controls
2) PWM (pulse width modulated)
3) Maximum power point tracking (MPPT)

DESCRIPTION:-

1) Simple 1 or 2 Controls: It has shunt transistors to control the voltage in one or two steps. This controller basically just shorts the solar panel when a certain voltage is arrived at. Their main genuine fuel for keeping such a notorious reputation is their unwavering quality – they have so not many segments, there is very little to break.
2) PWM (Pulse Width Modulated): This is the traditional type charge controller, for instance anthrax, Blue Sky and so on. These are essentially the industry standard now.
3) Maximum power point tracking (MPPT): The MPPT solar charge controller is the sparkling star of today's solar systems. These controllers truly identify the best working voltage and amperage of the solar panel exhibit and match that with the electric cell bank. The outcome is extra 10-30% more power out of your sun oriented cluster versus a PWM controller. It is usually worth the speculation for any solar electric systems over 200 watts.

BATTERY:-

Batteries in wind and solar applications have to meet the demands of unstable grid energy, heavy cycling (charging and discharging) and irregular full recharging. There's a variety of battery types fitted for these unique requirements. Considerations for choosing a battery include cost, cycle life and installation and maintenance.
So we use **Lead acid batteries for this use:-**
Deep-cycle, lead-acid batteries have been employed in renewable energy and reliably used in off-grid applications globally for decades.

COST: Typical deep-cycle, lead-acid batteries cost significantly less than lithium-ion.

CYCLING: Valve-regulated lead-acid (VRLA) batteries include absorbed glass mat (AGM) and gel models. Many AGM batteries available in the market are primarily built for dual-purpose or standby applications like emergency backup, but not deep cycling. However, new deep-cycle AGM designs have increased performance and total energy output making them a good choice for renewable energy applications at a lower price point than gel batteries.

REPLACEMENT/MAINTENANCE: Many factors including initial design and ongoing maintenance influence battery life so it's difficult to put a time frame on when the batteries will need replacement. Flooded lead-acid batteries have to be refilled regularly because the electrolyte that fully submerges the battery plates evaporates during charging. The battery enclosure needs ventilation to keep hydrogen gas from accumulating to dangerous levels.

WIND MILL :-

Wind power is the use of air flow through wind turbines to mechanically power generators for electric power. Wind power, as an alternative to burning fossil fuels, is plentiful, renewable, widely distributed, clean, produces no greenhouse gas emissions during operation, consumes no water, and uses little land. The net effects on the environment are far less problematic than those of nonrenewable power sources.
Wind farms consist of many individual wind turbines which are connected to the electric power transmission network.

 ISBN: 978-81-932966-9-1

Onshore wind is an inexpensive source of electric power, competitive with or in many places cheaper than coal or gas plants. Off shore wind is steadier and stronger than on land, and offshore farms have less visual impact, but construction and maintenance costs are considerably higher. Small onshore wind farms can feed some energy into the grid or provide electric power to isolated off-grid locations.

Wind power gives variable power which is very consistent from year to year but which has significant variation over shorter time scales. It is therefore used in conjunction with other electric power sources to give a reliable supply. As the proportion of wind power in a region increases, a need to upgrade the grid, and a lowered ability to supplant conventional production can occur. Power management techniques such as having excess capacity, geographically distributed turbines, dispatchable backing sources, sufficient hydroelectric power, exporting and importing power to neighboring areas, or reducing demand when wind production is low, can in many cases overcome these problems.In addition, weather forecasting permits the electric power network to be readied for the predictable variations in production that occur.

3.3.1 WIND CHARGE CONTROLLER:-

Wind power charge controllers that are compatible with most wind power systems and batteries. These charge controllers will protect and prolong the life of battery by controlling the amount of current that charges it.

3.4 BIOGAS :-

Biogas typically refers to a mixture of different gases produced by the breakdown of organic matter in the absence of oxygen. Biogas can be produced from raw materials such as agricultural waste, manure, municipal waste, plant materials, sewage green waste or food waste. Biogas is a renewable energy source. Biogas can be produced by anaerobic digestion with anaerobic organism, which digest material inside a closed system, or fermentation of biodegradable materials.[1]

Biogas is primarily methane (CH4) and carbon dioxide (CO_2) and may have small amounts of hydrogen sulfide (H 2S), moisture and siloxanes. The gases methane, hydrogen and carbon monoxide (CO) can be combusted or oxidized with oxygen. This energy release allows biogas to be used as a fuel; it can be used for any heating purpose, such as cooking. It can also be used in a gas engine to convert the energy in the gas into electricity and heat. Biogas can be used for electricity production on sewage works in a CHP gas engine, where the waste heat from the engine is conveniently used for heating the digester; cooking; space heating; water heating; and process heating. If compressed, it can replace compressed natural gas for use in vehicles, where it can fuel an internal combustion chamber or fuel cells and is a much more effective displacer of carbon dioxide than the normal use in on-site CHP plants.

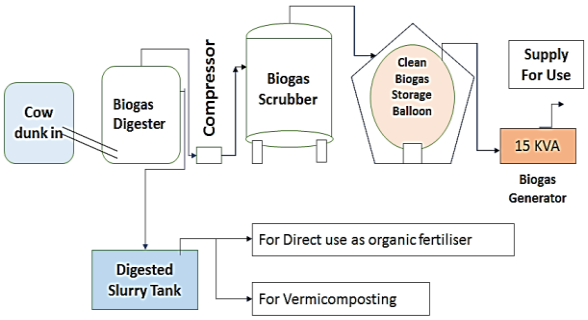

Fig 3.4 :- Block diagram of biogas plant

3.4.1 COMPOSITION

The composition of biogas varies depending upon the substrate composition, as well as the conditions within the anaerobic reactor (temperature, pH, and substrate concentration Landfill gas typically has methane concentrations around 50%. Advanced waste treatment technologies can produce biogas with 55%–75% methane,which for reactors with free liquids can be increased to 80%-90% methane using in-situ gas purification techniques. As produced, biogas contains water vapor. The fractional volume of water vapor is a function of biogas temperature; correction of measured gas volume for water vapor content and thermal expansion is easily done via simple mathematics which yields the standardized volume of dry biogas. In some cases, biogas contains siloxanes. They are formed from the anaerobic decomposition of materials commonly found in soaps and detergents. During combustion of biogas containing siloxanes, silicon is released and can combine with free oxygen or other elements in the combustion gas. Deposits are formed containing mostly silica (SiO2) or silicates and can contain calcium, sulfur, zinc, phosphorus. Such white mineral deposits accumulate to a surface thickness of several millimeters and must be removed by chemical or mechanical means. Practical and cost-effective technologies to remove siloxanes and other biogas contaminants are available. For 1000 kg (wet weight) of input to a typical biodigester, total solids may be 30% of the wet weight while volatile suspended solids may be 90% of the total solids. Protein would be 20% of the volatile solids, carbohydrates would be 70% of the volatile solids, and finally fats would be 10% of the volatile solids.

3.4.2 APPLICATION

Biogas can be used for electricity production on sewage works in a CHP gas engine, where the waste heat from the engine is conveniently used for heating the digester; cooking;
space heating; water heating; and process heating. If compressed, it can replace compressed natural gas for use in vehicles, where it can fuel an internal combustion engine or fuel cells and is a much more effective displacer of carbon dioxide than the normal use in on-site CHP plants.

3.4.3 BIOGAS GAS-GRID INJECTION

Gas-grid injection is the injection of biogas into the methane grid (natural gas grid). Injections includes biogas until the breakthrough of micro combined heat and power two-thirds of all the energy produced by biogas power plants was lost (the heat), using the grid to transport the gas to customers, the electricity and the heat can be used for on-site generation resulting in a reduction of losses in the transportation of energy. Typical energy losses in natural gas transmission systems range from 1% to 2%. The current energy losses on a large electrical system range from 5% to 8%. Before being injected in the gas grid, biogas passes a cleaning process, during which it is upgraded to natural gas quality. During the cleaning processtrace components harmful to the gas grid and the final users are removed.

IV. MICRO GRID PARAMETERS

4.1 DATA COLLECTION:

1) Solar panels rating, Area i.e their Length breadth, no of cells, Mono-crystalline info,
2) Battery specifications, connections (parallel), wire size.
3) Solar controller ratings.
4) Windmill ratings.

4.1 MICRO-GRID:-

Capacity :- 15 KW
Area :- 03 Acre
Type :- Off-grid

4.2 SOLAR PANELS:-

No. of solar Panels :- 08 Panels
Type :- Mono-crystalline
No. of cells :- 60 (6*10)
Cell vendor :-LG
Cell dimension :-156 x 156 mm^2/6 x 6 in2
Dimensions :- (L x W x H) 1640 x 1000 x 35 mm
Capacity :- 250 watts
Voltage :- 12v
Efficiency :-18.3%

4.3 CHARGE CONTROLLER :-

Type :- MPPT charge controller (Increase Output by 30%)
Make :- CS-30
Voltage input (Max.) :- 530v
Voltage Output :- 12V
Current :- 40 A

4.4 POWER INVERTER:-

Capacity :-1300 VA
Voltage :- 12V
Current :- 10A

4.5 BATTERY:-

No. of batteries :- 04
Make :- SF Sonic Stan Red-350
Type :- Lead-Acid Battery.
Rating :- 12v (100Ah)
Connections :- Parallel Connection

4.6 WIND MILL:-

RATING OF AXIAL FLUX PM GENERATOR (USED IN WIND MILL):-

SR NO.	PARAMETER	UNITS	SPECIFICATIONS
1	Rated power	KW	5
2	Rated speed	RPM	100
3	Rated voltage	V	380VAC
4	Rated Current	A	7.6
5	Efficiency		>85%
6	Resistance (Line-Line)	Ω	-
7	Winding type		Y
8	Insulation Resistance		100Mohm Min(500V DC)
9	Leakage level		<5 ma
10	Start torque	N/M	<0.5
11	Phase		Three phase
12	Structure		outer rotor
13	Stator		coreless
14	Rotor		Permanent magnet type (outer rotor)
15	Gen. Diameter	mm	765
16	Gen. Length	mm	406
17	Gen. Weight	Kg	165
18	Shaft. Diameter	mm	98
19	Housing Material		Aluminum (Alloy)
20	Shaft Material		Steel

TABLE. 4.6.1 RATING OF AXIAL FLUX PM GENERATOR (USED IN WIND MILL)

4.7 BIOGAS :-

Plant Capacity :- 25 m^3/day
Internal Diameter of Digester :- 23 m

 ISBN: 978-81-932966-9-1

External Diameter :- 23.7 m
Internal height of digester :- 6 m
Wall thickness of digester :- 0.3 m
Clean Biogas Balloon capacity :- 45 m^3
Clean Biogas Balloon material :- Rubber

4.7.1 BIOGAS COMBUTION ENGINERATING :- 15 KVA(WATER COOLED)

- 12v starter
- Radiator with and water pump
- Lub oil filter
- Flywheel suitable for Genset (Heavy)
- Panel with charging Ammeter, Oil Pressure Gauge,

  Water temperature gauge and starting switch
- Battery charging Alternator

  Air/ Gas mixture regulator
- Heavy Duty Air Filter

  Industrial Silencer

Biogas Combution Engine type :- 4 Stroke (110x125 110x120 110x120110x120 110x120)
Biogas Engine RPM :-1500
Combution Engine cylinder :- 02
Make :- Prakash India

4.7.2 BIOGAS GENERATOR:-

Rating	:- KVA-15 KVA
RPM	:-1500
Phase	:- 3 phase (AC)
Voltage	:-415 V
Current	:-21 Amp
Excitation Voltage	:-120V Excited
Frequecy	:-50 Hz
Power factor	:-0.8 pf
Generator output	:-12 kw
Make	:-Prakash India

4.2 DETAILS :

Our disc coreless PMG have advantage in low Rated speed, Low starting wind speed, Small volume, Energy Small, Light weight, Compact structure, High efficiency etc. Inner or outer rotor all available, and we can do customize generator accordingcustomer request magnetic levitation , Coreless, an hysteresis, slot less, have low starting torque. No iron loss, have high efficiency over 98% Adopt unique coreless precision winding technology design precision coil Adopt the rare earth permanent magnet, which is multipole, mean gap, high power density and high output power. Low speed direct driving, no torque fluctuations Compact structure, high ratio of power to volume No iron loss, low calorific value, small temperature rise Simple structure, easy to install The brushless structure, free maintenance.

V. CONCLUSIONS

This micro-grid is implemented currently in Sanjeevan foundation, The micro-grid consist of Solar plant, Wind Plant and Biogas plant whose collective generation capacity is 15 KW. Depending on the requirement of solar, wind and biogas energy sources can be utilized in micro-grid or it can be operate individually. Solar plant consist of 16 solar panels each of capacity 250 watt and 9 solar street lights , making the capacity of 2 KW. Wind mill had a capacity of 1 KW, which consist of AFPMG (axial flux permanent magnet generator) whose rated capacity is 5 KW. This types of micro grids can definitely reduce the pollution level and wastage of land as well retain there fertility. In central India this types of initiatives are needed in order to prevent environment and human health in the future. Making such institutes free from main grid will make them self dependent and after expansion they can provide their extra generated energy to the main grid also.

REFERENCE

1) Du Bo and Liu Wenzhou ”Research on control of energy storage by intelligent microgrid for wind/photovoltaic/energy storage”*IEEE*

2) K. Strunz, E. Abbasi, and D. N. Huu,”DC Microgrid for Wind and Solar Power Integration” IEEE journal of emerging and selected topics in power electronics, vol. 2, no. 1, march 2014

3) M. H. Nehrir, C. Wang, K. Strunz, H. Aki, R. Ramakumar, J. Bing,*et al.*, “A review of hybrid renewable/alternative energy systems for electric power generation: Configurations, control, and applications,”*IEEE Trans. Sustain. Energy*, vol. 2, no. 4, pp. 392–403, Oct. 2011.

4) H. Polinder, J. A. Ferreira, B. B. Jensen, A. B. Abrahamsen, K. Atallah, and R. A. McMahon, “Trends in wind turbine generator systems,” *IEEE J. Emerg. Sel. Topics Power Electron.*, vol. 1, no. 3, pp. 174–185, Sep. 2013.

5) B. S. Borowy and Z. M. Salameh, “Methodology for optimally sizing the combination of a battery bank and PV array in a wind/PV hybrid system,” *IEEE Trans. Energy Convers.*, vol. 11, no. 2, pp. 367–375, Mar. 1996.

6) A. L. Dimeas and N. D. Hatziargyriou, “Operation of a multiagent system for microgrid control,” *IEEE Trans. Power Syst.*, vol. 20, no. 3, pp. 1447–1455, Aug. 2005.

Embedded Solution for Aircraft Fault Detection and Passenger Safety System Using Wireless Technology

[1]JayendraChavan, [2]AjitShinde, [3]Hrishikesh More, [4]RavindraPatil, [5]SachinGurav
[1, 2, 3, 4,5]Sharad Institute of Technology College of Engineering, Yadrav-Ichalkaranji

Abstract: —**The recent years were quite bad for aviation world due to serious aircraft crashes. Lots of human being lost their lives in plane crashes over last 3 years and this became very serious & sensitive issue in the world. So we are proposing the idea of detachment of passenger compartment on the detection of major problem in an aircraft which predicts the fatal crash of airplane. We are using some advanced sensors to detect the accidental occurrences of defects or faults in an aircraft. These sensors are selected according to most common problems of aircraft crashes. On detection of sensors data, the data is compared with threshold limits & if the data reaches beyond threshold it predicts the possible crash of plane and gives signal to the detachment control panel On the signal of sensors, the passenger compartment will get ejected from the fuselage and with help of parachutes or will land safely on ground without any fatal loss. We are using arduino platform with AVR ATmega328 microcontroller. It is 8 bit microcontroller with 32kb memory. This controller board comes with 14 digital I/O pins and out of these 14 pins fro 6 pins provide Pulse Width Modulation (PWM) output signal. This board also comes with 6 analog input pins. This board can be powered by USB as well as external dc jack with 5 to 12 v input supply.**

Index Terms- **Aviation, detachment, predict, fatal, fuselage**

I. INTRODUCTION

Today we are living in 21st century in which human life safety is more important than any other things. But as century's increases technology also get increases similarly risk for human life too. But with that risk, humans get research the effective solution on that.

Similarly recent years were quite bad for aviation world due to serious aircraft crashes. Although today airplanes have become a lot safer over the past few decades. Much work goes into making sure that aircraft are safe since there's almost always a loss of life when a flight crashes. Lots of human being lost their lives in plane crashes. This became very sensitive & serious issue in the world. So companies are interested in improving safety in aircraft. So we are proposing idea of the ejection and the recovery system of passenger compartment in an accidental crash situation of aircraft. In this technique the passenger compartment of the aircraft gets ejected from its main body when any accidental or critical situation gets occurred. The ejected passenger compartment get fly in air with the help of parachute attached at the top of the compartment. Rubber tube filled with air used as floater which saves the compartment from drowns. Sensors are selected according to most common problems of aircraft crashes. On detection of sensors data, the data is compared with threshold limits & if the data reaches beyond threshold it predicts the possible crash of plane and gives signal to the detachment control panel On the signal of sensors, the passenger compartment will get ejected from the fuselage and with help of parachutes or will land safely on ground without any fatal loss.

We use arduino board with ATmeg328 controller. It is 32 kb 8 bit microcontroller. This controller board has 14 I/O digital pin from which 6 pins are used as Pulse Width Modulation (PWM) output, 6 analog input pins. A USB connector used for 5V power supply and a power jack is used for applying 3.3V-9V power supply to the board.

II. OBJECTIVE AND SCOPE

The main objective of our project is to make development in the aviation technology and make aircraft safer than past few decades. This technology can be readily

used by aviation industry for creating more safe aircrafts which saves the passenger life in critical situation like fire, wings fault, turbine fault etc. This project has the large scope as it has the following features which help in making it easy to use, modify and understand it.

- Parachute attached at the roof and rubber tubes inflate on bottom of cabin.
- Storage space holds passenger luggage underneath the cabin.
- Automatic excessive angle change system.

III.PRESENT STATE

➢ Present State:

- According to ICAO(International Civil Aviation
- Organization), over the past 10 years there are 8% of all accidents happen during takeoff, landing- 21% cruising flights-71%.
- The accident rate in Africa, for instance, is nearly five times that of the worldwide average, according to the International Civil Aviation Organization, part of the United Nations. Such trouble spots also happen to be where air travel is growing the fastest
- The analysis of causes of accident show that 75% of them happen because of human factor, other because of omission aeromechanics. To reduce the influence of human factor by rising up safety of airplane is impossible. The new principle of aircraft construction is needed for possibility of collective rescuing by evacuation of them crashing airplanes in the range from several hundreds of meters to several km.
- There are 12.25 fatalities per million flight deaths.
- A plane crashes one out of 1.2 million flights.
- There is a 24% survival rate of passengers on a fatal crash.
- There were 111 plane crashes in 2014, which went down from 138 in 2013.
- Technological improvements are also helping to lower the accident rate. Cockpits now come with systems that automatically warn if a jet is too low, about to hit a mountain or another plane. Others detect sudden wind gusts that could make a landing unsafe.

- The next generation of technology promises to help prevent even more accidents. Honeywell Aerospace launched a new system 18 months ago that gives pilots better awareness about severe turbulence, hail and lightning. The company is also developing a system to improve pilots' vision in stormy weather: an infrared camera will let them see runways through thick clouds earlier than the naked eye would.

➢ ***After implementation of project:***

- The year 2014 left a strong impression on the aviation industry, with Malaysian Airline's MH 370 going missing to various plane crashes. It was just a bad year and the industry had to fight out the odds. But, there was still no solution to prevent or at least battle plane crashes in a way it saves the lives of the passengers. But our project a small step to solve that problem.
- In this project such aircraft construction is offered. Which provides separation of the lower part of the fuselage with situated there passengers and their luggage, gradual decline of separated part and its soft landing(splashdown), afterwards providing an opportunity for its searching and finding by rescuers.
- The guaranty of success of offered airplane structure is in the fact that outlined in structure solutions are based on lifelong checked technical solution of landing in transport aviation
-

IV. PROCESS DESCRIPTION/METHODOLOGY

Block Diagram

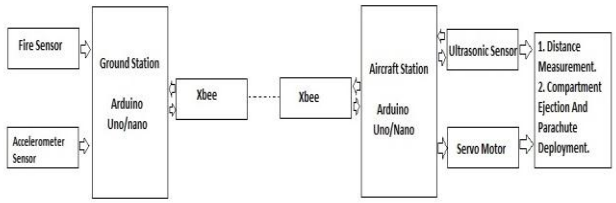

Fig.1 Bolck Diagram

There are two ARDUINO base stations present which are connected with each other through XBEE module. First Arduino Detect the fault occurred in aircraft by using fire sensor, Accelerometer sensor. And second Arduino board controls the servo motor and ultrasonic sensor, which is in aircraft station. XBEE module is the wireless communication model. It communicates with other XBEE which in line of sight with it. The fire/flame sensor detects the small fire in aircraft and sends that signal to the ground station Arduino. Ultrasonic sensor is used to detect the distance of falling compartment from ground. Servo motor is used for precise control of angular or linear position, velocity and acceleration. It consists of a suitable motor coupled to a sensor for position feedback.

B. Circuit Diagram

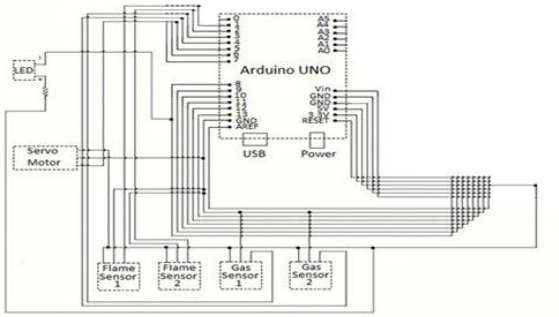

Fig 2. Interfacing Of Flame Sensor And Servo Motor.

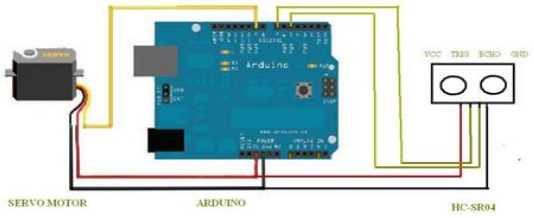

Fig 3.Interfacing of Ultrasonic Sensor with Servo Motor.

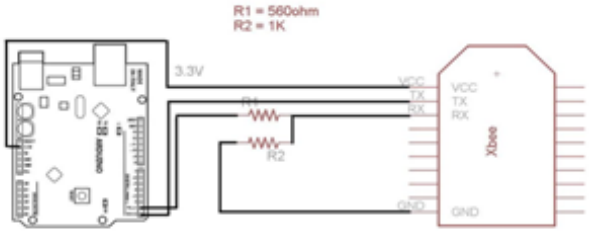

Fig 4.Interfacing of Xbee with ARDUINO.

V.PROPOSED WORK

- **Hardware Part:**
- **MCU: (Arduino unit)**

As Arduino are the simple and effective controller boards used in digital circuit design in industry, this system uses it for the centralized operation and digital processing. The embedded technology is used in arduino.

The Figure Shows Arduino board with ATmeg328 controller. It is 32 kb 8 bit microcontroller. This controller board has 14 I/O digital pin from which 6 pins are used as Pulse Width Modulation (PWM) output, 6 analog input pins. A USB connector used for 5V power supply and a power jack is used for applying 3.3V-9V power supply to the board.

It is a simple microcontroller board. It is an open source computing platform and has an environment for developing software for the Arduino board. It takes input from sensors or switches and controls the outputs. Arduino boards are inexpensive compared to other microcontroller based devices.

- ***SENSOR*:**
- ***Flame Sensor***

A flame sensor detects the presence of fire or flames. In extremely hazardous environments, flame sensors work to minimize the risks associated with fire. There are several different types of flame sensor - some will raise an alarm while others may activate a fire suppression system or deactivate a combustible fuel line. Among the many different types of flame sensor, ultraviolet flame sensors, near IR array flame sensors, infrared flame sensors and IR3 flame detection sensors are the most prominent.

- ***Ultrasonic Sensor(HC-SR 04)***

Ultrasonic sensors are based on measuring the properties of sound waves with frequency above the human audible range. They are based on three physical principles: time of flight, the Doppler Effect, and the attenuation of sound waves. Ultrasonic sensors are non-intrusive in that they do not require physical contact with their target, and can detect certain clear or shiny targets otherwise obscured to some vision-based sensors. On the other hand, their measurements are very sensitive to temperature and to the angle of the target.

- ***Accelerometer Sensor***

One of the most common inertial sensors is the **accelerometer**, a dynamic sensor capable of a vast range of sensing. Accelerometers are available that can measure acceleration in one, two, or three orthogonal axes. They are typically used in one of three modes. As an inertial measurement of velocity and position.As a sensor of inclination, tilt, or orientation in 2 or 3 dimensions, as referenced from the acceleration of gravity (1 g = 9.8m/s^2).As a vibration or impact (shock) sensor. There are considerable advantages to using an analog accelerometer as opposed to an inclinometer such as a liquid tilt sensor – inclinometers tend to output binary information (indicating a state of on or off), thus it is only possible to detect when the tilt has exceeded some threshold angle.

- ***SERVO MOTOR***

A servo motoris a rotary actuator or linear actuator that allows for precise control of angular or linear position, velocity and acceleration. It consists of a suitable motor coupled to a sensor for position feedback. It also requires a relatively sophisticated controller, often a dedicated module designed specifically for use with servomotors. Servomotors are not a specific class of motor although the term *servomotor* is often used to refer

to a motor suitable for use in a closed-loop control system.

- ***XBEE:***

Xbee is a device which is used for wireless technology which provides connection between the devices. It is the low cost, low power wireless network used for instrument control.784 MHz, 868MHz and 915 MHz Data rate varies from 20 Kb/s to 250 Kb/s.

Its transmission distance is limited to 10 to 100 meters line of sight. It depends on power output and environmental factors. It can use long distance communication using intermediate devices. It can be used in several applications such as wireless light switches, smart grid, medical devices etc. It is used for wireless transmission purpose.Xbee was designed to provide high data throughput in applications where the duty cycle is low and low power consumption is an important consideration.

IV.RESULT

From our project we got some sensor result.
For Accelerometer Sensor

For Servo motor:

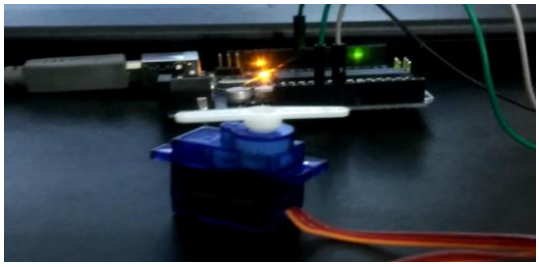

For Ultrasonic Sensor

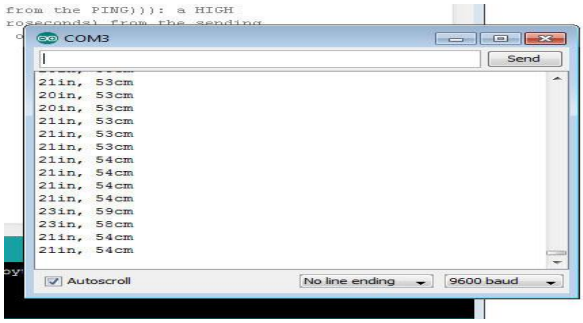

VII. CONCLUSION

From all above the project, we said that the project is very useful to increase the percentage of human safety when plane get crashed. It will become a very important life saving technology in plane engineering. But Passenger might have to pay more money to fly on a plane.

REFERENCES

[1] Nusratfatema, Rafat shams, Shafkathossain, Shaonipriyom, Automated fire extinguishing system with GSM alarm, 2014

[2] MdIftekharulMobin, MdAbid-Ar-Rafi, MdNeamul Islam, And MdRifat.Hasan, An Intelligent Fire Detection and Mitigation System Safe from Fire (SFF), January 2016, Volume 133 - No.6.

Enhancement to CCTV Footage Technology using Keyframes and Background Substraction

[1] Shivam Bhatia, [2] Chethan S
[1][2] Department of Information and Technology Manipal Institute of Technology Manipal,India

Abstract:-- **This paper deals with two very important concepts in Image Processing i.e. Video Summarization and Background Subtraction. Video Summarization is one of the most important concepts in today's image processing world. Video Summarization is a process of creating and presenting a meaningful abstract view of the entire video in a summary. There are two main types of Video Summarization techniques available in the literature, key frame based and video skimming. This paper will deal with key frame based approach. Background Subtraction also known as foreground detection is a technique in the field of image processing and computer vision where an image's background is extracted for further processing. The idea of the research paper is mainly focused on the problem of ever increasing CCTV footage length that has to be monitored. My project aims to reduce the CCTV video length based on key frames and also incorporates the concept of Background Subtraction enabling the user to focus on Object of Interest.**

Keywords—**Video Processing, Background Subtraction, Video Summarization, Key frame, Video Skimming, Region of Interest(ROI).**

I. INTRODUCTION

Wondered how tiring and exhausting it is for the CCTV footage invigilators to go through CCTV footage in case of an unfortunate incident. Keeping in mind the above issue we have come up with an idea which will incorporate concept of Video Summarization using key frame based approach and Background Subtraction.

Video processing systems are based on the stream processing architecture. In this architecture the video frames from a continuous stream are processed one (or more) at a time. This type of processing becomes handy where systems have live video or where the video data is so large that incorporating the entire visual data into the workspace is inefficient [1]. Keeping in mind the need of the hour, a large number of cameras are installed to record video 24*7 which results in a large amount of data. Processing this large amount of visual data requires a large amount of resources like time, man power, and hardware storage and so on [2]. This is where concept of Video Summarization comes to rescue. Video Summarization is one the most important concept in present image processing world. It is a process of creating and presenting a meaningful abstract view of the entire video in a shorter video. There are two main types of Video Summarization techniques available in the technical world. One of them is based on key frames generation concept while the other one is based on the concept of video skimming. The research paper incorporates the concept of key frame generation where key frames are generated from a video using MATLAB. A plot of mean gray values of the frames generated along with Adaptive Background and Binarized Difference Image is also generated.

There are certain cases where you need to focus on an object of interest; this is where Background Subtraction comes in the picture. Background Subtraction is one of the most common and widely used techniques which let you calculate the foreground mask by performing a subtraction operation between the current frame and the background which more or less is the static part of the scene and lets you to focus on the Object of Interest [3].

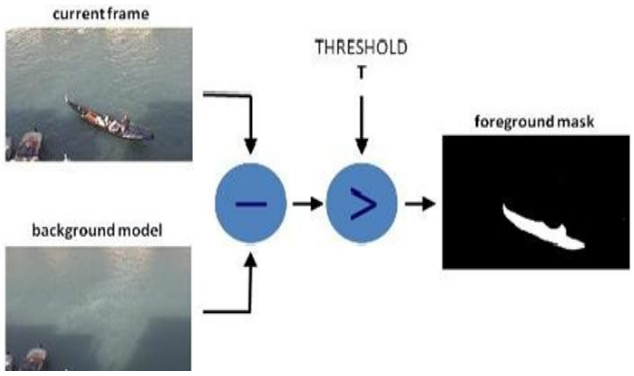

II. LITERATURE SURVEY

Priyamvada R Sachan and Keshaveni [4] presented a paper on Video Summarization in which the CCTV Footage video is segmented into contagious shots. From the contagious shots generated one or more key frames are generated from each shot and a summary video is

generated from the keys frames selected. Saran K B and Sreelekha G [5] published a paper on Background Subtraction in which the moving vehicles are detected, number of vehicles is estimated and the detected vehicles are estimated using the mixture of Gaussians and Artificial Neural Network (ANN) with a new set of features. Ashvini A. Tonge and Sudeep D Thepade [6] put forward a paper on Video Summarization keeping in mind the large amount of CCTV footage available. In the above paper key frame are extracted for video content summarization using the concept of Orthogonal Transforms and Fractional Energy Coefficients. Ijiya Chugh, Ridhima Gupta, Rishi Kumar and Prashast Sahay [7], published a paper on Video Summarization in which various possible techniques for key frame extraction from the video stream are discussed This paper was published keeping in mind the various problems faced by various researchers and projects to properly execute or create a system which can perform video frame extraction and face recognition. The paper makes sure that only those scenes which are required by the user are taken into consideration hence saving a considerable amount of resources. Yijie Lan , Shikui Wei , Ruoyu Liu and Yao Zhao [8] ,presented in a paper on Video Summarization in which an approach of summarizing a video based on viewpoint of emotion. Ground-truth emotion scores of each frame are firstly obtained from dataset annotated by humans. Then, we extract emotional features of each frame from training video sets. Later, using linear regression predictive model is trained from the feature vectors and emotion scores. Concurrently, the videos are segmented into various segments. Then, a subset of segment whose length is below a specific value is selected by optimizing the sum of their emotion scores. This subset of segment is what is treated as a desired summarized video. Yanghong Zhang, Qing He, Haibin Wang, Guan Guan, Tao Xu and Haodong Chen [9], proposed a paper on Background Subtraction in based on a detection algorithm in which pixel level is used to construct the background model for background segmentation. The authors based on this algorithm proposed a spatiotemporal-based algorithm which helps in construction of the background model for the background segmentation. The paper has adopted the property of color clustering to determine the similarity dynamically. The experimental result on the 2012 Change Detection dataset depict that the above algorithm outperforms most of the algorithms. Gongyan Wang , Jing Xu and Ming Fang [10] , put forth a paper on Background Subtraction in which 11 different are compared using the BMC dataset and gives guidelines to choose different algorithms by computing the F- measure , Peak Signal-Noise Ratio , Structural Similarity and D-Score etc. Ali Javed, Khalid Bashir Bajwa, Hafiz Malik, Aun Irtaza and Muhammad Tariq Mahmood [11], proposed a study where an automatic summary of cricket video using first rule induction to detect audio clips in cricket videos and then a decision tree framework is designed for video summarization. This paper has evaluated on a diverse dataset with an average accuracy of 95% signifies the effectiveness of Video Summarization. This helps in broadcast over the low- bandwidth networks and transmission over time constraints.

III. METHODOLOGY

The paper incorporates two basic concepts i.e. Video Summarization and Background Subtraction.

A. Video Summarization

For Video Summarization, a key frame based approach is used. There are five basic steps that govern the Video Summarization:-

1. Number of frames is determined along with the height and width of the frames. Then, the key frames are generated from the uploaded video.

2. The frames are converted from RGB format to gray scale format. The mean red level, green level and blue levels is determined. A plot between Frame number and Gray level is displayed with mean red level, green level and blue level.

3. An adaptive background window is displayed where slight difference between each frame and background is displayed. This helps to track the movement of the object of interest.

4.A Binarized Difference Image window is displayed where the difference between current and previous frame is displayed. A binary image is a digital image that has only two possible values for each pixel i.e. 0 and 1.[12]

5. A summary video is generated from the key frames generated using Blender.

Pseudo Code for Key Frame Generation is as follows:-

```
Select the video file you want to generate frames for
//video Object = Video Reader(NameOfTheMovieFile)
Determine the number of frames
//numberOfFrames=videoObject.NumberOfFrames
Determine the height of the frame
//vidHeight = videoObject.Height
Determine the width of the frame
//vidWidth = videoObject.Width
for frame = 1 : numberOfFrames//Loop through all the frames
thisFrame = read(videoObject, frame)// Extract the frame from the movie structure.
hImage = subplot(2, 2, 1) //Display the Frame
image(thisFrame)
```

 ISBN: 978-81-932966-9-1

caption = sprintf('Frame %4d of %d.', frame, numberOfFrames)//Caption the frame
title(caption, 'FontSize', fontSize) [1].

B. Background Subtraction

The second concept i.e. Background Subtraction is a unique method by which a subject is identified in the first frame and then followed in subsequent frames n the presence of a moving background. The write-up tends to provide insight on how background subtraction is done and how for better vigilance you can concentrate on object of interest.

The method incorporated for Background Subtraction in this paper is Frame Differencing. The region of interest being white in some cases like a white car you might need to use some morphological operators to find the center of Region of Interest (ROI) and the bounding box. In this method, the background model at each pixel location is based on pixel's recent history. The history can be the average or the median of the previous n frames:

$Bi(x,y)=median\{Ii-n+1(x,y),Ii-n(x,y),...,Ii-2(x,y),Ii-1(x,y)\}$.

A pixel belongs to the foreground if

$|Ii(x,y)-Bi(x,y)| > T$,

Where T is a defined threshold. The estimated background can

be updated as follows:

$Bi(x,y) = \alpha Ii(x,y) + (1-\alpha)Bi-1(x,y)$ if Ii−1 is foreground,

$Bi(x,y)=Bi-1(x,y)$ if Ii−1 is background,

Where α is the learning rate, usually a small value(0.05). [13][14]

IV. RESULT

This paper focuses on the concept of Background Subtraction and Video Summarization. Keeping in mind the basic idea of the research work, a CCTV video footage was taken into consideration. The Video Summarization part of the research paper was taken care by using the key frame generation concept and Blender. From the key frames generated a clip was generated with background subtracted and main focus on Region of Interest (ROI).

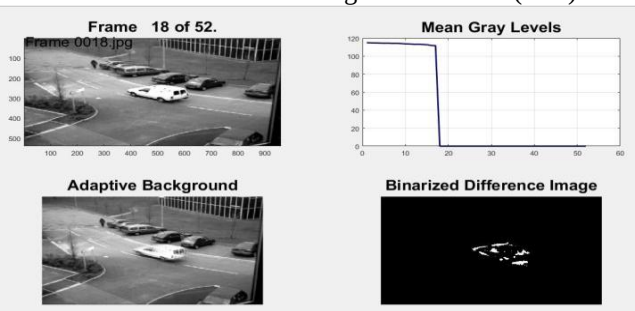

Figure 2: Depicting key frame generation, Graph displaying mean gray levels, Adaptive Background and Binarized Difference Image.

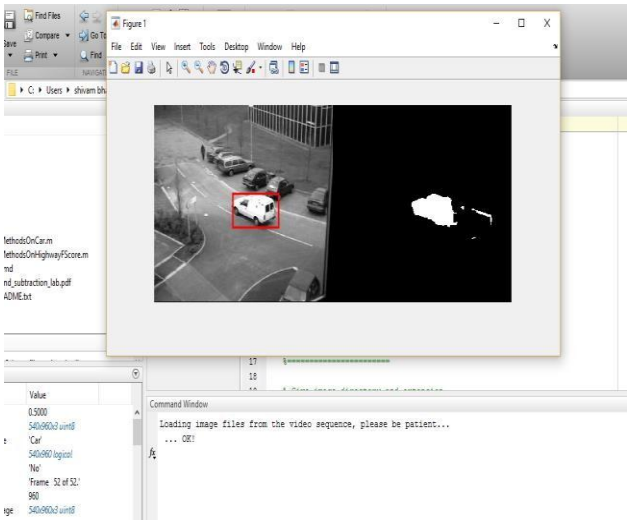

Figure 3: Depicting background subtraction as per the Region of Interest(ROI).`

Figure4: Depicting how a video is generated from key frames generated.

V. CONCLUSION

The paper incorporates two very important concepts of Video Processing i.e. Video Summarization and Background Subtraction. The project encompasses Video Summarization is by generating a summarized clip of a large CCTV video using the key frame based approach. The key frames generated are then taken in consideration for Background Subtraction and a video clip is generated with background subtracted based on the Region of Interest (ROI). The Background Subtraction is based on an important concept of Frame Differencing. [14]

REFERENCES

[1] https://in.mathworks.com/solutions/image-video-processing/video- processing.html

[2] Ajmal M., Ashraf M.H., Shakir M., Abbas Y., Shah F.A. (2012) Video Summarization: Techniques and Classification. In: Bolc L., Tadeusiewicz R., Chmielewski L.J., Wojciechowski K. (eds) Computer

Vision and Graphics. ICCVG 2012. Lecture Notes in Computer Science, vol 7594. Springer, Berlin, Heidelberg
[3] How to Use Background Subtraction Methods. Available online at: http://docs.opencv.org/trunk/d1/dc5/tutorial_background_subtraction.ht ml
[4] Priyamvada R Sachan and Keshaveni, "Frame Clustering Technique towards Single Video Summarization," in 2016 Second International Conference on Cognitive Computing and Information Processing (CCIP).
[5] Saran K B and Sreelekha G, "Traffic Video Surveillance: Vehicle Detection and Classification," in 2015 International Conference on Control, Communication & Computing India (ICCC) | 19-21 November
2015 | Trivandrum.
[6] Ashvini A. Tonge and Sudeep D Thepade, "Key frame extraction for video content summarization using orthogonal transforms and fractional energy coefficients," in Information Processing (ICIP), 2015
International Conference | 16-19 Dec. 2015 |Pune.
[7] Ijiya Chugh ,Ridhima Gupta , Rishi Kumar and Prashast Sahay, "Techniques for key frame extraction: Shot segmentation and feature trajectory computation," in Cloud System and Big Data Engineering (Confluence), 2016 6th International Conference |14-15 Jan,2016| Noida.
[8] Yijie Lan , Shikui Wei , Ruoyu Liu and Yao Zhao, "Creating video summarization from emotion perspective," in Signal Processing (ICSP),
2016 IEEE 13th International Conference |6-10 Nov,2016| Chengdu,China.

[9] Yanghong Zhang , Qing He , Haibin Wang , Guan Guan , Tao Xu and Haodong Chen, "Background subtraction based on pixel clustering," in Information and Automation (ICIA), 2016 IEEE International Conference | 1-3 Aug. 2016 |Ningbo, China.
[10] Gongyan Wang , Jing Xu and Ming Fang, "A comparison of background subtraction algorithms evaluated with BMC dataset," in Intelligent Control and Automation (WCICA), 2016 12th World Congress|12-15 June,2016|Guilin,China.
[11] Ali Javed , Khalid Bashir Bajwa , Hafiz Malik , Aun Irtaza and Muhammad Tariq Mahmood "A hybrid approach for summarization of cricket videos, " in Consumer Electronics-Asia (ICCE-Asia), IEEE International Conference |26-28 Oct,2016| Seoul, South Korea.
[12] Video Processing, Copyright (c) 2014, Image Analyst Available online at: http://in.mathworks.com/matlabcentral/fileexchange/47726-video- processing-tutorial?focused=3812055&tab=function

[13] Emre Ozan Alkan, "Tracking a Moving Object I : Background Subtraction" The MIT License (MIT), Copyright (c) 2014 Emre Ozan Alkan, Available Online at: "https://github.com/emreozanalkan/BackgroundSubtraction"
[14] Nishu Singla, "Motion Detection Based on Frame Differencing Method," International Journal of Information & Computation Technology, ISSN 0974-2239 Volume 4, Number 15 (2014), pp. 1559-
1565.

Effect of Inorganic and Organic Fertilisers on Walnut Quality and Leaf Macro Nutrient Status

[1] Imtiyaz A. wani, [2] Rayees A. Ahanger
Division of Fruit science, Sher-e-kashmir University of Agricultural Sciences and technology of Kashmir, Shalimar, Srinagar 191121 (India)

I. INTRODUCTION

Supply of all the essential plant nutrients in sufficient quantity and appropriate proportion is one of the major factors controlling the nut quality and leaf nutrient status. Production of fruit crops has undergone enormous change due to continuous use of inorganic fertilizer over a long period causing serious damage to soil fertility, environment and health. Sustainability in horticulture with respect to maintenance of soil fertility and stabilized fruit production is the main concern in the present situation. Hence, there is a need to think of alternate source of safe fertilizers which may improve quality and leaf nutrient status without having adverse effects on soil properties. The high nutrient requirement of fruit crops can be met through an integrated use of organic manures and chemical fertilizer since organic manures in INM generally improve the physical, chemical and biological properties of the soil along with its moisture holdings capacity which results in enhanced crop productivity and the quality of crop produced. Therefore, present investigation will be carried out to standardize integrated nutrient management programme for sustainable walnut production as no systemic work has been done in relation to walnut nutrient management.

II. MATERIAL AND METHODS

The experiment consisted of four selections [SKAU/002 (S1), SKAU/008 (S2), SKAU/024 (S2) and SKAU/040 (S2)] and six treatments [T1 (NPK recommended as per package of practices through inorganic fertilizers), T2 {100 % through manure (FYM 50% + vermicompost 25% + poultry manure 25%)}, T3 (75% NPK through inorganic fertilizers + 25 % through FYM), T4 (75 % NPK through inorganic fertilizers + 25 % through vermicompost), T5 (75 % NPK through inorganic fertilizers + 25 % through poultry manure) and T6 {75 % NPK through inorganic fertilizers + 25 % through manure (1/3 FYM + 1/3 vermicompost + 1/3 poultry manure)} replicated thrice in Factorial Randomised Block Design during 2011 and 2012. The observations were recorded on kernel weight, Kernel percentage,Kernel fill,kernel protein content and kernel oil content by following standard procedures. Leaf samples from walnut trees were collected and analysed for macronutrient status.

III. RESULTS AND DISCUSSION

The results obtained in present study indicate that kernel weight, kernel protein and kernel fill were significantly affected by different fertilizer treatments. Maximum kernel protein content was found in treatment T4 which differ significantly from treatments T1, T2, T3 and T6 but is statistically at par with treatment T5. The improvement in nut quality might be due to improvement in physical properties of soil and increase growth of micro-organisms. The maximum kernel protein content in treatment T4 might be due to the fact that protein is made up of amino acid which is mostly constituent of nitrogen. Treatment T4 enhanced the uptake of nitrogen which must have assimilated in amino acid and finally into protein. The increase in oil content under combined fertiliser application may be due to increased availability of micronutrients and K that help in converting primary fatty acids to their end products by increased activity of acetyl CO-A.This increase in nut parameter with combined application of vermicompost and inorganic fertilisers might be due to the fact that vermicompost would have improved soil texture and provided micronutrients such as zinc, iron, copper, manganese etc. and better microbial establishment in the soil. The biological activity of the micro-organism would have helped the soil to become ready to serve zone for essential nutrients to plant root system. Zinc is involved in the biochemical synthesis of the most important phytohormone IAA through the pathways of conversion of tryptophan to IAA. Iron is involved in the chlorophyll synthesis besides being part of co-enzymes of respiratory chain reaction. Copper and manganese are important

 ISBN: 978-81-932966-9-1

activators of co-enzymes. Organic manures in combination with inorganic fertilisers must have helped in metabolic changes through the supply of such important micro-nutrients and enzyme activation which ultimately must have improved nut parameters.

Among selections S1 showed highest kernel weight, which differed significantly from S3 and S4 but is at par with S2. Kernel percentage was maximum in S1 followed by S3 and S2. This difference in nut parameters among different selections might be due to their genetic make-up. Different selections showed marked differences with regard to, kernel protein content and maximum protein content was observed in selection S2 which differed significantly from S1, S2 and S3. Kernel fat content was highest in selection S2 followed by S1, S4 and S3. This difference in quality parameters of nut may be due to genetic constitution of individual selections.

Maximum leaf nitrogen content was observed in treatment T4 followed by T5, T1 and T3 while lowest was recorded in treatment T2 and T6. Phosphorus content of leaves differed significantly with different fertiliser treatments and recorded higher P content in treatment T2 which showed marked difference with all other treatments but is statistically at par with treatment T4. Potassium content also showed marked difference among different treatments. The highest K content was observed in treatment T4 followed by T1 and T5, while as lowest was found in treatment T6. The highest leaf N content in treatment T4 might be due to the fact that application of vermicompost alongwith NPK must have enhanced mineralization of organic nitrogen thus making more nitrogen available to the plants. Higher nitrogen can also be attributed to the improvement in soil aeration, better soil moisture retention in root zone, increased microbial nitrogen fixation due to the conjoint application and improved its availability to the plants. The addition of vermicompost improves physical properties of soil, moisture retention in soil rhizosphere, improved root development by mycelial network of arbuscular mycorrhizal fungi, thus increased the water absorption and hence improved nutrient contents of leaf Phosphorus applied to the soil in inorganic form get fixed but addition alongwith organic manure release P slowly due to microbial culture present in the soil, solubilised the fixed phosphorus and make it easily and readily available to plants.

It is evident from the data that maximum leaf calcium was observed in treatment T4 followed by T5 and T3, while as lowest was found in treatment T1. Highest magnesium content was recorded in treatment T4 and minimum in T1. This increased calcium and magnesium content in leaves might be due to the fact that vermicompost is a rich source of calcium and with the application of higher quantity of vermicompost, availability of Ca would have increased hence more leaf Ca.

IV. CONCLUSION

Thus it may conclude that conjoint application of organic and inorganic fertilizers showed substantial improvement nut quality and leaf macro nutrient status. Application of 75% RDF through inorganic coupled with 25% vermicompost was the best treatment for optimum nut quality and leaf nutrient status. Among the selections, S2 showed better performance with respect to yield and quality followed by selection S1 in walnut under Kashmir conditions.

Effect of integrated nutrient management on kernel weight (g) in walnut

Treatment	2011					2012					Pooled				
	S_1	S_2	S_3	S_4	Mean	S_1	S_2	S_3	S_4	Mean	S_1	S_2	S_3	S_4	Mean
T_1	6.40	6.73	5.70	6.37	**6.30**	6.53	6.73	5.84	6.43	**6.38**	6.47	6.73	5.77	6.40	**6.34**
T_2	6.15	6.07	5.53	5.71	**5.87**	6.61	6.13	5.70	5.89	**6.08**	6.38	6.10	5.62	5.80	**5.97**
T_3	6.07	6.55	5.78	5.99	**6.10**	6.67	6.68	5.78	6.46	**6.40**	6.37	6.62	5.78	6.23	**6.25**
T_4	7.46	7.40	6.87	6.66	**7.10**	7.53	7.50	6.97	7.00	**7.25**	7.50	7.45	6.92	6.83	**7.17**
T_5	7.21	6.52	6.57	5.90	**6.55**	7.21	6.76	6.63	6.07	**6.67**	7.21	6.64	6.60	5.99	**6.61**
T_6	6.47	6.15	5.86	5.67	**6.04**	6.70	6.39	5.89	6.01	**6.25**	6.58	6.27	5.88	5.84	**6.14**
Mean	**6.63**	**6.57**	**6.05**	**6.05**		**6.88**	**6.70**	**6.14**	**6.31**		**6.75**	**6.63**	**6.09**	**6.18**	
C.D≤0.05 (S)			**0.27**					**0.37**					**0.21**		
C.D≤0.05 (T)			**NS**					**0.48**					**0.45**		
C.D≤0.05 (S× T)			**NS**					**NS**					**NS**		

T_1 = NPK (recommended as per package of practices) through inorganic fertilizers — S_1 = SKAU/002

T_2 = 100 % through manure (FYM 50% + vermicompost 25% + poultry manure 25%) — S_2 = SKAU/008

T_3 = 75% NPK through inorganic fertilizers + 25 % through manure (FYM) — S_3 = SKAU/024

T_4 = 75 % NPK through inorganic fertilizers + 25 % through manure (vermicompost) — S_4 = SKAU/040

T_5 = 75 % NPK through inorganic fertilizers + 25 % through manure (poultry manure)

T_6 = 75 % NPK through inorganic fertilizers + 25 % through manure (1/3 FYM + 1/3 vermicompost + 1/3 poultry manure)

Effect of integrated nutrient management on kernel percentage in walnut

Treatment	2011					2012					Pooled				
	S_1	S_2	S_3	S_4	Mean	S_1	S_2	S_3	S_4	Mean	S_1	S_2	S_3	S_4	Mean
T_1	56.99	52.18	53.57	52.22	**53.74**	56.76	52.45	53.71	52.31	**53.81**	56.88	52.32	53.64	52.27	**53.78**
T_2	57.01	54.20	53.53	50.71	**53.86**	57.01	54.20	53.53	52.47	**54.30**	57.01	54.20	53.53	51.59	**54.08**
T_3	54.05	52.69	52.59	52.20	**52.88**	54.80	53.13	52.73	52.40	**53.27**	54.43	52.91	52.66	52.30	**53.07**
T_4	58.01	55.43	55.05	53.32	**55.45**	58.14	55.62	55.37	53.55	**55.67**	58.08	55.53	55.21	53.43	**55.56**
T_5	56.77	54.33	54.16	52.40	**54.42**	56.85	54.22	54.44	52.60	**54.53**	56.81	54.28	54.30	52.50	**54.47**
T_6	53.96	53.35	53.71	52.35	**53.34**	55.46	54.01	53.81	52.57	**53.96**	54.71	53.68	53.76	52.46	**53.65**
Mean	**56.13**	**53.70**	**53.77**	**52.20**		**56.50**	**53.94**	**53.93**	**52.65**		**56.32**	**53.82**	**53.85**	**52.43**	
C.D≤0.05 (S)			**1.76**					**1.56**					**1.18**		
C.D≤0.05 (T)			**NS**					**NS**					**NS**		
C.D≤0.05 (S× T)			**NS**					**NS**					**NS**		

T_1 = NPK (recommended as per package of practices) through inorganic fertilizers — S_1 = SKAU/002

T_2 = 100 % through manure (FYM 50% + vermicompost 25% + poultry manure 25%) — S_2 = SKAU/008

T_3 = 75% NPK through inorganic fertilizers + 25 % through manure (FYM) — S_3 = SKAU/024

T_4 = 75 % NPK through inorganic fertilizers + 25 % through manure (vermicompost) — S_4 = SKAU/040

T_5 = 75 % NPK through inorganic fertilizers + 25 % through manure (poultry manure)

T_6 = 75 % NPK through inorganic fertilizers + 25 % through manure (1/3 FYM + 1/3 vermicompost + 1/3 poultry manure)

Effect of integrated nutrient management on kernel protein content (%) in walnut

Treatment	2011					2012					Pooled				
	S_1	S_2	S_3	S_4	Mean	S_1	S_2	S_3	S_4	Mean	S_1	S_2	S_3	S_4	Mean
T_1	16.26	16.84	15.41	16.21	**16.18**	16.19	16.8	15.52	15.28	**15.95**	16.23	16.82	15.47	15.74	**16.06**
T_2	14.41	15.48	15.07	14.33	**14.82**	15.15	15.48	15.23	15.33	**15.30**	14.78	15.48	15.15	14.83	**15.06**
T_3	15.26	16.35	16.57	16.49	**16.17**	17.17	16.55	16.75	16.29	**16.19**	15.21	16.45	16.66	16.39	**16.18**
T_4	18.79	18.81	17.58	17.8	**18.25**	18.85	19.07	17.63	17.97	**18.38**	18.82	18.94	17.61	17.88	**18.31**
T_5	16.92	17.95	17.14	17.13	**17.29**	17.21	17.85	17.14	17.23	**17.36**	17.06	17.9	17.14	17.18	**17.32**
T_6	15.32	16.74	15.29	16.1	**15.86**	15.52	16.75	15.39	16.27	**15.98**	15.42	16.75	15.34	16.18	**15.92**
Mean	**16.16**	**17.03**	**16.18**	**16.34**		**16.35**	**17.08**	**16.28**	**16.39**		**16.25**	**17.05**	**16.23**	**16.37**	
C.D≤0.05 (S)			**0.70**					**0.62**					**0.58**		
C.D≤0.05 (T)			**1.45**					**1.85**					**1.22**		
C.D≤0.05 (S× T)			**NS**					**NS**					**NS**		

T_1 = NPK (recommended as per package of practices) through inorganic fertilizers — S_1 = SKAU/002

T_2 = 100 % through manure (FYM 50% + vermicompost 25% + poultry manure 25%) — S_2 = SKAU/008

T_3 = 75% NPK through inorganic fertilizers + 25 % through manure (FYM) — S_3 = SKAU/024

T_4 = 75 % NPK through inorganic fertilizers + 25 % through manure (vermicompost) — S_4 = SKAU/040

T_5 = 75 % NPK through inorganic fertilizers + 25 % through manure (poultry manure)

T_6 = 75 % NPK through inorganic fertilizers + 25 % through manure (1/3 FYM + 1/3 vermicompost + 1/3 poultry manure)

Effect of integrated nutrient management on kernel fat content (%) in walnut

Treatment	2011					2012					Pooled				
	S_1	S_2	S_3	S_4	Mean	S_1	S_2	S_3	S_4	Mean	S_1	S_2	S_3	S_4	Mean
T_1	57.34	58.12	55.93	56.57	**56.99**	57.6	58.15	56.09	56.67	**57.13**	57.47	58.13	56.01	56.62	**57.06**
T_2	54.97	56.23	51.73	55.9	**54.71**	57.26	58.16	56.31	56.16	**56.97**	56.11	57.19	54.02	56.03	**55.84**
T_3	59.63	59.03	56.89	57.47	**58.26**	59.13	59.17	57.3	57.57	**58.29**	59.38	59.1	57.1	57.52	**58.27**
T_4	61.4	62.76	57.47	59.07	**60.18**	61.83	63.22	57.67	59.66	**60.60**	61.62	62.99	57.57	59.37	**60.39**
T_5	59.01	60.27	57.27	58.21	**58.69**	59.01	60.58	57.27	58.35	**58.80**	59.01	60.43	57.27	58.28	**58.75**
T_6	58.21	58.2	52.78	56.36	**56.39**	58.34	58.34	54.52	56.61	**56.95**	58.28	58.27	53.65	56.49	**56.67**
Mean	**58.43**	**59.1**	**55.35**	**57.26**		**58.86**	**59.6**	**56.53**	**57.5**		**58.64**	**59.35**	**55.94**	**57.38**	
C.D≤0.05 (S)			**2.55**					**2.21**					**1.65**		
C.D≤0.05 (T)			**NS**					**1.98**					**1.24**		
C.D≤0.05 (S× T)			**NS**					**NS**					**NS**		

T_1 = NPK (recommended as per package of practices) through inorganic fertilizers — S_1 = SKAU/002

T_2 = 100 % through manure (FYM 50% + vermicompost 25% + poultry manure 25%) — S_2 = SKAU/008

T_3 = 75% NPK through inorganic fertilizers + 25 % through manure (FYM) — S_3 = SKAU/024

T_4 = 75 % NPK through inorganic fertilizers + 25 % through manure (vermicompost) — S_4 = SKAU/040

T_5 = 75 % NPK through inorganic fertilizers + 25 % through manure (poultry manure)

T_6 = 75 % NPK through inorganic fertilizers + 25 % through manure (1/3 FYM + 1/3 vermicompost + 1/3 poultry manure)

Effect of integrated nutrient management on leaf nitrogen (%)

Treatment	2011					2012					Pooled				
	S_1	S_2	S_3	S_4	Mean	S_1	S_2	S_3	S_4	Mean	S_1	S_2	S_3	S_4	Mean
T_1	2.73	2.75	2.75	2.73	**2.74**	2.74	2.76	2.75	2.75	**2.75**	2.73	2.75	2.75	2.74	**2.74**
T_2	2.66	2.64	2.68	2.64	**2.66**	2.74	2.76	2.78	2.76	**2.76**	2.70	2.70	2.73	2.70	**2.71**
T_3	2.69	2.73	2.68	2.68	**2.70**	2.73	2.75	2.74	2.75	**2.74**	2.71	2.74	2.71	2.72	**2.72**
T_4	2.77	2.78	2.75	2.78	**2.77**	2.78	2.80	2.83	2.83	**2.81**	2.78	2.79	2.79	2.81	**2.79**
T_5	2.71	2.75	2.74	2.75	**2.74**	2.73	2.76	2.76	2.78	**2.76**	2.72	2.76	2.75	2.77	**2.75**
T_6	2.68	2.69	2.68	2.72	**2.69**	2.70	2.73	2.76	2.75	**2.74**	2.69	2.71	2.72	2.74	**2.71**
Mean	**2.71**	**2.72**	**2.71**	**2.72**		**2.74**	**2.76**	**2.77**	**2.77**		**2.72**	**2.74**	**2.74**	**2.75**	
C.D≤0.05 (S)			**NS**					**NS**					**NS**		
C.D≤0.05 (T)			**0.06**					**0.04**					**0.04**		
C.D≤0.05 (S× T)			**NS**					**NS**					**NS**		

T_1 = NPK (recommended as per package of practices) through inorganic fertilizers — S_1 = SKAU/002

T_2 = 100 % through manure (FYM 50% + vermicompost 25% + poultry manure 25%) — S_2 = SKAU/008

T_3 = 75% NPK through inorganic fertilizers + 25 % through manure (FYM) — S_3 = SKAU/024

T_4 = 75 % NPK through inorganic fertilizers + 25 % through manure (vermicompost) — S_4 = SKAU/040

T_5 = 75 % NPK through inorganic fertilizers + 25 % through manure (poultry manure)

T_6 = 75 % NPK through inorganic fertilizers + 25 % through manure (1/3 FYM + 1/3 vermicompost + 1/3 poultry manure)

Effect of integrated nutrient management on leaf phosphorus (%)

Treatment	2011					2012					Pooled				
	S_1	S_2	S_3	S_4	Mean	S_1	S_2	S_3	S_4	Mean	S_1	S_2	S_3	S_4	Mean
T_1	0.25	0.24	0.25	0.24	**0.25**	0.26	0.25	0.26	0.25	**0.26**	0.25	0.26	0.24	0.25	**0.25**
T_2	0.29	0.29	0.26	0.26	**0.28**	0.3	0.3	0.31	0.3	**0.30**	0.3	0.29	0.29	0.28	**0.29**
T_3	0.24	0.23	0.25	0.25	**0.24**	0.25	0.25	0.25	0.26	**0.25**	0.25	0.24	0.25	0.25	**0.25**
T_4	0.21	0.80	0.22	0.23	**0.36**	0.27	0.26	0.27	0.28	**0.27**	0.24	0.53	0.25	0.25	**0.32**
T_5	0.27	0.26	0.25	0.25	**0.26**	0.28	0.27	0.26	0.28	**0.27**	0.27	0.27	0.26	0.27	**0.27**
T_6	0.25	0.25	0.25	0.22	**0.24**	0.26	0.26	0.26	0.27	**0.26**	0.26	0.25	0.25	0.25	**0.25**
Mean	**0.25**	**0.34**	**0.25**	**0.24**		**0.27**	**0.28**	**0.27**	**0.26**		**0.26**	**0.31**	**0.26**	**0.25**	
C.D≤0.05 (S)			**NS**					**NS**					**NS**		
C.D≤0.05 (T)			**0.07**					**0.02**					**0.02**		
C.D≤0.05 (S× T)			**NS**					**NS**					**NS**		

T_1 = NPK (recommended as per package of practices) through inorganic fertilizers — S_1 = SKAU/002

T_2 = 100 % through manure (FYM 50% + vermicompost 25% + poultry manure 25%) — S_2 = SKAU/008

T_3 = 75% NPK through inorganic fertilizers + 25 % through manure (FYM) — S_3 = SKAU/024

T_4 = 75 % NPK through inorganic fertilizers + 25 % through manure (vermicompost) — S_4 = SKAU/040

T_5 = 75 % NPK through inorganic fertilizers + 25 % through manure (poultry manure)

T_6 = 75 % NPK through inorganic fertilizers + 25 % through manure (1/3 FYM + 1/3 vermicompost + 1/3 poultry manure)

Effect of integrated nutrient management on leaf potassium (%)

Treatment	2011					2012					Pooled				
	S_1	S_2	S_3	S_4	Mean	S_1	S_2	S_3	S_4	Mean	S_1	S_2	S_3	S_4	Mean
T_1	1.63	1.66	1.66	1.68	**1.66**	1.64	1.66	1.67	1.69	**1.67**	1.63	1.66	1.67	1.69	**1.66**
T_2	1.42	1.43	1.36	1.44	**1.41**	1.64	1.69	1.68	1.71	**1.68**	1.53	1.56	1.52	1.57	**1.55**
T_3	1.55	1.49	1.47	1.51	**1.51**	1.59	1.51	1.57	1.60	**1.57**	1.57	1.50	1.52	1.56	**1.54**
T_4	1.70	1.69	1.69	1.68	**1.69**	1.71	1.74	1.74	1.71	**1.73**	1.70	1.71	1.72	1.70	**1.71**
T_5	1.56	1.64	1.65	1.64	**1.62**	1.61	1.67	1.69	1.68	**1.66**	1.59	1.66	1.67	1.66	**1.64**
T_6	1.52	1.51	1.47	1.55	**1.51**	1.59	1.53	1.57	1.58	**1.57**	1.55	1.52	1.52	1.56	**1.54**
Mean	**1.56**	**1.57**	**1.55**	**1.58**		**1.63**	**1.62**	**1.66**	**1.67**		**1.59**	**1.60**	**1.61**	**1.62**	
C.D≤0.05 (S)			**NS**					**NS**					**NS**		
C.D≤0.05 (T)			**0.16**					**0.04**					**0.05**		
C.D≤0.05 (S× T)			**NS**					**NS**					**NS**		

T_1 = NPK (recommended as per package of practices) through inorganic fertilizers — S_1 = SKAU/002

T_2 = 100 % through manure (FYM 50% + vermicompost 25% + poultry manure 25%) — S_2 = SKAU/008

T_3 = 75% NPK through inorganic fertilizers + 25 % through manure (FYM) — S_3 = SKAU/024

T_4 = 75 % NPK through inorganic fertilizers + 25 % through manure (vermicompost) — S_4 = SKAU/040

T_5 = 75 % NPK through inorganic fertilizers + 25 % through manure (poultry manure)

T_6 = 75 % NPK through inorganic fertilizers + 25 % through manure (1/3 FYM + 1/3 vermicompost + 1/3 poultry manure)

Effect of integrated nutrient management on leaf calcium (%)

Treatment	2011					2012					Pooled				
	S_1	S_2	S_3	S_4	Mean	S_1	S_2	S_3	S_4	Mean	S_1	S_2	S_3	S_4	Mean
T_1	2.26	2.24	2.25	2.24	**2.25**	2.27	2.25	2.26	2.25	**2.26**	2.27	2.25	2.26	2.24	**2.25**
T_2	2.31	2.31	2.31	2.32	**2.31**	2.37	2.38	2.35	2.34	**2.36**	2.34	2.35	2.33	2.33	**2.34**
T_3	2.43	2.42	2.42	2.44	**2.43**	2.44	2.42	2.43	2.45	**2.44**	2.44	2.42	2.43	2.45	**2.43**
T_4	2.57	2.58	2.59	2.57	**2.58**	2.58	2.59	2.61	2.59	**2.59**	2.58	2.58	2.6	2.58	**2.58**
T_5	2.54	2.56	2.54	2.57	**2.55**	2.55	2.56	2.55	2.58	**2.56**	2.55	2.56	2.55	2.58	**2.56**
T_6	2.45	2.43	2.44	2.44	**2.44**	2.46	2.44	2.45	2.45	**2.45**	2.46	2.44	2.45	2.44	**2.45**
Mean	**2.43**	**2.42**	**2.43**	**2.43**		**2.45**	**2.43**	**2.44**	**2.44**		**2.45**	**2.42**	**2.43**	**2.44**	
C.D≤0.05 (S)			**NS**					**NS**					**NS**		
C.D≤0.05 (T)			**NS**					**0.24**					**NS**		
C.D≤0.05 (S×T)			**NS**					**NS**					**NS**		

T_1 = NPK (recommended as per package of practices) through inorganic fertilizers — S_1 = SKAU/002

T_2 = 100 % through manure (FYM 50% + vermicompost 25% + poultry manure 25%) — S_2 = SKAU/008

T_3 = 75% NPK through inorganic fertilizers + 25 % through manure (FYM) — S_3 = SKAU/024

T_4 = 75 % NPK through inorganic fertilizers + 25 % through manure (vermicompost) — S_4 = SKAU/040

T_5 = 75 % NPK through inorganic fertilizers + 25 % through manure (poultry manure)

T_6 = 75 % NPK through inorganic fertilizers + 25 % through manure (1/3 FYM + 1/3 vermicompost + 1/3 poultry manure)

Effect of integrated nutrient management on leaf Magnesium (%)

Treatment	2011					2012					Pooled				
	S_1	S_2	S_3	S_4	Mean	S_1	S_2	S_3	S_4	Mean	S_1	S_2	S_3	S_4	Mean
T_1	0.5	0.49	0.51	0.5	**0.50**	0.51	0.5	0.52	0.51	**0.51**	0.51	0.5	0.51	0.51	**0.51**
T_2	0.52	0.52	0.52	0.52	**0.52**	0.53	0.53	0.53	0.53	**0.53**	0.53	0.53	0.52	0.53	**0.53**
T_3	0.53	0.54	0.53	0.54	**0.54**	0.54	0.55	0.54	0.54	**0.54**	0.54	0.55	0.54	0.54	**0.54**
T_4	0.55	0.55	0.54	0.56	**0.56**	0.57	0.57	0.56	0.57	**0.57**	0.56	0.56	0.55	0.57	**0.56**
T_5	0.57	0.55	0.54	0.55	**0.55**	0.57	0.55	0.55	0.56	**0.56**	0.57	0.55	0.55	0.56	**0.55**
T_6	0.52	0.51	0.52	0.51	**0.52**	0.53	0.52	0.53	0.52	**0.53**	0.53	0.52	0.52	0.52	**0.52**
Mean	**0.54**	**0.52**	**0.53**	**0.53**		**0.56**	**0.53**	**0.54**	**0.54**		**0.55**	**0.53**	**0.53**	**0.54**	
C.D≤0.05 (S)			**NS**					**NS**					**NS**		
C.D≤0.05 (T)			**NS**					**0.05**					**NS**		
C.D≤0.05 (S× T)			**NS**					**NS**					**NS**		

T_1 = NPK (recommended as per package of practices) through inorganic fertilizers — S_1 = SKAU/002

T_2 = 100 % through manure (FYM 50% + vermicompost 25% + poultry manure 25%) — S_2 = SKAU/008

T_3 = 75% NPK through inorganic fertilizers + 25 % through manure (FYM) — S_3 = SKAU/024

T_4 = 75 % NPK through inorganic fertilizers + 25 % through manure (vermicompost) — S_4 = SKAU/040

T_5 = 75 % NPK through inorganic fertilizers + 25 % through manure (poultry manure)

T_6 = 75 % NPK through inorganic fertilizers + 25 % through manure (1/3 FYM + 1/3 vermicompost + 1/3 poultry manure)

New Records of Bloodsucking Flies Associated with Wild Birds of Haftad-Gholleh Protected Area, Iran (Diptera: Hippoboscidae, Calliphoridae)

[1] Araghi MP, [2] Gilasian E, [3] Samaie A
[1] Insect Taxonomy Research Department, Iranian Research Institute of Plant Protection, Agricultural Research, Education and Extension Organization (AREEO), Tehran, Iran
[2] Department of Environment of Markazi province, Arak, Iran

***Abstract*— We have studied the parasitic flies of wildlife of Haftad-Gholleh Protected Area, Iran, for the first time and report here the three hematophagous fly species of birds: the louse fly Ornithophila metallica (Schiner) (Hippoboscidae), and bird nest flies Trypocalliphora braueri (Hendel) and Protocalliphora azurea (Fallen) (Calliphoridae). The genera and species O. metallica and T. braueri are new to Iran**

***Keywords*: Avian myiasis; Louse flies; Ornithophila metallica; Trypocalliphora braueri; Protocalliphora azurea; Blow flies**

I. INTRODUCTION

Avian myiasis-causing flies and bird's blood-feeding ectoparasite flies mainly belong in the family's Calliphoridae and Hippoboscidae. The family Hippoboscidae, commonly known as louse flies, consists of 213 hematophagous species of birds and mammals worldwide [1]. This family is known in Iran only by the single species Pseudolynchia canariensis (Macquart), pigeon fly that has been repeatedly recorded from various cities across the country [2-5]. Aside from being a nuisance to their hosts, hippoboscids are capable transmitters of pathogenic and parasitic agents, including avian trypanosomes and mammals' bacteria, causing serious diseases in wild birds [6] and ruminant animals [7,8]. They are also the only known vectors of apicomplexan parasites of the genus Haemoproteus to birds and transmitters of filarial nematodes to domestic and wild mammals [9,10].

The majority of myiasis-inducing species belong to the family Calliphoridae, esp. subfamily Chrysomyinae, whose members are known as important facultative and obligatory parasites. Bird myiasis records are not as frequent as mammals' most likely due to the inaccessibility of the hosts. With respect to Iran, the reports of avian myiases have been poorly documented [11,12], mainly because of difficulties in larval identification. Although the said technical problem often necessitates the rearing of the maggots for a reliable identification at adult stage, in a recent case of avian wound myiasis in southwestern Iran the myiatic agent was successfully identified at larval stage [13]. The genera Protocalliphora Hough and Trypocalliphora Peus contain specialist bird nest parasites whose larvae feed on the blood of nestling birds through tunneling under their skin, causing a type of myiasis called subcutaneous myiasis, and eventually leading to heavy damages to the tissues or death of young birds [14]. The species P. azurea (Fallen) is widely spread in the Palaearctic region and remains the only species of birds' subcutaneous myiasis agents that has been recorded from Iran so far [15].

II. MATERIAL AND METHODS

Haftad-Gholleh Protected Area covers an estimated area of 97,400 hectares (240,680 acres) and is home to a large number of vulnerable mammal and bird species (Figure 1). Using Malaise traps, the specimens were collected in 75% ethyl alcohol and preserved at the Hayk Mirzayans Insect Museum (HMIM), Tehran, Iran. In case of the examination of male genitalia, we detached the whole abdomen to clear it in hot 10% KOH and then washed it lightly in glacial acetic acid

Figure 1: A general view of Chekab valley, Haftad-Gholleh protected area, Iran.

 ISBN: 978-81-932966-9-1

to remove the base. After dissecting the male genitalia, the abdomen was glued back to its original place and the genitalia transferred to a microvial and pinned below the associate specimen. Specimen data: 1♂ 1♀ Ornithophila metallica; 2♂♂ 3♀♀ Protocalliphora azurea; 1♀ Trypocalliphora braueri; Iran: Markazi province, Amr-abad village, Haftad-Gholleh Protected Area, Chekab valley, 2219 m, 34°07′05.3"N 050°16′25.3"E, 28 May-15 June, 2016, Malaise trap near pool, E. Gilasian & M. Parchami-Araghi. Birds of haftad-gholleh protected area Hafted-Gholleh is home to an estimated 71 species within 26 families of wild birds and serves as a sanctuary for a number of migrating birds as well. We have listed the following common avian taxa of this area to underline the impact of hematophagous flies on the bird fauna: Monticola solitarius (L.) (blue rock thrush), Accipiter spp. (hawks), Falco spp. (falcons and kestrels), Coturnix spp. (quails), Columba spp. (pigeons), Cuculus spp. (cuckoos), Coracias spp. (rollers), Merops spp. (bee-eaters), Upupa spp. (hoopoes), Galerida spp. (larks), Hirundo spp. (passerines), Muscicapa striata (Pallas) (spotted flycatcher), Emberiza melanocephala Scopoli (black-headed bunting), E. cia (L.) (rock bunting), E. citrinella L. (yellowhammer), Turdus spp. (true thrushes), Motacilla spp. (wagtails), Lanius spp. (typical shrikes), Parus spp. (tits), Passer spp. (sparrows.), Sturnus spp. (starlings), Corvus spp. (crows), Pica pica (L.) (Eurasian magpie), Ammoperdix spp. (partridges), Gypaetus spp. (vultures), Aquila spp. (eagles), Athene noctua (Scopoli) (little owl), swifts (Apodidae) and woodpeckers (Picidae) [16].

III. RESULTS AND DISCUSSION

We, for the first time, collected three species of bloodsucking flies from Haftad-Gholleh Protected Area where strictly feed on wild birds. The recorded fly species are as follows: Ornithophila metallica (Schiner), Protocalliphora azurea (Fallen) and Trypocalliphora braueri (Hendel). Both O. metallica and T. braueri are new genus and species records for the Iranian fauna.

Ornithophila metallica (Schiner)

Both sexes of the hippoboscid O. metallica are hematophagous ectoparasites and ingest blood from a wide variety of birds (Figures 2 and 3). Maa [17] listed the host birds for the two Palaearctic members of Ornithophila Rondani, O. metallica and O. gestroi Rondani, and categorized the former as a species with "having high population density and very wide host and distributional ranges" and found the latter to be a species with "low population density and much more restricted host/ or distributional ranges." O. metallica is widely distributed in the Old World including Iran's neighboring countries of Pakistan, Afghanistan and Turkey (Figures 4-10) [17]. These species are commonly known as bird blow flies or bird nest flies. Trypocalliphora is a monotypic genus, with a single Holarctic

Figure 2: Ornithophila metallica (Schiner): Dorsal view.

Figure 3: Ornithophila metallica (Schiner): Lateral view.

species T. braueri which differs from its closest related genus Protocalliphora in having additional notopleural setae. Although some Dipterists consider Trypocalliphora a subgenus within Protocalliphora [18], other calliphorid taxonomists argued that Trypocalliphora is to be considered as a valid genus [19-21]. These species display different types of parasitic strategies as the larvae of P. azurea feed on the blood of young birds of the order Coraciiformes and remain on the surface of the birds, but the hematophagous larvae of T. braueri infest nestlings of the order Falconiformes and burrow beneath the skin of their hosts, causing a form of parasitism called subcutaneous myiasis [18].

Figure 4: Protocalliphora azurea (Fallen): Dorsal view

Figure 5: Protocalliphora azurea (Fallen): Lateral view.

Figure 6: Protocalliphora azurea (Fallen): Male genitalia, lateral view

Figure 7: Protocalliphora azurea (Fallen): Male genitalia, posterior view.

Figure 8: Protocalliphora azurea (Fallen): Male sternite

Figure 10: Trypocalliphora braueri (Hendel): Lateral view

IV. CONCLUSION

Haftad-Gholleh Protected Area, like most of Iranian natural habitats, has been experiencing destructive interventions from illegal human activities, including poaching, that aggravating the vulnerability of its wildlife to epidemics and parasites as an ovine rinderpest epidemic heavily emaciated the population of wild goats of this area in 2015. In terms of birds, the sprawling build-up areas, power lines and transmission towers pose significant threats to migrating birds of the area and nearby parks. In a framework of a faunistic project, we are working to document the insect diversity of Haftad-Gholleh Protected Area to underscore the need for improving the conservation measures and policies towards a standard protection of the area and its fauna and flora.

V. ACKNOWLEDGEMENTS

We wish to thank Dr Nil Rahola (Université de Montpellier, Montpellier, France) for confirming the identity of Ornithophila metallica. We are also grateful to the Department of Environment of Markazi province and the rangers at Haftad-Gholleh Protected Area for facilitating our research through the area.

REFERENCES

1. Dick CW (2006) Checklist of world Hippoboscidae (Diptera: Hippoboscoidea). Department of Zoology, Field Museum of Natural History, Chicago p: 7.

2. Borji H, Moghaddas E, Razmi GR, Azad M (2012) A survey of ecto-and endoparasites of domestic pigeons (Columba livia) in Mashhad, Iran. Iran J Vet Sci Technol 4: 37-42.

3. Radfar MH, Fathi S, Norouzi AE, Mirzaei DM, Rezaei SH (2011) A survey of parasites of domestic pigeons (Columba livia domestica) in South Khorasan, Iran. Vet Res 4: 18-23.

4. Pirali KK, Dehghani SA, Ahmadi BN, Najafzadeh V (2016) A First report of infestation by Pseudolynchia canariensis in a herd of pigeons in Shahrekord (Southwest of Iran). J Arthropod-Borne Dis 10: 426-430.

5. Khoobdel M, Akhoond MR (2015) The survey on Pseudolynchia canariensis (Diptera: Hippoboscidae) in military sites and human bite cases reported in Tehran, Iran. J Milit Med 16: 243-251.

6. Kucera J (1983) Incidence and some ecological aspects of avian trypanosomes in Czechoslovakia. Folia Parasitol 30: 209-222.

7. Halos L, Jamal T, Maillard R, Girard B, Guillot J, et al. (2004) Role of Hippoboscidae flies as potential vectors of Bartonella spp. infecting wild and domestic ruminants. Appl Environ Microbiol 70: 6302-6305.

8. Reeves WK, Nelder MP, Cobb KD, Dasch GA (2006) Bartonella spp. in deer keds, Lipoptena mazamae (Diptera: Hippoboscidae), from Georgia and South Carolina, USA. J Wildlife Dis 42: 391-396.

9. Nelson GS (1963) Dipetalonema dracunculoides (Cobbold, 1870), from the dog in Kenya: with a note on its development in the lousefly, Hippobosca longipennis. J Helminthol 37: 235-240.

10. Daynes P (1964) Note sur les helminthoses des animaux domestiques reconnues à Madagascar. Revue d'Élevage et de Médecine Vétérinaire des Pays Tropicaux 17: 477-490.

11. Halajian A, Tavakol S, Mansoori J (2012) The first report of pigeon maggot, Protocalliphora sp. (Diptera: Calliphoridae) from domestic pigeons in Iran. Comp Clin Pathol 21: 361-362.

12. Pirali KK, Cheraghchi BM, Navidpour S (2010) Infestation of an owl (Bubo bubo) with Lucilia spp. Comp Clin Pathol 19: 221-2214.

13. Parchami AM, Eskandari F, Gilasian E (2015) Avian wound myiasis caused by Calliphora vicina Robineau Desvoidy (Diptera: Calliphoridae) in an immature migrating Eastern Imperial Eagle (Aquila heliaca Savigny) (Aves: Accipitridae) in southwestern Iran. Vet Sci Technol 6.

14. Little SE (2009) Myiasis in wild birds. Parasitic Diseases of Wild Birds. In: Atkinson CT, Thomas NJ, Hunter DB (ed.) Wiley-Blackwell, Oxford pp: 546-556.

15. Parchami AM, Peris SV, Gonzalez MD (2001) New records of Iranian Calliphoridae and Sarcophagidae, with a guide to the males of Palaearctic Protocalliphora (Diptera, Calyptratae). Boletín de la Real Sociedad Española de Historia Natural (Sección Biológica) 96: 175-181.

16. (2003) Reports of wildlife of Hafta-Gholleh Protected Area.

17. Maa TC (1969) Synapses of the genera Ornithophila and Ornithoctona with remarks on their habitat diversification (Diptera: Hippoboscidae). Pacific Insects Monograph 20: 1-23.

18. Sabrosky CW, Bennett GF, Whitworth TL (1989) Bird blow flies (Protocalliphora) in North America (Diptera: Calliphoridae) with notes on the Palearctic species. Smithsonian Institution, Washington, DC, USA.

19. Rognes K (1985) Revision of the bird-parasitic blowfly genus Trypocalliphora Peus, 1960 (Diptera: Calliphoridae). Entomologica Scandinavica 15: 371-382.

20. Whitworth TL (2003) A key to the puparia of 27 species of North American Protocalliphora Hough (Dipetera: Calliphoridae) from bird nests and two new puparial descriptions. Proc Entomol Soc Wash 105: 995 1033.

21. Whitworth TL (2006) Key to the genera and species of blow flies (Diptera: Calliphoridae) of America north of Mexico. Proc Entomol Soc Wash 108: 689-725.

Real Time Distribution Transformer Monitoring System with Data Logging

[1]SonaliPatil, [2]PriyankaPatil, [3]PallaviKhot, [4]SurajPatil,
[1, 2, 3, 4]BE ETC,[5] ShitalGhorpade
Sharad Institute of Technology College of Engineering, IchalkaranjiYadrav, Ichalkaranji

Abstract: **—This project is about design and implementation of a mobile embedded system to monitor and record parameters of a distribution transformer like load currents, oil level and winding temperature, different gases and humidity present in the atmosphere. The idea of on-line monitoring system integrates a GSM Modem, with an Arduino UNO board and different sensors. It is installed at the distribution transformer site and the above parameters are recorded of the embedded system. The obtained parameters are processed and recorded in the system memory. If any abnormality or an emergency situation occurs the system sends SMS messages to the mobile phones containing information about the abnormality according to some predefined levels programmed in the microcontroller. This mobile system will help the transformers to identify problems before any serious failure.**

Index Terms*—Distribution transformer, *Arduino UNO board, RF module, GSM, Sensors

I. INTRODUCTION

Distribution transformer is electrical equipment which distributes power to the end users directly, and its operation is an important parameter of the entire distribution network.

Distribution transformers are currently monitored manually where a person periodically visits a transformer site for maintenance and records parameter. This type of monitoring cannot provide information about overloads and overheating of transformer oil and windings. All these factors can significantly reduce transformer life. Our system is designed based upon online monitoring of key parameters of distribution transformers and which can provide useful Information about the health of transformers.

Operation of distribution transformer under certain condition guarantees their long life. However their life is reduced due to the failures of transformers in Temperature rise, low oil levels, over load, moisture present in the oil, and increase in unwanted dissolved gases in the transformer oil. Overloading and ineffective cooling of transformers are the major causes of failure in distribution transformers.

Online monitoring system consists of embedded system, GSM modem, mobile-users and sensors installed at transformer site. Sensors are installed on transformer side which reads and measures the physical quantity from the distribution transformer. The embedded module is located at the transformer site. It is used to acquire process, display, transmit and receive the parameters from the GSM modem. GSM module is the link between the embedded system and the public GSM network. Another module that has a PC-based -server located at the control center.

Monitoring system based on RFID technology that has been used to monitoring and controls the parameters potential to be a more accurate and cheaper technique for health assessment of transformers.

II.RELEVANCE

Distribution transformers are one of the most important equipment in power network and today's society. Because of the large number of transformers distributed in a wide area in power electric systems, the data acquisition and transformer monitoring is an important issue. The main aim of this system is distribution transformer monitoring and controlling through GSM modem, RFID and Arduino based microcontroller.

III.OBJECTIVE

The objective of this project is to implement the accurate, good maintained and less human power for the distribution transformers, also to reduce the damages and increases the life of the distribution transformers.

IV.METHODOLOGY

1. First all sensors are installed in the transformer site for sensing the parameters of distribution transformers.
2. This sensed data is then connected to Arduinoanalog port by using connectors.
3. Then the signal is passed to the PC for monitoring purpose by using RF transmitter.
4. At the receiving end RF receiver is attached for receiving signals from the transformer site.
5. On the PC data of all sensors will collected in the VB based software and it compares with predefined level.
6. If any abnormal situation occurs then the SMS will be sent to the control room by using a GSM modem.

V.BLOCK DIAGRAM

In this project we dividing the total system into mainly two parts –

1. Data acquisition
2. Online monitoring

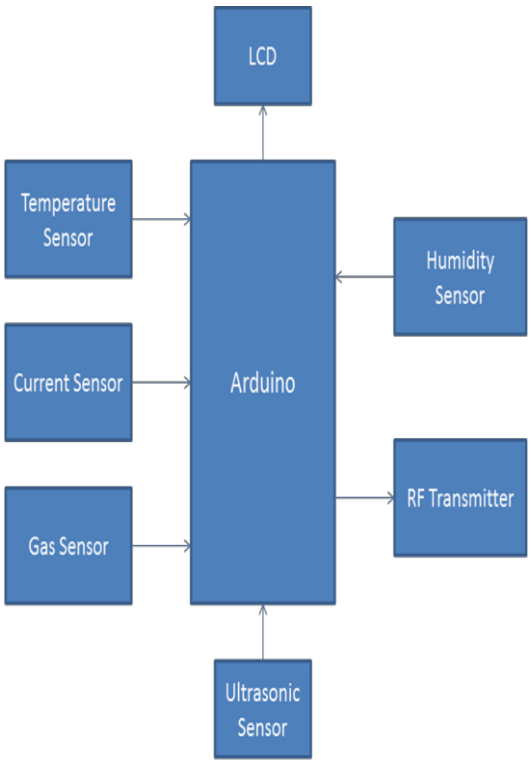

Fig- Transformer Data acquisition unit

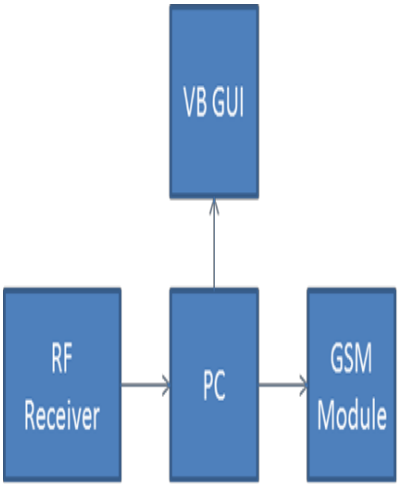

Fig-Transformer online monitoring unit

VI. OPERATION

In this system, when we switched on the power supply the system will start working. When temperature of transformer increases above the set point then there is possibility of damage of the winding of transformer , then this message will displayed on LCD to avoid this we can provide solution that is fans are get started to avoid the overheating of transformer. Also when current of transformer increase due to sudden increase in load in end user side, then immediately message is send to the operator, then operator read this message and immediate action is takes place. Hence, transformer gets protected. A humidity sensor senses moisture present in the oil, measures and reports the relative humidity in the air, if humidity increases beyond set point then is chances of short circuit or damage of transformer so immediate action takes place. Ultrasonic sensor used for level measurement of oilThese outputs of the all sensors are in analog form and connected to the analog port of the Arduino basedmicrocontroller this data is send to the data monitoring unit by using an RF transmitter.

At the side of transformer monitoring unit for online monitoring purpose the VB GUI software is developed which receives the data by using an RF receiver. In this software the sensor data is compared with threshold set values of all sensors if values is in the given range then normal procedure will takes place but if the sensor value exceeded beyond set point then there is an SMS will be sent to control room by using a GSM modem and required immediate action will takes place.

 ISBN: 978-81-932966-9-1

VII. FLOWCHART

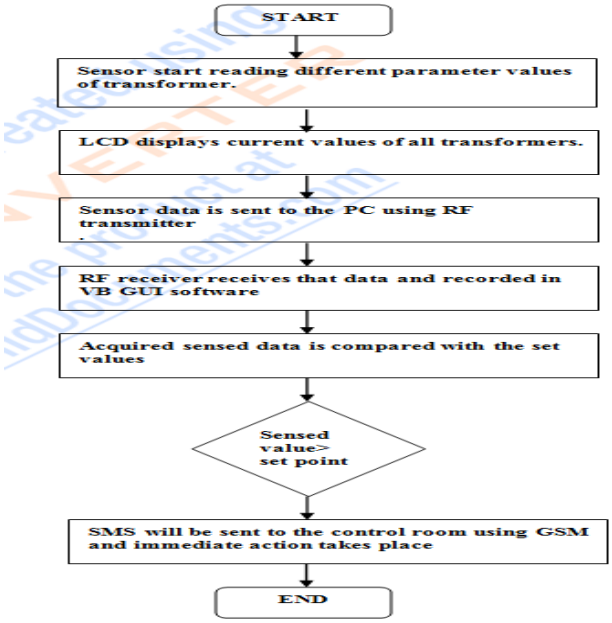

VIII.HARDWARE

1. Arduino UNO board(ATMega 328)
2. GSM SIM 300 Modem
3. RF Transmitter
4. RF Receiver
5. 16*2 alphanumeric LCD Display
6. Temperature sensor
7. Humidity sensor
8. Current sensor
9. Gas sensor
10. Ultrasonic sensor

IX. SOFTWARE

1. VB GUI

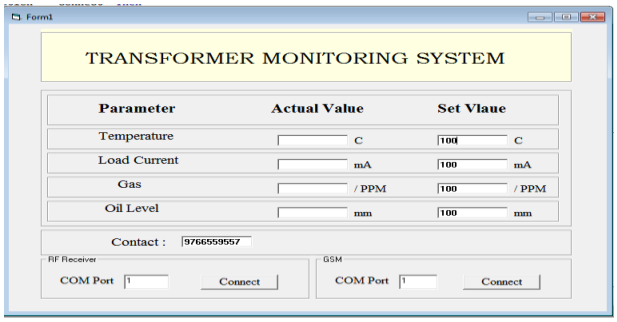

X. CONCLUSION

In real time distribution transformer monitoring system by using GSM, RFID module and different sensors online monitoring of transformer is possible instead of manual monitoring. So we can reduce the man power and provides the effective security.

REFERENCES

1. Ansuman Sharma, Rajesh Behura, "GSM based Distribution Transformer Monitoring System" National Institute of Technology Rourkela-769008 (ODISHA) May-2013
2. Rakesh Kumar Pandey, Dilip Kumar, "Distributed Transformer Monitoring System Based On Zigbee Technology" International Journal of Engineering Trends and Technology (IJETT) - Volume4Issue5- May 2013
3. NagargojeSurekha, Abhishek Kumar, Mr. Daniel A. Figueiredo, "Monitoring and Controlling Of Distribution Transformer via GSM Modem", Volume 4, Issue 7, July 2014 ISSN: 2277 128X

International Journal of Advanced Research in Computer Science and Software Engineering.
XII.

.

CO_2 Purification using an Aqueous Amine Absorbent in the Syngas

[1] Jeong Ho Choi, [2] Soung Hee Yun, [3] Yeo Il Yoon, [4] Jung-Hyun Lee
[1][2][3] Greenhouse Gas Laboratory, Climate Change Research Division, Korea Institute of Energy Research, 152 Gajeong-ro, Yuseong-gu, Daejeon 34129, Korea
[1] [4] Department of Chemical & Biological Engineering, Korea University, 145 Anam-dong, Seongbuk-gu, Seoul 02841, Korea

Abstract: -- **The acetic acid production using syngas in the BP chemical process showed superior performance compared to using rhodium-based catalyst. However, CO2 in the syngas causes poison of the promoted-iridium and the performance of the catalyst degrades. Therefore, CO2 must remain at extremely low concentration below 20 ppmv. In this study, we try to develop the new CO2 capturing absorbent for replacing with BASF a-MDEA (activated MDEA). The absorption performance of amine absorbents was evaluated to keep the CO2 concentration low and the applicability of the absorbent for acetic acid production process was evaluated. A continuously stirred-tank reactor and differential reaction calorimeter were used to measure the CO2 absorption capacity and heat of reaction, respectively. As results among the amine absorbents, KIERSOL-N and KIERSOL-P showed better performance in both CO2 absorption capacity and heat of reaction than MEA's results and a- MDEA's results.**

Index Terms — Acetic acid, Gas purification, CO2 control, amine absorbent.

I. INTRODUCTION

Acetic acid is used as a raw material for fine chemical products such as vinyl acetate and acetic acid ester. It is also a chemical substance widely used in such as terephthalic acid solution and dye [1]. A projected increase in the consumption of acetic acid has been reported at 4.0–4.5 % annually in China through 2020. China is expected to consume an average of 3–4 % of worldwide production [2]. The annual production of acetic acid is about 11.8 Mt/year, of which the production of acetic acid based on the methanol carbonylation technology is equivalent to about 80% [3],[4]. Processes for production of acetic acid using methanol carbonylation technology generally use noble metal catalysts such as iridium and ruthenium. The acetic acid production process based on ruthenium was widely used after being commercialized by Monsanto in 1970 [5]. In 1996, BP Chemical developed an improved methanol carbonylation process based on promoted iridium-iodide catalyst [6]. However, Bu4NI catalyst has the disadvantage that the iodide poisons the catalyzed reaction and reduces the reaction rate to 67% or less [7]. Therefore, many researchers have tried to improve the performance of catalyst using the iridium-complex [8],[9]. The annual production of acetic acid using iridium-complex catalyst was very high, but the problem of catalyst poisoning by CO2 occurred. Therefore, the use of CO2 capture technology was required to separate CO2 from the syngas.

A primary syngas manufactured through partial oxidation is commonly used to produce acetic acid [10]. The primary syngas is composed of CO (60–70 %), H2 (30–40 %), CO2 (1–5 %), along with CH4 and other impurities. The H2S present in the syngas was removed via desulfurizer, and the CO/H2 was separated by the pressure swing adsorption process (PSA). The CO2 in the syngas was removed by CO2 capture technology, and the remaining CO2 should be limited to less than 20 ppm to prevent poisoning of the catalyst. Thus, high-level purification of CO2 is very important for increasing efficiency in the acetic acid production process. The CO2 capture technology used in the petrochemical industry was developed for gas purification purposes. In particular, the gas purification method using amines has been widely used commercially since its development by R. Richards in 1930 [11]. The typical amine absorbents are monoethanolamine (MEA), diethanolamine (DEA), and N-methyldiethanolamine (MDEA) [12]. Amines are classified as primary, secondary, or tertiary amines depending on their structural characteristics. MEA is a primary amine, which has the advantages of low cost and high CO2 absorption rate, but the disadvantages of low CO2 capacity, thermal degradation, oxidative degradation, corrosion, etc [13]-[16]. DEA has a relatively lower CO2 absorption rate than MEA does. MDEA is an absorbent used in early 1950, and has the advantage of treating H2S and CO2 simultaneously [17], but it has the disadvantage of a very low absorption rate [18]. In the 2000s, gas purification technology using amines was considered for application in carbon capture and storage (CCS) technology. The core technology of CCS is absorbents, and CO2 capacity, absorption rate and regeneration energy for CO2 capture process using a wet absorption method have been studied to evaluate the performance of absorbents. Recently, alternative absorbents in the form of cyclic amines such as

piperazine (PZ) and 2-methylpiperazine (2MPZ) have been reported for use as commercial absorbents in power plants because of their advantages of low absorption heat, high CO2 capacity and rapid reaction rate [19],[20]. In this study, various cyclic absorbents with potassium carbonate were evaluated to control CO2 in an acetic acid production process, one of petrochemicals. The CO2 absorption capacity and heat of reaction were measured and compared with MEA (30 wt%) and activated MDEA (α-MDEA; 40 wt% MDEA + 5 wt% PZ), in order to confirm the applicability of cyclic amines. When each absorbent was used, the concentration of emitted CO2 was kept below 20 ppm.

II. EXPERIMENT

The CO2 absorption capacity and heat of reaction were measured using a continuously stirred-tank reactor (CSTR) and differential reaction calorimeter (DRC), respectively. The mixed gases (3 vol% CO2 / balanced N2) used in the DRC experiment were purchased from Special Gas Co. in Korea. The CSTR experiments were conducted by mixing N2 (99.9999%) and CO2 (99.9999%) gas. MEA (2-aminoethanol; ≥99%), PZ (piperazine; 99.0%), and potassium carbonate (K2CO3; 99.5%) were from Samchun Chemicals. MDEA (N-methyldiethanolamine; ≥99.0) from Sigma Aldrich and 2MPZ (2-methylpiperazine; 98%) from Acros Organics were also used. The following four different absorbents mixed with deionized water were used for the experimental comparison of performance: 1) Commercially available and widely used aqueous 30 wt% MEA solution, 2) α-MDEA for simultaneous treatment of H2S and CO2, 3) KIERSOL-N (a brand of the Korea Institute of Energy Research) [21], and 4) KIERSOL-P (a brand used for petrochemical applications).

III. EXPERIMENTAL SETUP AND PROCEDURE

A. Continuously stirred-tank reactor (CSTR)

The experimental apparatus used in this study is shown in Fig. 1. The pressure in the CSTR was maintained at 9.50 to 9.52 bar to simulate the absorber of the CO2 capture process. In the CO2 absorption capacity experiment, the measurement was made by supplying 500 mL of absorbent to a reactor with an internal volume of 750 mL. The reaction temperature during the experiment was controlled by a water bath. CO2 was supplied using a sparger to maximize contact with the surface of the absorbent; the stirring was done at a constant rate of 500 r min-1 during the reaction. CO2 (3 vol%) was supplied at a constant concentration, in combination with nitrogen, using a mass flow controller. The gas supplied was injected into each reactor at a rate of 1,000 cm¬3 min-1. The concentration of CO2 was inspected at five-minute intervals using GC (gas chromatography; Agilent Technologies, model 7890A).

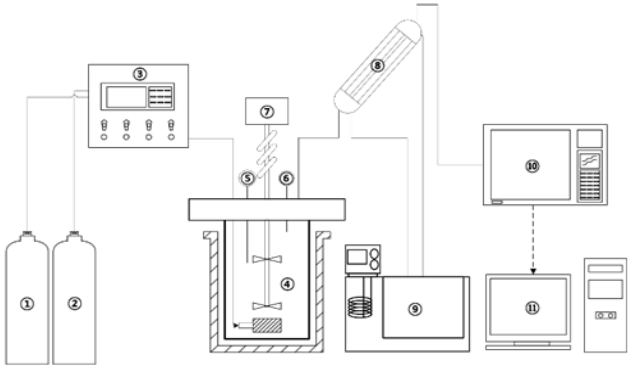

B. Differential reaction calorimeter (DRC)

Fig. 2 shows the configuration for the differential reaction calorimeter (DRC) experiment. The reactor had a double jacket structure with an inner volume of 250 mL. A total of 150 mL of the absorbent was injected into each reactor. The temperature in the reactors was kept constant during the reaction time using a thermostat. Two types of reactors were used: a reference reactor and a measurement reactor. The gas injected into the reactor was 3 vol% CO2 mixed gas. In order to maximize the reaction area of the absorbent, a sparger was used to give the injection a constant flow rate of 150 cm3 • min-1. The absorbent was stirred at a constant rate of 250 r • min-1 over the entire reaction time. Gas chromatography was used to analyze the concentration of CO2 exhausted after reaction with the absorbent inside the reactor. The absorbent underwent an exothermic reaction as it reacted with CO2; this reaction was measured in real time by the thermocouple located inside the reactor. Differences in the measured reaction heat were stored on the computer in real time. The details of the experimental procedure are available in a previous report [22].

IV. THEORETICAL FOUNDATIONS

A. Measurement of CO2 capacity using CSTR

The moles of CO2 absorbed by the absorbents (n_absorbed CO2) at each measurement point was calculated using Equation (1)-(3).

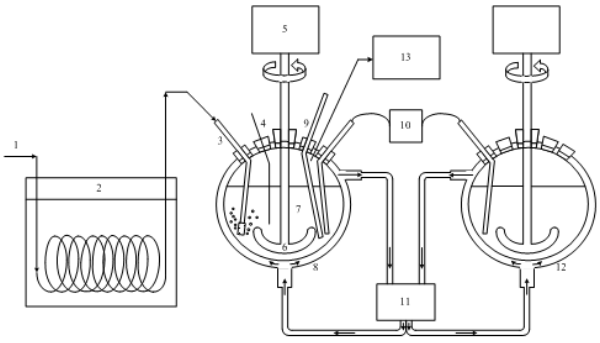

 ISBN: 978-81-932966-9-1

Figure 2. Schematic diagram of differential reaction calorimeter: 1) CO2 gas (3 vol% CO2 / balanced N2), 2) Water bath, 3) Inlet gas port, 4) Optional probe, 5) Motor, 6) impeller, 7) Absorbent, 8) Double jacketed reactor, 9) Calibration probe, 10) Temperatures and ΔT measurements, 11) Thermostat, 12) Reference reactor, 13) Gas chromatography.

$$n_{CO_2,out} = \frac{P_{CO_2,in} \times V_{CO_2,in}}{\mathrm{R} \times T_{CO_2,in}} \quad (1)$$

$$n_{CO_2,out} = \frac{P_{CO_2,out} \times V_{CO_2,out}}{\mathrm{R} \times T_{CO_2,out}} \quad (2)$$

$$n_{absorbed\ CO_2} = n_{CO_2,in} - n_{CO_2,out} \quad (3)$$

$$n_{absorbed\ co_2} = \int_0^t n_{absorbed\ CO_2} tdt \quad (4)$$

where PCO2 (atm), VCO2 (mol/min), and TCO2 (K) are the partial pressure, volume, and temperature of CO2, respectively. The subscripts, 'in' and 'out' indicate inlet and outlet. CO2 absorption capacity at saturated point was calculated using equation (4).

B. Measurement of the heat of reaction using DRC

]The measurement of the heat of reaction between the absorbent and CO2 was conducted three times: (1) calibration time before the CO2 reaction, (2) for the CO2 reaction, and (3) calibration time after the CO2 reaction. The heat of reaction is indicated by temperature changes per unit time in the reference reactor and the measurement reactor. As can be seen in equation (5), the heat of reaction calibration factor Q (kJ) can be calculated using the reaction-heat-transfer coefficient (UA; W• K-1) and the cumulative time changes (ΔT; K).

$$Q_{cal\ (1)} = UA_1 \times \int_{t_o}^{t_{end}} \Delta T dt \quad (5)$$

The UA was calculated by injecting constant energy via the calibration probe; in this study, the measurement was made three times. The heat of reaction calibration after the reaction was calculated in the same way as the heat of reaction calibration before reaction. As shown in equation (6), the total heat of reaction calibration within the reactor was calculated as the arithmetic mean of the heat of reaction calibration before the reaction and the heat of reaction calibration after the reaction.

$$UA_{average} = \frac{UV_1 + UV_2}{2} \quad (6)$$

In order to measure the heat of reaction between CO2 and absorbent, the enthalpy of the standard state was measured based on the heat of reaction per mole of CO2, and was found to be 40 °C.

V. RESULTS AND DISCUSSION

A. CO_2 absorption capacity

The CO_2 absorption capacity was expressed in mol of CO_2 dissolved in the absorbent per mol of absorbent (mol CO_2 • mol absorbents-1). Absorbents with high absorption capacity can dissolve large amounts of CO_2 in the CO_2 capture process and can thereby reduce operating cost. The CO_2 absorption capacity was measured to evaluate the absorption performance of each absorbent. The breakthrough curve of CO_2 is shown in Fig. 3–5 at the reaction temperature of 40–80 °C. In this figure, the y-axis is the ratio of the concentration of injected CO_2 (C_i) to the concentration of

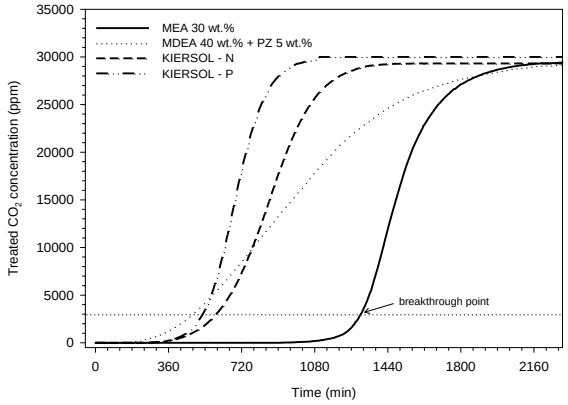

Figure 3. CO2 absorption curve of absorbents at 40 °C.

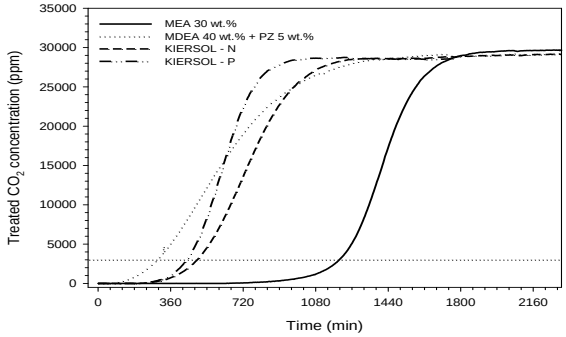

Figure 4. CO2 absorption curve of absorbents at 60 °C.

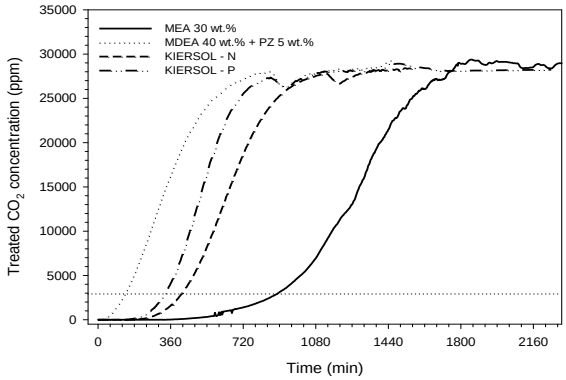

Figure 5. CO2 absorption curve of absorbents at 80 °C

emitted CO_2 (C_o), and the x-axis is the reaction time of the CO_2 and absorbent. In general, the point at which the outlet concentration is 10% of the inlet concentration is called the breakthrough point. As shown in Fig. 3–5, the breakthrough point is reached in a short time as the temperature increases. From these results, it can be shown that the amount of absorption of CO_2 depends on the reaction temperature. Table 1 shows the amount of absorbed CO_2 in each absorbent at different temperatures. The maximum CO_2 capacity of a primary amine such as MEA is generally limited to 0.5 mol CO_2 · mol amine^{-1} due to formation of MEA carbamate ($MEACOO^-$) and protonated MEA ($MEAH^+$). However, the absorption capacity of the MEA in this experiment was 0.74 mol CO_2 · mol amine^{-1}, which is higher than the theoretical value.

Table 1. CO2 absorption capacity of each absorbent at temperatures from 40 to 80 °C

Absorbents	CO_2 absorption capacity (mol CO_2 · mol absorbent^{-1})		
	40 °C	60 °C	80 °C
MEA	0.74	0.70	0.64
α-MDEA	0.63	0.38	0.23
KIERSOL-P	1.14	0.98	0.81
KIERSOL-N	1.17	1.00	0.84

These results were affected by the simulated pressure of the absorber (9.50–9.52 bar). The results for KIERSOL-P and KIERSOL-N at 40 °C were 1.14 and 1.17 mol CO_2 · mol absorbent^{-1}, respectively. KIERSOL-P showed 1.54 times greater CO_2 absorption than MEA and 1.81 times greater CO_2 absorption than a-MDEA. The difference in CO_2 absorption capacity at 60 °C was greater than at 40 °C. And, the difference in CO_2 absorption capacity at 60 °C was higher than at 40 °C. KIERSOL-P showed 1.40 times greater CO_2 absorption capacity than MEA, and 2.58 times greater CO_2 absorption capacity than a-MDEA. The CO_2 concentration remains low (< 20 ppm) after the absorbent. The curve of CO_2 in a low range of concentration is shown in Fig. 6-8, and the time is shown in Table 2 until the concentration of CO_2 reaches 20 ppm.

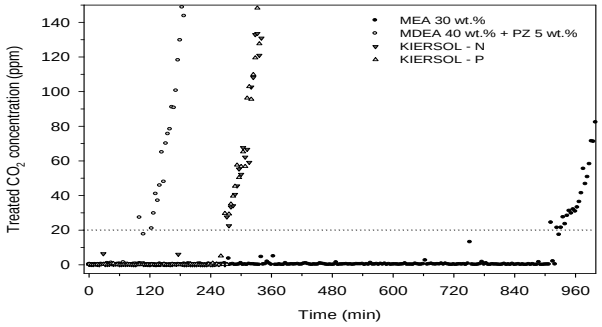

Figure 6. Initial CO2 concentration for CO2 absorption curve at 40 °C.

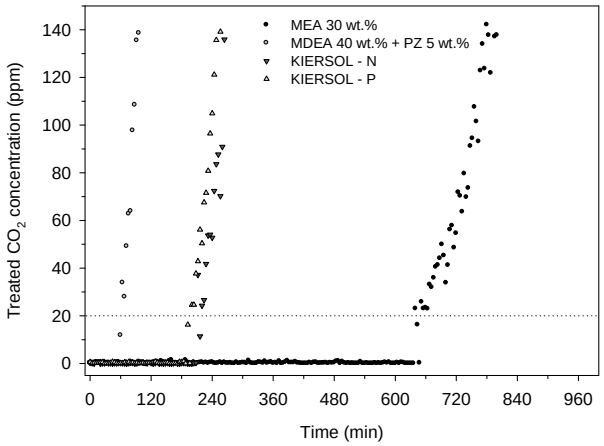

Figure 7. Initial CO2 concentration for CO2 absorption curve at 60 °C.

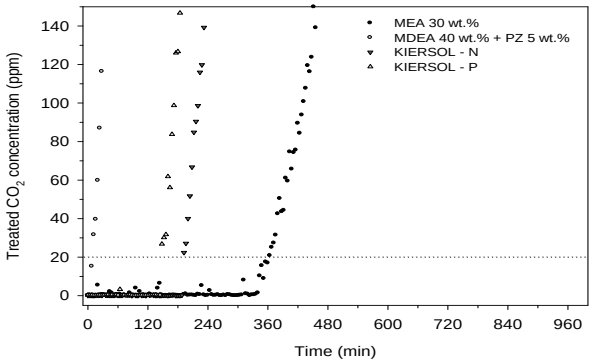

Figure 8. Initial CO2 concentration for CO2 absorption curve at 80 °C.

Table 2. Interval for absorbent to reach CO2 concentration of 20 ppm.

Temperature (°C)	Interval (min)			
	MEA	MDEA+PZ	KIERSOL-N	KIERSOL-P
40	912	100	272	268
60	640	64	212	200
80	364	12	192	148

MEA provided the highest absorbent concentration at which the concentration of CO2 was kept below 20 ppm. Interval of absorbents with a CO2 concentration of less than 20 ppm increased following the order MEA > MDEA > KIERSOl-N > KIERSOl-P.

B. Heat of reaction

High CO_2 absorption rate, high cyclic capacity and low reaction heat are required to reduce the energy requirement in the CO_2 capture process [23]. In general, the heat of reaction accounts for more than 50% of the total energy requirement and is an important indicator for evaluating the performance of the absorbent. As the reaction between CO_2 and absorbents is reversible reaction, it is possible to anticipate the heat of adsorption by measuring the heat of

endothermic reaction produced during the reaction between CO_2 and absorbents. The heat of reaction is the energy (kJ • mol-1) that has increased through exothermic reaction per mol of CO_2 of each absorbent. Kim et al. found that when 30wt% MEA and CO_2 were made to react with each other at 40℃, the heat of reaction was 87.098 kJ • mol-1 [24], and Carson et al. reported that the reaction between 30 wt% MEA and CO_2 at 25 oC resulted in the heat of reaction 83.15kJ • mol-1 [24]. The results of this study showed that the heat of reaction of MEA was 96.00 kJ • mol-1, which was higher than previous report. Although preceding research was conducted using 10-30 vol% CO_2 based on flue gases of the power plant, this study used low concentration CO_2 (3 vol%) of petrochemical process. The heat of reaction of MEA was 96.00 kJ • mol-1 and that of a-MDEA was 68.22 kJ • mol-1. As a result of the experiment, while the heat of reaction of KIERSOL-N and P were similar to that of a-MDEA, it was 0.73-0.65 times lower than that of MEA. As a result of measuring the heat of reaction, it could be found that KIERSOL-N and P were better than MEA in the aspects of absorption capacity and heat of reaction.

Table 3. Heat of absorption of saturated CO_2 at 40 °C

Absorbent	Absorbed CO_2 (mol)	CO_2 loading (CO_2 mol · absorbent mol^{-1})	Enthalpy ($\triangle H$: kJ · mol^{-1})
MEA	0.356	0.48	96.00
α-MDEA	0.145	0.25	68.22
KIERSOL-P	0.137	0.65	69.76
KIERSOL-N	0.160	0.59	62.83

VI. CONCLUSIONS

We assessed CO_2 absorption capacity, low concentration duration of CO_2, and the heat of reaction between absorbents and CO_2 in order to control 3vol.% CO_2 emitted during the acetic acid production process under ultra-low concentration 20ppm, As a result of the experiment, the absorption capacity of KIERSOL-N and KIERSOL-P at 40℃ was 1.14-1.17 mol CO2 • mol absorbent-1, which was rather higher than that of MEA (0.74 mol CO_2 • mol absorbent-1) or MDEA (0.63 mol CO_2 • mol absorbent-1). Although MEA kept the concentration of CO_2 under 20ppm longer than the others, KIERSOL-N and KIERSOL-P emitted low concentration CO_2 longer than MDEA. As for the heat of reaction, α-MDEA, KIERSOL-N and KIERSOL-P showed similar results, and MEA was found to have very high heat of reaction. The study results indicate that KIERSOL-N and KIERSO-P have high absorption capacity, low heat of reaction, and long low concentration carbon dioxide duration. Thus, KIERSOL-N and KIERSOL-P are expected to improve the efficiency of the acetic acid production process.

V. ACKNOWLEDGEMENTS

This work was supported by the Energy Demand Management Technology Program of the Korea Institute of Energy Technology Evaluation and Planning (KETEP), granted financial resource from the Ministry of Trade, Industry and Energy, Republic of Korea. (No. 20172010202060)

REFERENCES

[1] M. T. Ashtiany, A. M. Rezaee, and M. R. Jafari Nasr, "An investigation on the effects of iodide salts in iridium catalyst in methanol carbonylation process" Journal of Applied Chemical Researches, vol. 4, pp. 11-18, August 2010.

[2] HIS Market "Monochlroacetic acid" Chemical economics handbook, November 2016.

[3] Grand view research, "Acetic Acid Market Analysis By Application (VAM, Acetic Anhydride, Acetate Esters, PTA) And Segment Forecasts To 2022", ISBN: 978-1-68038-0774-4, July 2015.

[4] S. Bhaduri, and D. Mukesh "Homogeneous Catalysis: Mechanisms and Industrial Applications" John Wiley & Sons, 2014.

[5] A. Haynes, P. M. Maitlis, G. E. Morris, G. J. Sunley, H. Adams, P. W. Badger, C. M. Bowers, D. B. Cook, P. I. P. Elliott, T. Ghaffar, H. Green, T. R. Griffin, M. Payne, J. M. Pearson, M. J. Taylor, P. V. Vickers, and R. J. Watt, "Promotion of Iridium-Catalyzed Methanol Carbonylation: Mechanistic Studies of the Cativa Process" Journal of the American Chemical Society, vol. 126, pp. 2847-2861, February 2004.

[6] J. H. Jones "The CativaTM Process for the Manufacture of Acetic Acid" Platinum Metals Rev, vol. 44, pp. 94-105, 2000.

[7] G. J. Sunley, and D. J. Watson, "High productivity methanol carbonylation catalysis using iridium The CativaTM process for the manufacture of acetic acid" Catalysis Today, vol. 58, pp. 293-307, 2000.

[8] P. I. P. Elliott, S. Haak, A. J. H. M. Meijer, G. J. Sunley, and A. Haynes, "Reactivity of Ir(III) carbonyl complexes with water: alternative by-product formation pathways in catalytic methanol carbonylation" Dalton Transactions, vol. 42, pp. 16538-16546, September 2013.

[9] G. Borah, and D. Boruah, "Ruthenium(Ⅱ), rhodium(Ⅰ) and iridium(Ⅰ) complexes with [p-(N,N-dimethylamino)phenyl]diphenylphosphine ligand: Synthesis, characterization and rhodium-catalysed carbonylation of methanol" Indian Journal of Chemistry, vol. 52A, pp. 334-341, March 2013.

[10] S. A. Al-Sayari, "Recent Developments in the Partial Oxidation of Methane to Syngas" The Open Catalysis Journal, vol. 6, pp. 17-28, June 2013.

[11] A. L. Kohl, and R. B. Nielsen, "Gas Purification" Gulf Publishing Company, ISBN: 978-0-88415-220-0, 1997.

[12] J. H. Choi, Y. E. Kim, S. C. Nam, S. H. Yun, Y. I. Yoon, and J-H Lee, "CO2 absorption characteristics of a piperazine derivative with primary, secondary, and tertiary amino groups" Korean J. Chem. Eng. Vol. 33, pp. 3222-3230, June 2016.

[13] C. Han, K. Graves, J. Neathery, and K. Liu, "Simulation of the Energy Consumption of CO2 Capture by Aqueous Monoethanolamine in Pilot Plant" Energy Environment Research, vol. 1, pp. 67-80, December 2011.

[14] Y. E. Kim, J. H. Choi, S. C. Nam, and Y. I. Yoon, "CO2 Absorption Characteristics in Aqueous K2CO3 / Piperazine Solution by NMR Spectroscopy" Industrial & Engineering Chemistry Research, vol. 50, pp. 9306-3913, June 2011.

[15] J. Davison, "Performance and costs of power plants with capture and storage of CO2" Energy, vol. 32, pp. 1163-1176, July 2007.

[16] S. H. Yun, Y. E. Kim, J. H. Choi, S. C. Nam, J. Chang, and Y. I. Yoon, "CO2 absorption, density, viscosity and vapor pressure of aqueous potassium carbonate + 2-methylpiperazine" Korean Journal of Chemical Engineering, vol. 33, pp. 3473-3486, December 2016.

[17] S. Y. Khan, M. Yusuf, and A. Malani, "Selection of Amine in Natural Gas Sweetening Process for Acid Gases Removal: A Review of Recent Studies" Petroleum & Petrochemical Engineering Journal, vol. 1, pp. 1-7, June 2017.

[18] H. Kierzkowska-pawlak, and A. Chacuk, "Kinetics of Carbon Dioxide Absorption into Aqueous MDEA Solutions" Ecological Chemistry and Engineering S, vol. 17, pp. 463-475, 2010.

[19] B. Sherman, X. Chen, T. Nguyen, Q. Xu, H. Rafique, S. A. Freeman, A. K. Voice, and G. T. Rochelle, "Carbon Capture with 4 m Piperaizine / 4 m 2-methylpiperazine" Energy Procedia, vol. 37, pp. 436-447, 2013.

[20] Y. E. Kim, J. H. Choi, S. C. Nam, and Y. I. Yoon, "CO2 absorption capacity using aqueous potassium carbonate with 2-methylpiperazine and piperazine" Journal of Industrial and Engineering Chemistry, vol. 18, pp. 105-110, January 2012.

[21] Y. I. Yoon, Y. E. Kim, S. C. Nam, S. K. Jeong, S. Y. Park, M. H. Youn, and K. T. Park. "Characteristics of CO2 capture system using KIERSOL in the LNG flue gas" Energy Procedia, vol. 63, pp. 1745-1750, 2014.

[22] J. H. Choi, S. H. Yoon, Y. E. Kim, Y. I. Yoon, and S. C. Nam, "The Effect of Functional Group Position of the Piperidine Derivatives on the CO2 Absorption Characteristics in the (H2O-Piperidine-CO2) System" Korean Chemical Engineering Research,vol. 53, pp. 57-63, November 2014.

[23] F. A. Chowdhury, H. Yamada, T. Higashii, K. Goto, and M. Onoda, "CO2 Capture by Tertiary Amine Absorbents: A Performance Comparison Study", Industrial & Engineering Chemistry Research, vol. 52, pp. 8323-8331. 2013.

[24] I. Kim, and H. F. Svendsen, "Heat of Absorption of Carbon Dioxide (CO2) in Monoethanolamine (MEA) and 2-(Aminoethyl) Ethanolamine (AEEA) Solutions." Industrial & Engineering Chemistry Research. vol. 46, pp. 5803-5809, July 2007.

[25] J. K. Carson, K. N. Marsh, and A. E. Mather, "Enthalpy of Solution of Carbon Dioxide in (Water + Monoethanolamine, or Diethanolamine, or N-Methyldiethanolamine) and (Water + Monoethanolamine + N-Methyldiethanolamine) at T= 298.15 K." The Journal of Chemical Thermodynamics, vol. 32, pp. 1285-1295. September 2000.

An Approach to Measure Similarity of Software Projects at the Design Phase

[1] Asif imran
Institute of Information Technology, University of Dhaka

Abstract:-- **Estimation of software comparability is one of the ideal approach to utilize experiences of effectively developed software. Experiences obtained from previous projects can help software industries to deliver software project in a short pe- riod of time. Although various approaches have been proposed throughout years on software similarity that helps to utilize the previous projects knowledge, none of these are based on design diagrams. However, research on measuring software similarity based on design paradigm is expected to use the historic projects knowledge in early phase of software development. This paper proposes an approach of measuring similarity by developing a tool named Software Design Similarity Measurement Tool (DeSiMeT). DeSiMeT ascertains a similarity score between two software projects utilizing class diagram, sequence diagram and state transition diagram. An experimental analysis has been conducted by running the tool using seven software projects to verify the approach. The analysis of the tool appears in a precision of 0.83, recall of 1 and F-measure of 0.91 which concludes that the tool performs well as a novel work.**

Index Terms—**Software Similarity, Historic Project, Software Design, Class Diagram, Sequence Diagram, State Transition Diagram**

I. INTRODUCTION

In today's fast changing business environment, software industries attempt to rapidly develop their products so that they can speed up the delivery of their latest innovations to customers. This makes software development more chal- lenging as software developers need to design, implement, and test complex software systems as early as possible. As a result, software companies are in search of some solutions that can help to deliver good quality and error free software in right time. Experiences obtained from historic projects can help software industries to adopt shorter release cycles. In this regard, measurement of software similarity is one of the best way to use experiences of already developed software [1]. Proper identification of similar software helps to select development methods, design patterns and reliability testing models as well as is applicable in the areas of data mining, software testing, plagiarism detection and software security [2]. This helps software industries to decrease their efforts, costs and time of development cycle [3].

In this research, a method to measure similarity between software projects were proposed based on software design paradigm. The proposed method computes similarity between intended software project and historic software projects to use previous knowledge. More precisely, the problem can be addressed by the following questions:

- How to utilize the experiences of historic software

Here, we use design paradigms of different projects to measure similarity among those. The proposed method solely focuses on the quantitative similarity measure. For this pur- pose, we use different design diagrams i.e. class diagram, sequence diagram and state diagram. To measure similarity score, a tool named Software Design Similarity Measurement Tool (DeSiMeT) is developed.

II. RELATED WORK

In the software engineering literature, a less work has been done that addressed the issue of measuring similarity between two software projects. Some works have been done based on fuzzy logic, Euclidean Distance, Graph Matching and Source code corresponded but these are not enough to solve the existing problems. Two approaches for measuring similarity between software projects based on fuzzy C-means clustering and fuzzy logic were presented in [7]. The proposed approaches overcame the problems of nearest neighborhood techniques. First approach was developed based on identification features of fuzzy sets and second approach was based on partition matrix that is obtained by fuzzy C-means. They stated that first approach outperforms second approach based on some experimental results. This approach is not applicable for linguistic values and only suitable for numerical and categorical data. Some specific research has been done for computing difference between class diagrams. A generic difference algorithm proposed for computing similarity of two UML models which were encoded in XML files from design diagram [14]. The implemented algorithm performed well on runtime for small documents but not good for a large documents. A

comparative result were presented using basic graph by denoting node and edge. In this approach, at first the elements of each document were detected and then calculated similarity by a defined function that worked with some predefined criteria. Weight was defined for each criteria in a way that may mislead to a missed correspondences. To optimize cost-resource for cloud environment an empirical analysis investigation was proposed in [13]. Authors presented a comparison analysis between open source cloud and organizational cloud to increase the performance of open source cloud by optimizing cost and resource. However, performance,of open source cloud can be enhanced by applying software similarity approach to find out the best result. Although various approaches have been proposed throughout years, none of these are based on design diagrams. However, research is expected to use the historic projects knowledge in software development. In this research, we mainly focused on the design phase of SDLC.

III. PROPOSED APPROACH

The novelty of this research is to measure similarity of software projects based on some design diagrams in the design phase of SDLC. Firstly, in order to measure design similarity, we consider several design diagrams: (a) Class Diagram (CD) (b) Sequence Diagram (SD) and (c) State Transition Diagram (STD). These diagrams cover the overall design of any object oriented software project to the maximum extent. Later on, the diagrams are parsed by an open source automated tool i.e. StarUML and converted to XML format. Then the XML files are parsed by XML parser and compared using the structure and some comparison criteria. To demonstrate the approach, we have developed a tool and named it as Software Design Similarity Measurement Tool (DeSiMeT).

A. Overview of DeSiMeT

Top level view of the proposed tool's architecture is shown in the Fig. 1. The tool developed in a way that measured similarity between current project and historic project based on design diagrams those are declared in the previous section. Selected design diagrams are converted to XML format using an open source converter as the tool takes XML file as input.

B. Similarity Measurement Approach

Main purpose of this research is to find out the best similarity match of a current project with some historic projects. The proposed approach to measure similarity between software projects based on design depends on different UML diagrams which describe the external behavior of a project.

a) Structural Matching: In the view of a class diagram, the whole system can be compared by relationships of classes. At first, class diagrams of a system are converted to XMLs and inputted to the tool. Then elements are parsed by an XML parser to proceed the next step. Class diagrams are considered as a graph where classes are denoted as node and relationships are denoted as edge.

($A \xrightarrow{Ag} D$, $A \xrightarrow{As} C$, $B \xrightarrow{Ag} C$, $D \xrightarrow{As} C$, $D \xrightarrow{G} E$ and $C \xrightarrow{As} E$)

Historic class also contains five classes and relation among the classes are:

($B \xrightarrow{Ag} A$, $B \xrightarrow{As} C$, $A \xrightarrow{Ag} C$, $A \xrightarrow{G} G$, $A \xrightarrow{G} F$ and $C \xrightarrow{As} F$)

b) Criteria Matching:

In the view of class each of the classes a similarity can be measured by comparing some criteria that is presented by Ketle et al. [14]. Due to the generic approach a function is defined by setting some criteria i.e. number of operations and number of attributes. In every case, graph matching can not provide accurate similarity score. Thus, quantitative value need to be considered as an important fact of measuring similarity of class diagram. A criteria matching algorithm is developed that is shown in Algorithm 2. For measuring criteria similarity, a class of first diagram is compared with all of the classes of the second diagram and stored.The same class can not be matched with any other class of the second diagram. The criteria similarity score is Ncalculated (Algorithm 2 Line 19). Finally, the total similarity between two class diagrams are measured by integrating the score of structural matching and criteria matching.

Algorithm 1 Structural Matching

```
1: input: XMLs (CD, SD, STD)
2: output : finalScore_structural
3: initialize mat[u][v] ← 0
4: initialize setofrelations ← R
5: for edges(u, v) in diagrams do
6:     mat[u][v] ← getValue()
7: end for
8: procedure GETVALUE
9:     if relations ∈ R then
10:        setValue = value
11:    end if
12: end procedure
13: finalScore_structural ← matchBFS()
```

1) Similarity of Sequence Diagram: SD is used to show the interaction among the objects in a given scenario based on a time sequence. It is a logical view of a system under development that is typically associated with the use cases. A sequence of messages are exchanged among the

 ISBN: 978-81-932966-9-1

participating instances through the interactions of the system and some actors or different subsystems or classes [17]. Sequence diagram is considered as a part of project to measure similarity as it represents the dynamic interactions of classes in execution [11]. Similarity measurement of sequence diagram is similar as class diagram using two phases such as :structural matching and criteria matching. The phases are described in the following sections.

a) Structural Matching: For structural matching, sequence diagram is also considered as a graph to measure similarity like class diagram. At first, the UML sequence diagrams of the system are converted to XMLs and inputted to the tool. The XMLs are parsed by the XML parser and a n n matrix is generated like class diagram. The lif elines are considered as node and sendMessage and replyMessage are considered as edge of the graph for generating matrix. Fig. 3 presents a sample example of sequence diagram and fig. 4 presents the generated matrix of fig. 3. For generating matrix, the values of edges are set as prime number to keep track the multiple call between two lif elines. Different values are set for sendMessage and replyMessage where sendMessage is defined by 2 and replyMessage is defined by 3 because these two edges are not same and address a different meaning for sequence diagram. Generated matrix is compared by the same algorithm that is used in class diagram is presented in Algorithm 1. The algorithm describes that all matrix is generated (Algorithm 1 Line 6). Value of edges are set based on message type between lif elines (Algorithm 1 Line 9-10). Similarly, for measuring similarity between two matrices of

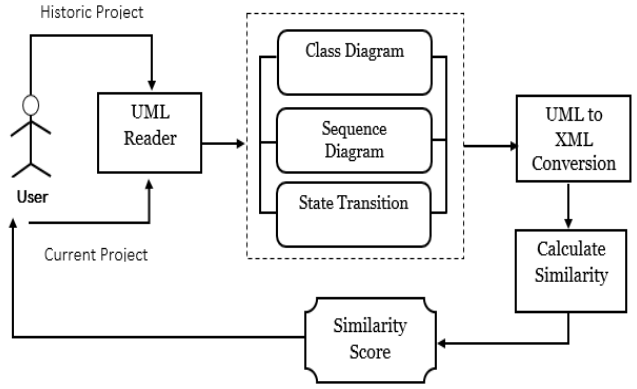

Fig. 1: Overview of Framework DeSiMeT

	A	B	C	D	E
A	0	0	2	5	0
B	0	5	0	0	0
C	0	0	0	0	2
D	0	0	2	0	3
E	0	0	0	0	0

Current Project

	B	C	A	G	F
B	0	2	5	0	0
C	0	0	0	0	2
A	0	5	0	3	3
G	0	0	0	0	0
F	0	0	0	0	0

Historic Project

Fig. 2: Generated Matrices of Fig. 2

sequence diagram, a customize Breath First Search algorithm is used (Algorithm 1 Line 13) that is proposed by smith et al. [20]. b) Criteria Matching: Criteria matching of sequence diagram is a statistical similarity measured based on some criteria i.e. number of lif elines, number of sendMessage and number of replyMessage. Algorithm 2 is used to measure criteria matching like class diagram. However, a function is defined for this purpose and a sequence diagram from first project is compared with all of the sequence diagram of the second project and store the max value. If a match is found in the next step then it is ignored as it is already compared. Then, the similarity score is calculated (Algorithm 2 Line 19). Finally, similarity of sequence diagrams are measured by integrating the score of structural matching and criteria matching.

2) Similarity of State Diagram: STD describes the behavior of a system using states of the system and transitions between states [18]. It shows different states of an entity as well as how an entity respond to events by changing the states. Similarity of state diagram is measured into two phases like class diagram.

a) Structural Matching: State diagram is considered as a graph to measure similarity where the states are considered

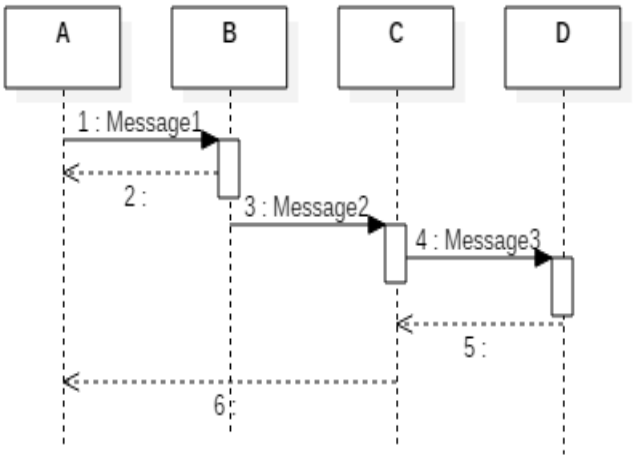

Fig. 3: Example of Sequence Diagram

	A	B	C	D
A	0	2	0	0
B	3	0	2	0
C	3	0	0	2
D	0	0	3	0

Fig. 4: Generated Matrix of sequence diagram

 ISBN: 978-81-932966-9-1

as node and transitions are considered as edge of the graph. At first, the UML state diagrams of the system are converted to XMLs and inputted to the tool. Then, the XMLs are parsed by the XML parser and a n n matrix is generated like class diagram. The value of edges are set as: start state to

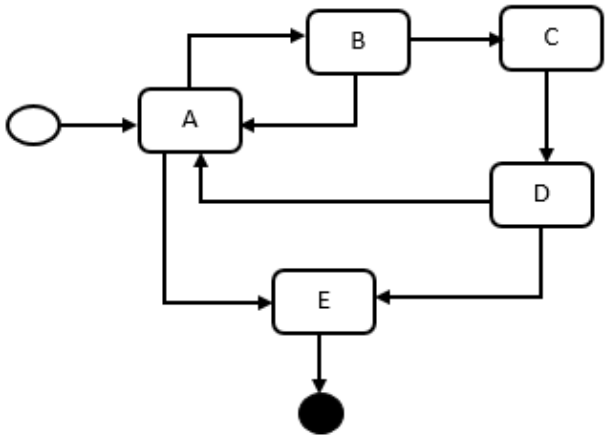

Fig. 5: Example of State Diagram

general state is defined by 1, general state to general state is defined by 2 and general state to final state is defined by 3. Algorithm 1 is also used for structural matching of state diagram. Similarly, for generating matrix the function is used (Algorithm 1 Line 6). The value of edges are set based on transition type between state that is shown (Algorithm 1 Line 9-10). The matrices are compared like class diagram that is used (Algorithm 1 Line 13).

b) Criteria Matching: Some criteria i.e. number of states, and number of transitions are defined for measuring the statistical similarity of two state diagrams. A function is defined based on these criteria and the similarity is computed using the algorithm 2 like other two diagrams. However, a state diagram from first project is compared with all of the state diagram of the second project and store the max value. If a match is found in the next step then it is ignored as it is computed. The similarity score is calculated (Algorithm 2 Line 19). Then, the similarity of state diagrams are measured by integrating the score of structural matching and criteria matching. Finally, total similarity score of two projects is calculated by integrating the similarity score of class diagram, sequence diagram and state transition diagram.

IV. CASE STUDY

The goal of this case study is to evaluate approximation of the proposed approach. The experiment have been conducted on some design diagram of software projects. A tool DeSiMeT has been implemented in java for this purpose.

A. Dataset

The analysis was performed on 7 different software project requiring different diagrams those are used in this research. These projects have been collected from the student of Institute of Information Technology, University of Dhaka. These projects are Inventory Management System (IMS), Student Management System (SMS), AmaderChakri.com (AC.com), Program Office Management System (POMS), Library Circulation System (LCS), Cricket Circle (CC) and Cloud Portal(CP). The project set is converted to XMLS using StarUml before running DeSiMeT as it takes XMLs as input. Table I shows the dataset in details. Project name, number of classes in class diagram, number of sequence diagrams and number of state diagrams of each project are presented in this table.

B. Study Result

For experimental result, dataset projects were run using DeSiMeT. The similarity score was measured between current project and historic project. In the dataset, IMS is the selected as current project and other projects as historic projects. For each historic projects, similarity values of class diagram, sequence diagram and state diagram were measured by comparing with current project that is presented in Table II. Here, first column presents the current project and second column presents historic project. Similarity values of Class Diagram (CD), Sequence Diagram (SD) and State Transition Diagram (STD) are also presented that were obtained from DeSiMeT. In the last column, similarity score of two projects are presented that is calculate d from the average value of CD, SD and STD.

C. Analysis

For the justification of DeSiMeT, an empirical analysis was performed. Table III presents the expected result and actual result of this tool. The expected similarity result was identified from a manual analysis that was performed by some software design experts. The actual result was generated from DeSiMeT and the similar project were chosen based on a threshold value that is greater than or equal 0.6 (threshold 0:6).

TABLE I: Result Analysis

CP	HP	Actual Result (threshold $\geq$ 0.60)	Expected Result
IMS	SMS	Yes	Yes
	AC.com	Yes	No
	POMS	Yes	Yes
	LCS	Yes	Yes
	CC	No	No
	CP	No	No

 ISBN: 978-81-932966-9-1

Now, from the actual and expected result that is shown in the table III, the precision and recall of DeSiMeT can be measured. Let, tp =true positive, fp =false positive, fn =false negative. From Table I, tp = 5, fp = 1, fn = 0. Thus,

$$Precision = \frac{tp}{tp + fp} = \frac{5}{5 + 1} = 0.83$$

As, DeSiMeT provides 1 false negative result, it possesses the maximum recall. Using the precision and recall, the F-measure or the balanced F-score (F1 score) can be calculated.

$$F_1 = 2 \cdot \frac{Precision \cdot Recall}{Precision + Recall} = 2 \cdot \frac{0.83 \cdot 1}{0.83 + 1} = 0.91$$

V. CONCLUSION

In this paper, a generic approach for measuring similarity between software projects is proposed. The approach is based on a series of design diagrams those are converted to XMLs. One of the challenges to measure similarity between complex types which are represented by XML, is handled by different techniques for getting the best scores as described previously. The task is performed in three steps: similarity of class diagrams in first step, similarity of sequence diagram in the second step and similarity of state diagram in third step are measured. A prototype tool DeSiMeT is developed to prove the feasi-bility of the approach. A case study is presented that evaluates the applicability of the approach. In this case study, seven projects were selected to perform the empirical study. For DeSiMeT, the precision, recall and F-measure were calculated that possesses a precision of 0.83, recall of 1 and F-measure of 0.91. The result shows that the proposed approach performs well as a novel work. In this approach, only three UML diagrams are considered for similarity Measurement, in future more diagrams will consider for performing better result. This work directs to our next work to software reliability model selection based on similarity score between current project and historic project.

REFERENCES

[1] Zeng, Jintao, et al. ”A prototype system of software reliability prediction and estimation.” in proceedings of the Third International Symposium on Intelligent Information Technology and Security Informatics (IITSI), 2010.

[2] Reungsinkonkarn, Arun. ”Hierarchical similarity measurement model of program execution.” in proceedings of the Software Engineering and Service Science (ICSESS), 2013 4th IEEE International Conference on IEEE, 2013.

[3] Salami, Hamza Onoruoiza, and Moataz A. Ahmed. ” UML artifacts reuse:
state of the art.” arXiv preprint arXiv:1402.0157 (2014).

[4] Fenton, Norman, and James Bieman. Software metrics: a rigorous and practical approach. CRC Press, 2014.

[5] Idri, Ali, and Alain Abran. ”A fuzzy logic based set of measures for software project similarity: validation and possible improvements.” Soft- ware Metrics Symposium, 2001. METRICS 2001. Proceedings. Seventh International. IEEE, 2001.

[6] Idri, Ali, and Alain Abran. ”Evaluating software project similarity by using linguistic quantifier guided aggregations.” IFSA World Congress and 20th NAFIPS International Conference, 2001. Joint 9th. Vol. 1. IEEE, 2001.

[7] Azzeh, Mohammad, Daniel Neagu, and Peter Cowling. ”Software project similarity measurement based on fuzzy C-means.” Making Globally Distributed Software Development a Success Story. Springer Berlin Heidelberg, 2008. 123-134.

[8] Shepperd, Martin, and Chris Schofield. ”Estimating software project effort using analogies.” Software Engineering, IEEE Transactions on 23.11 (1997): 736-743.

[9] Tibermacine, Okba, Chouki Tibermacine, and Foudil Cherif. ”A practical approach to the measurement of similarity between WSDL-based web services.” Revue des Nouvelles Technologies de l’Information (2014): 03-18.

[10] Nahar, Nadia, and Kazi Sakib. ”SSTF: A novel automated test gener- ation framework using software semantics and syntax.” Computer and Information Technology (ICCIT), 2014 17th International Conference on. IEEE, 2014.

[11] Nahar, Nadia, and Kazi Sakib. ”Automatic Recommendation of Soft- ware Design Patterns Using Anti-patterns in the Design Phase: A Case Study on Abstract Factory.” 3rd International Workshop on Quantitative Approaches to Software Quality.

[12] Yamamoto, Tetsuo, et al. ”Measuring similarity of large software sys- tems based on source code correspondence.” Product Focused Software Process Improvement. Springer Berlin Heidelberg, 2005. 530-544.

[13] Imran, Asif, Alim Ul Gias, and Kazi Sakib. ”An empirical investigation of cost-resource optimization for running real-life applications in open source cloud.” Procedings of High Performance Computing and Simulation (HPCS), 2012 International Conference on. IEEE, 2012.

[14] Kelter, Udo, Jrgen Wehren, and Jrg Niere. ”A Generic Difference Algorithm for UML Models.” Software Engineering 64.105-116 (2005): 4-9.

[15] Szlenk, Marcin. ”Formal semantics and reasoning about uml class diagram.” Dependability of Computer Systems, 2006. DepCos- RELCOMEX’06. International Conference on. IEEE, 2006

[16] Chen, Peter. ”Entity-relationship modeling: historical events, future trends, and lessons learned.” Software pioneers. Springer Berlin Heidel- berg, 2002. 296-310.

[17] Firley, Thomas, et al. ”Timed sequence diagrams and tool-based anal- ysisa case study.” UML99 The Unified Modeling Language. Springer Berlin Heidelberg, 1999. 645-660.

[18] Klein, Cornel, Christian Prehofer, and Bernhard Rumpe. ”Feature Spec- ification and Refinement with State Transition Diagrams.” FIW. 1997.

[19] Dong, Jing, Dushyant S. Lad, and Yajing Zhao. ”DP-Miner: Design pattern discovery using matrix.” Engineering of Computer-Based Sys- tems, 2007. ECBS’07. 14th Annual IEEE International Conference and Workshops on the. IEEE, 2007.

[20] Smith, S., and D. R. Plante. ”Dynamically recommending design pat- terns.” SEKE. 2012.

Effect of Ultrasonic stress in Semiconductor Materials and Devices

Awadhesh Prasad
Associate Professor (Physics)
Jagjiwan College, Arrah – 802301, Bhojpur, Bihar
email: draprasadjjc@rediffmail.com

***Abstract:*-- Effect of Ultrasonic Stress in solid state devices and materials have been discussed with the help of electromagnetic wave theory. Ultrasonic stress (radiation pressure) changes the characteristics of solid state devices and materials. Analytical treatment of changed characteristics of solid state devices and materials have been discussed.**

***Index Terms*— Maxwell's wave equation, Poisson's equation, Space Charge density, Attenuation and Dispersion of Stress Wave, Ultrasonic Radiation Pressure.**

I. INTRODUCTION

Effect of ultrasonic stress is known in pure materials. Further, a systematic study has been made in solid state devices made from pure materials defined as Acoustoelectic effect. [1-13] due to ultrasonic radiation pressure effect when a sound wave propagates through a material containing free electrons, its momentum, as well as energy is attenuated. The momentum attenuation acts a dc force, causing the electrons to drift in the direction of force. When there is a closed circuit in this direction, a direct current is produced called "Acoustoelectric current" which is proportional to the sound intensity, as the momentum attenuation itself is. If on the other hand, the circuit is open, the drifting electrons produce a space charge whose electric field cancels the dc force due to the sound wave momentum attenuation. This back electric field is the "Acoustoelectric Effect" due to ultrasonic radiation pressure effect. The resistance of the material is changed due to acountic stress. There is a simultaneous bunching of electrons and holes in the solid state devices under the action of deformation potential of the travelling ultrasonic wave.

The phenomenon of phonon drag contributes to the thermometric power due to the momentum transfer to electrons from thermal phonons streaming down temperature gradient. It is qualitatively equivalent to the acoustoelectric effect, while quantitatively, it is different, since the ralations between typical wave length, mean free times and frequencies are entirely changed. For the propagation of acountic wave in piezoelectric semiconductor, there is a possibility of achieving acoustic gain by applying a dc electric field which causes the interacting charge carriers to drift in the direction of wave propagation faster than the sound. Ultrasonic wave carries a flux of momentum. A loss in energy from wave is equivalent to a proportional loss in momentum. This loss in momentum constitute a constant force acting on the object absorbing the energy (radiation pressure). The absorbers are the free charged carriers, and the ultrasonic radiation pressure is the acoustoelectric effect.

There is a simultaneous bunching of electrons and holes in a solid state devices under the action of deformation potential of the travelling acoustic wave. A sound wave in a solid gives rise to electric fields which accelerate electrons in much the same way as an electromagnetic wave. An analytical treatment of ultrasonic radiation pressure effect has been discussed.

II. ANALYTICAL TREATMENT: DESCRIPTION

Stress waves and Electrical Phenomena in Piezoelectric Semiconductors

For a one dimensional approximation, Electric field E produces a stress in the x_1 direction as follows:

$$\sigma = c\varepsilon - eE \quad (1)$$

$$D = eE + pE \quad (2)$$

c = elastic constant, E = electric field
D = electric displacement
ε = permitivity of a medium
σ = surface charge density

e = piezoelectric constants relating electric field to stress
p = magnitude of the elastic displacement component
Expressing E in terms of ε and differentiating (1) with respect to x leads to a wave equation. If D is assumed constant, this equation takes the form

$$\rho \frac{\partial^2 S}{\partial t^2} = c \left(1 + \frac{e^2}{cp}\right) \frac{\partial^2 S}{\partial x^2} \quad (3)$$

S is the displacement. The change in c due to the presence of the electric fields is thus obvious. The condition of constant D further leads to a zero space charge density through Poisson' s equation

$$\frac{\partial \mathrm{D}}{\partial X} = Q \quad (4)$$

where as the continuity relation

$$\frac{\partial J}{\partial X} = -\left(\frac{\partial \mathrm{Q}}{\partial t}\right) \quad (5)$$

For an extrinsic semiconductor in thermal equilibrium, the total space charge density Q may be expressed in terms of the energy levels and densities of the impurity states in the forbidden band, and the concentration of electrons in the conduction band. The condition of electrical neutrality corresponds to Q=0, and the acoustically produced space charge is the periodic variation of Q about zero.
J is the current density, indicates that in this case the varying current density due to the piezoelectric fields is zero, which corresponds to a very low conductivity in the medium.
In the case of very high conductivity, the field E accompanying the wave will be zero, and the elastic constant C will remain unaffected (Equation 1), whereas the stress wave will be accompanied by D fields, currents and varying space charge.
The case of specific interest here is that corresponding to intermediate values of conductivity, in the range encountered in semiconductors. In this range, equation (4) and (5) are used, together with an appropriate expression for J, to obtain values of D and E. These, in turn permit one to eliminate E from the wave equation.
For an extrinsic semiconductor (assumed to be n type), the current density may be expressed by

$$J = q\,(n + f n_s)\mu E + (\mu K T) f \left(\frac{\partial \mathrm{n_s}}{\partial \mathrm{X}}\right) \quad (6)$$

where the first term is due to drift and the second term is due to diffusion, q is the electronic charge, K is Boltzman's constant, T is the temperature, n is the mean density of electrons in the conduction band, and f is the fraction of acoustically produced space charge density n_s which is mobile.
Thus, $(n + f n_s)$ is the instantaneous local density of electrons in the conduction band. Equation (1) to (4) combined with plane wave representations of D and E

$$D = \frac{-i(nq\,\mu/\omega)E}{1 + i\omega\left(\frac{k}{\omega}\right)^2 (\mu f K T/q)} \quad (7)$$

In the case of small conductivity modulation $(f n_s \ll n)$, equation (7) may be further simplified and written in the form

$$D = \frac{-i(b/\omega)E}{1 + i\omega\left(\frac{k}{\omega}\right)^2 (\mu f K T/q)} \quad (8)$$

$b = nq\mu$represents the average conductivity.
The condition of small conductivity modulation $(f n_s \ll n)$ is satisfied when the effective drift velocity of the carriers in the piezoelectric field $f\mu E$ is much less than the velocity of the stress wave v. This imposes a limitation on the strain value:

$$\varepsilon \ll pv/f\mu e \quad (9)$$

In order to determine the attenuation and dispersion of stress waves, use is made of the conductivity frequency, defined by $\omega_c = \frac{b}{p}$, and the diffusion frequency, defined by,

$$\omega_D = \frac{q}{f\mu K T}\left(\frac{\omega}{K}\right)^2 \approx \left(\frac{q}{f\mu K T}\right) v^2$$

From equation (1), (2) and (8), one obtains

$$E = -\frac{e\varepsilon}{p}\left[\frac{1 + i(\omega/\omega_D)}{1 + i(\omega/\omega_D) + i(\omega_c/\omega)}\right]$$

In the case of negligible charge carrier diffusion $(\omega_D \gg \omega_c)$ equation (9) may be simplified to:

$$E = -\frac{e\varepsilon}{p}\left[\frac{1 - i(\omega_c/\omega)}{1 + \left(\frac{\omega_c}{\omega}\right)^2}\right] \quad (10)$$

and the effective elastic constant is obtained by substitution into (1)

$$\sigma = C\left[1 + \frac{e^2}{cp}\frac{1 - i\left(\frac{\omega_c}{\omega}\right)}{1 + \left(\frac{\omega_c}{\omega}\right)^2}\right]\varepsilon \quad (11)$$

The velocity and attenuation are obtained in terms of the real and imaginary parts of the complex elastic constant

$$V = V_0\left[1 + \frac{\frac{e^2}{2Cp}}{1 + \left(\frac{\omega_c}{\omega}\right)^2}\right] \quad (12)$$

 ISBN: 978-81-932966-9-1

$$\alpha = \frac{\omega}{V_0}\frac{e^2}{2Cp}\left[\frac{\frac{\omega_c}{\omega}}{1+\left(\frac{\omega_c}{\omega}\right)^2}\right] \quad (13)$$

This expression show that at very low frequency V tends to V_0 and α tends to zero, whereas in the high frequency limit the become.

$$V = V_\infty = V_0\left[1 + \frac{e^2}{2Cp}\right] \quad (14)$$

$$\alpha = \alpha_\infty = \frac{\omega_c e^2}{V_0 2Cp} \quad (15)$$

$\omega_D$is the frequency above which the wave length is sufficiently short for diffusion to smooth out carrier density fluctuations associated with the periodicity of the stress wave.

Expression (11) and (12) are obtained on the assumption that $\frac{e^2}{Cp}$ is small.

In the vicinity of $\omega = \omega_c$, a simple relaxation –type dispersion occurs. It should be emphasized that the relaxation frequency is given by the conductivity of the material.

When carrier diffusion is taken into account, the complete expression for velocity and attenuation become

$$V = V_0\left[1 + \frac{e^2}{2Cp}\frac{1+(\omega_c/\omega_D)+\left(\frac{\omega}{\omega_D}\right)^2}{1+2\left(\frac{\omega_c}{\omega_D}\right)+\left(\frac{\omega}{\omega_D}\right)^2+\left(\frac{\omega_c}{\omega}\right)^2}\right] \quad (16)$$

$$\propto = \frac{\omega}{V_0}\frac{e^2}{2Cp}\left[\frac{\omega_c/\omega}{1+2(\omega_c/\omega_D)+\left(\frac{\omega}{\omega_D}\right)^2+\left(\frac{\omega_c}{\omega}\right)^2}\right] \quad (17)$$

In this case, for $\omega_D \gg \omega_c$, expression (12) and (13) retain their validity for all frequencies, except that $\propto$ approaches a constant value $\left(\frac{\omega_c}{V_0}\right)\left(\frac{e^2}{2Cp}\right)$ in the frequency range between ω_C and ω_D, and drops to zero as ω becomes larger than ω_D. For $\omega_C \gg \omega_D$, the velocity and attenuation may be expressed by:

$$V = V_0\left[1 + \frac{e^2}{2Cp}\frac{(1+\omega^2/\omega_D\omega_C)}{2+(\omega^2/\omega_D\omega_C)+(\omega_D\omega_C/\omega^2)}\right] \quad (18)$$

And

$$\propto = \frac{\omega}{V_0}\frac{e^2}{2Cp}\left(\frac{\omega_D/\omega}{2+(\omega^2/\omega_D\omega_C)+(\omega_D\omega_C/\omega^2)}\right) \quad (19)$$

The maximum velocity change occurs at the frequency $\omega = \left(\frac{\omega_D}{\omega_C}\right)^{1/2}$, whereas the frequency corresponds to maximum attenuation is

$$\omega = \left(\frac{\omega_D\omega_C}{3}\right)^{\frac{1}{2}}$$

Ultrasonic radiation pressure has been discussed analytically [13].

II. CONCLUSION

Discussion of the interaction of ultrasonic waves with lattice vibrations or with defects in a solid follows a pattern very close to that of thermal conductivity theory. The interaction or coupling between ultrasonic waves and conduction electrons proceeds through the absorption and emission of phonons. At sufficiently low temperature there is also energy transfer from ultrasonic waves to conduction electrons.

Electrons are coupled to the lattice and interact with stress waves in at least two distinct ways. Lattice waves interact with ultrasonic stress waves, and nuclear quadrupole coupling link the nucleus with the lattice and hence with ultrasonic stress waves.

REFERENCES

1. V. R. Singh and Awadhesh Prasad, “Effect of Ultrasonic stress on the sensitivity of Silicon Strain devices and application to acoustic power measurement” Sensors and Actuators A. Netherlands, Vol. 28, pp 7 – 11, 1991.
2. V. R. Singh and Awadhesh Prasad, “Effect of Ultrasonic Stress on Amplification of an Operational Amplifier Device”, Applied Acoustics, UK, Vol 27, pp 69 – 73, 1989.
3. V. R. Singh and Awadhesh Prasad, “Acoustoelectric Effect in semiconductor materials Devices”, Chinese Journal of Acoustics, Vol. 9, No. 3, pp 275 – 279, 1990.
4. V. R. Singh, Awadhesh Prasad and Sanjay Yadav, “Ultrasonic Stress Effect on a Germanium Based Junction Transistor”, Acustica, Great Britain, Vol. 71, pp 79 – 80, 1990.
5. Awadhesh Prasad and V. R. Singh, “Characteristics of Silicon Laser p-i-n photodiodes in Ultrasonic Field”, IETE, New Delhi, Technical Review, Vol. 7, No. 1, pp 64 – 65, 1990.
6. V. R. Singh and Awadhesh Prasad, “Technical Note: Effect of Ultrasonic Stress on offset voltage of operational Amplifier Devices”, Noise control Engineering Journal, USA, Vol. 35 No.2, pp 65 – 67.
7. V. R. Singh and Awadhesh Prasad, “Effect of Ultrasonic Stress on the N-Type Silicon

Photodiodoes", ITBM, France, Vol. 10 No, pp 567-571, 1989.
8. Awadhesh Prasad, "Effect of Ultrasonic Stress on the Solid State Devices and Materials", ISST Journal of Applied physics, Vol. 3 No. 1, pp 41 – 47, 2012.
9. Awadhesh Prasad, "Effect of ultrasonic Stress on the Silicon Based p-n-junction diodes", Vol. 3, No. 1, pp 17 – 20, 2012 ISSN No. 0976 – 903x, Intellectuals Society for Socio – Techno Welfare (ISST) Journal of Applied Physics.
10. Awadhesh Prasad, "Effect of Ultrasonic stress on the solid state devices and Materials", ActaCineciaIndica, Vol. XXXVIIP, No. 2, pp 85 – 88, 2011, Meerut, UP.
11. Awadhesh Prasad, "UtrasonicRadiation Pressure Effect in Materials and Devices", ISST Journal of Applied Physics, Vol. 3, No . 2, pp 1-6, 2012.
12. Awadhesh Prasad, "Effect of Ultrasonic Stress on Solid State Devices and Materials," ISST Journal of Applied Physics, Vol . 7, No .1, 2016.
13. RohnTruell, Charles Elbaum and Bruce B. Chick, Ultrasonic Methods in Solid State Physics, Academic Press, New York, 1969.

Mechanical Properties of A β–Ti -Xnb-3.5sn Alloy Synthesized by Mechanical Alloying and Cold Isostatic Pressure

[1] Abdel-Nasser Omran, [2] Mohammed Y. Abdellah, [3] Soltan Ghanim Al-Fadli
[1] Mining and Metallurgical Dept. Faculty of Engineering, Al-Azhar University, Qena Egypt
[2] Mechanical Engineering Department, Faculty of Engineering South Valley University, Egypt
[3] Ministry of public Work, Kuwait

Abstract: **-- A developed □-Ti-xNb-3.5%Sn (wt%) alloy was synthesized by mechanical alloying of high energy ball milled powders and powder consolidation with cold isostatic pressure (CIP). The starting powder materials were as mixed powders and powders were produced by high energy ball milling (HEBM) for 1 hr, 2 hr and 4 hr respectively. The bulk solid samples were fabricated by the (CIP at temperature of 900-1050 oC for 2 hrs. It was found that the Ti was completely transformed from □ to □ phase after milling for 4 hr in powder state, and almost transformed to □-Ti phase with the sintered specimen at 1000 oC. The homogeneity of the sintered specimen increases as the milling time, Nb contents and sintering temperature increase. Also the hardness of the sintered alloys increases as increase of sintering temperature, Nb contents and milling time, reached to a value of 400 HV with 4 hr milling time. The Young's modulus is almost constant for all sintered Ti-x%Nb-3.5%Sn specimens at different milling time. Young's modulus is law (62.-66Gpa) compared to the standard alloy of Ti-6Al-4V about (110 Gpa).**

Index Terms: - Biomedical materials, Ti-Nb-Sn alloys, □ titanium, mechanical alloying, mechanical properties, Young' Modulus.

I. INTRODUCTION

Ti has a lustrous finishing and characterized with silver color, low density and high strength. It has a high ability to resist corrosion in various media such as sea water, aqua regia and chlorine [1]. Ti is also claimed to be biocompatible since it is nontoxic nor rejected by the human body. Thus, Ti and its alloys can be used in various medical usages, e.g. surgical implements and implants, and in dentistry So that these materials and their alloys could be widely used as permanent implant materials in the replacement of damaged hard tissues such as those in artificial hip joints and teeth due to their excellent corrosion resistance, high strength and biocompatibility [2- 4]. Some of these materials have been registered as standard materials for biomedical applications, but there have been some problems for using these materials [5-6]. For example, the vanadium in the standard Ti-6Al-4V alloy which is a standard registered material for making implants is known to be a toxic element, both in the elemental state and in its oxide form. Also the applications of Ti–Ni shape memory alloys are limited by the toxicity and hypersensitivity of nickel in spite of having been applied successfully in many medical areas [7,8]. In order to overcome these problems, new Ti-based alloys with non-cytotoxic and biocompatible elements such as Nb, Ta, Sn and Mo have been developed, as a result, Nb, Ta, Mo, Zr and Sn are selected as the safest alloying elements to titanium. [9, 10]. A lower elastic modulus between the bones and implant materials is preferable for an orthopedic alloy [11]. Recently, □-titanium alloys, and Ti–Nb, and Ti–Ta based alloy systems have been studied to achieve both lower elastic modules and higher tensile strengths than commonly possible with metals and alloys. These studies mostly utilized casting processes to make the test samples of the alloys [5, 12]. In terms of the effects of alloying elements on the phase transformation of titanium alloys, some elements such as Mn, Cr, Fe, Mo, V and Nb are the □□phase stabilizing alloying elements, and some alloying elements such as Zr and Sn have principally no effect on the □-to-□ transformation temperature [13,14]. The favored titanium alloy for biomedical applications should have low elastic modulus, excellent mechanical strength, corrosion resistance, formability, and no potential toxic elements [17,18]. When the clinical durability of a renewal is considered, its wear resistance is one of the important characteristics that must be studied. However, wear testing procedures are not standardized, and many types of wear testing have been used [19,20]. In general, metals with low theoretical tensile and shear strengths exhibit higher coefficients of friction than high-strength materials [19, 21]. Therefore, in order to select a suitable

dental material, it is the most important to understand wear behavior of experimental materials [22, 23]. The aims of this study are to characterize the microstructure, mechanical properties as well as hardness for a new biomedical material. The new alloys are prepared from Ti , Nb and Sn at different niobium contents using mechanical alloying of elemental powders and consolidation of the powders using cold isostatic pressure (CIP) at different temperatures.

II. EXPERIMENTAL PROCEDURE

Elemental powders of high purity Ti (99.9%), 100 mesh, Nb 99.9%, and Sn 99.8% 325 mesh were used as the starting reactant materials. The powders were blended for 4 hours using a low speed milling machine in a plastic jar, with a ball to powder ratio of 10:1. The other experiments were carried out using a high-energy Ball Mill (HEBM) model TH1080. The materials were placed in a stainless steel vial with a stainless steel ball. Isopropyl alcohol (7 drops) was placed in the vial before the vial was sealed in a glove box under Ar gas atmosphere. The desired ball-to-powder weight ratio was 6:1. The milling procedure was conducted at room temperature for three different milling times (1, 2 and 4 hours) using HEBM.

The milled powder was tested by X-ray diffraction (XRD) with CuK radiation and transmission electron microscopy (TEM) operated at 200 kV for observation of the structural changes of the powders. The morphological (shape and size) changes of the produced powders were analyzed using scanning electron microscopy (SEM) operated at 15 to 25 kV. Energy dispersive spectroscopy (EDS), via SEM techniques, was used to analyze the concentration of the constituent elements. The produced powders were placed in a cylindrical stainless steel die 15 mm diameter and pressed using a uniaxial pressure of 60 MPa for 5 min was applied to the powder compact. The perfumes were sintered in a muffle furnace under Ar atmosphere at 1173, 1273 and 1373 K (900, 1000 and 1050oC). After sintering, the samples were ground and polished for subsequent indentation and microscopy studies. Density is determined by Archimedes' principle, using an accurate balance with 0.1 mg accuracy. The microstructure of the sintered samples was characterized using X-ray diffractometry (XRD) with Cu-K radiation and scanning electron microscopy (SEM) operated at 15 to 25 kV. Energy dispersive spectroscopy (EDS) via SEM was used to analyze the concentration of the constituent elements. After sintering, the samples were ground and polished for subsequent indentation and microscopy studies. Density is determined by Archimedes' principle, using an accurate balance with 0.1 mg accuracy. The microstructure of the sintered samples was characterized using X-ray diffractometry (XRD) with Cu-K radiation and scanning electron microscopy (SEM) operated at 15 to 25 kV. Energy dispersive spectroscopy (EDS) via SEM was used to analyze the concentration of the constituent elements. The hardness test was carried out using Vickers hardness (load 0.5 Kgf). The compressive strength was carried out using compression tensile test equipment on the sintered specimen at 1000℃, the Young' Modulus was estimated and compare with Ti-6Al-4V.

III. RESULTS AND DISCUSSION

3.1 Sintering behavior of the powder compacts using CIP

XRD analysis was carried out to observe the phase changes during milling times as shown in Fig 1. This figure shows the XRD patterns for Ti-36%Nb-3.5%Sn powders produced by 4 hrs. From this figure, it can be seen that the intensity of the -Ti peaks is completely disappeared after 4 hr milling. Also, the intensity of the Sn peaks also is completely disappeared after 4 hr milling. The as-mixed powder contain only the -Ti peaks, Nb and Sn peaks as starting materials, thereby during mixing the reaction between the elemental phases was started. The Nb and Sn may have been dissolved in Ti phase to form a solid solution and the presence of Nb act as -Ti stabilizer as shown in Figure 1.

Figure 2 shows the SEM micrographs of the (a) as-mixed and (b) 1 hs, (c) 2 hrs, and (d) 4 hrs HBEM powders. The figure indicates that the particle size decreased with an increasing milling time. The as-mixed and 1 hr HEBM particles were plate shaped, as shown in Figures 2(a) and (b), while the particles shown in Figs. 2(c) and (d) were smaller and more rounded. From Fig. 2, the average particle sizes were 15 μm, 12 μm, 9 μm, and 7 μm for the as-mixed, 1 hr, 2 hrs., and 4 hrs. HBEM powders, respectively.

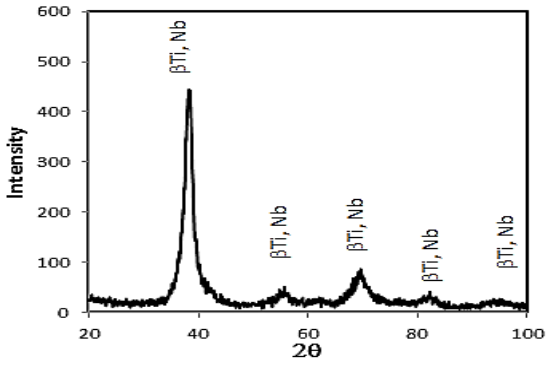

Fig. 1 XRD diffraction patterns for Ti-36Nb-3.5Sn

alloys produced by mechanical alloying at milling time 4hr using HEBM.

Fig 3 shows the XRD patterns of the sintered samples produced by CIP using as mixed and milled powders for 1, 2 and 4 hrs. The XRD analysis shows that there are 3 phases: □-Ti, □-Ti and FeO in all sintered samples. The intensity of FeO was appeared due to Fe formed by collision between vial and steel balls. From the comparison of the intensity of the (101) plane of □-Ti phase in the XRD patterns, it is clear that the fraction of □-Ti phase in the sintered samples clearly decreased in the order of as-mixed powder, and 1 hr, 4 hr and 12 hr HEBM powders. In the meantime, the fraction of the new phase increased in the same order. Decreasing particle size made a stabilizing of □-Ti phase by Nb and made high surface area between Ti and Nb. It encourages creating good homogeneity of solid solution. It can be concluded that the sintered sample by PCAS using 4 hr HEBM powder was almost the □-Ti phase [23].

Fig. 4 shows the SEM micrographs for the sintered samples produced by CIP of different powders at 1000 oC. From this figure, the sintered samples using as mixed and 1 hr HEBM powders showed large Ti rich □-Ti phase regions as shown in Figures 4 (a) and (b). The size of the Ti rich □-Ti phase regions decreased with increasing milling time, and in the meantime, the homogeneity of the □-Ti (or new phase) particles also increased dramatically. The chemical compositions of the dark and light phases in the as mix sample sintered at 1000 oC were analyzed using EDS and marked as points 1, 2 as shown in Fig. 5(a). As shown by the EDS spectra in Figure 5, a composition of the light phase (Point 1) almost niobium while a composition of the dark or black phase (Point 2) was much closer to that of Ti. From this result, it is clear that the dark phase is □ metastable phase containing Nb, while the light phase is Nb rich □-Ti phase. This is confirmed by Ti-Nb phase diagram[24] the □-Ti phase increased with increasing Nb content at temperature lower □-Ti to □-Ti transformation temperature (882℃).

Fig 6 shows the backscattered electron SEM micrographs for the sintered samples at 1000℃ at different milling time using CIP of as mixed and milled powders for 1, 2 and 4hrs.

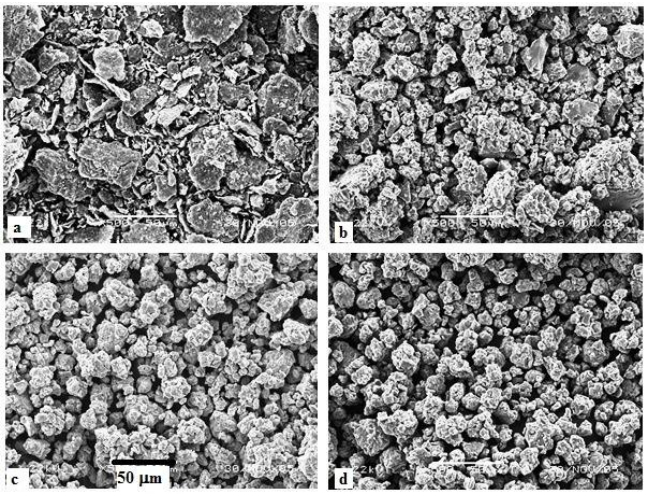

Fig.2 Shows the SEM micrographs for Ti-36Nb-3.5Sn alloys produced by mechanical alloying at (a) as-mixed and (b) 1 h, (c) 2 h, and (d) 4 h HBEM powders

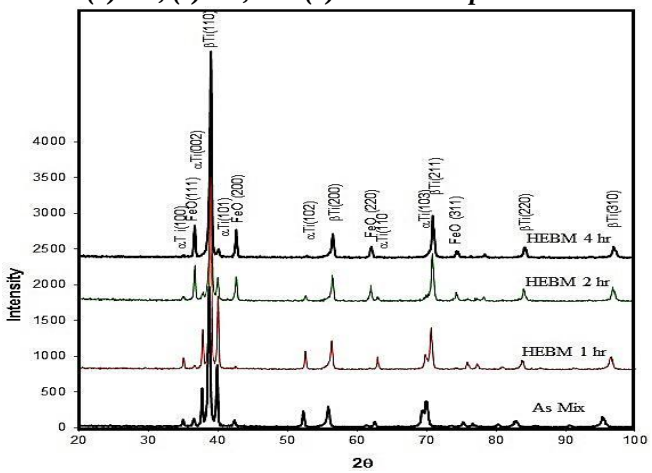

Fig. 3 XRD diffraction patterns of the bulk samples produced by CIP of different powders at 1000℃[29].

From this figure, the sintered samples using as mixed consists of large white area (particles) within black matrix and the white particles increase as milling time increase. Also the particles size of the mixture decreased with increasing milling time, and in the meantime, the homogeneity of the mixture also increased dramatically. Fig. 7 EDS point analysis for point "1" and "2" in Fig. 6(a). The chemical compositions of the dark and light phases in the sample at (point 1) almost twice higher than that of Nb (Ti~65% and Nb ~32%), while a concentration of Nb (about 41%) of the light phase (point 2) was much closer to that of Ti (about 54%). From this result, it is clear that the dark phase is a metastable □□Ti phase containing Nb, while the light phase is Nb rich □-Ti phase. This is confirmed by Ti-Nb phase diagram [24]; the □-Ti phase

 ISBN: 978-81-932966-9-1

increased with increasing Nb content at temperature lower than the □-Ti to □-Ti transformation temperature (882℃). Fig 8 shows X- ray mapping images indicating the distribution of Ti, Nb and Sn in the bulk samples produced by CIP at 4hrs milling and sintering temperature at 1000℃. From this figure, it can be seen that Ti, Nb and Sn formed a □-Ti based homogeneous solid solution. This was confirmed by the XRD analysis Fig 3.

The variation of relative density versus temperature of sintered specimens by CIP under a pressure of 60 MPa and sintered at 1000 oC using as mixed powder and milled powder for 1 hr, 2 hrs and 4 hrs are shown in Fig 9. The density of specimens increased with increasing temperature up to 1000℃ and then slightly decreased with temperature. The increase of density at the temperature range from 900 to 1000℃ reaches to the maximum value of 0.87 at milling time 4 hrs and the sintering temperature of 1000oC. It can be noticed that, as the temperature increases, porosities decrease might be due to the higher liquid phase transaction during sintering that could be the main reason for increasing relative density But the slight decrease of density with temperature is due to the grain gross leads to increasing the inter-granular vacancies. At the same temperature the relative density increases due to the decrease of particles size as the milling time increases.

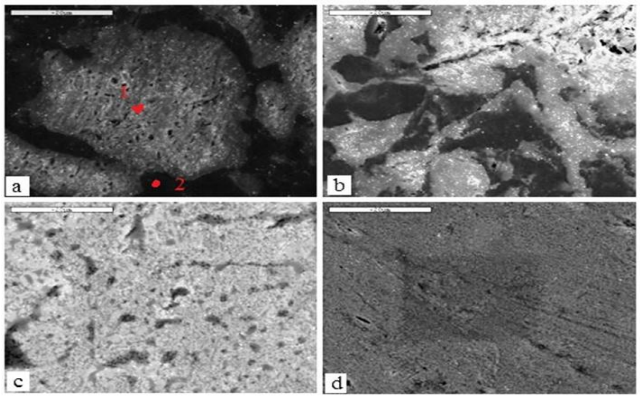

Fig.4 Shows the SEM micrographs for Ti-36Nb-3.5Sn alloys produced by mechanical alloying sintered at 1000 oC at (a) as-mixed and (b) 1 hr, (c) 2 hrs, and (d) 4 hrs HBEM powders

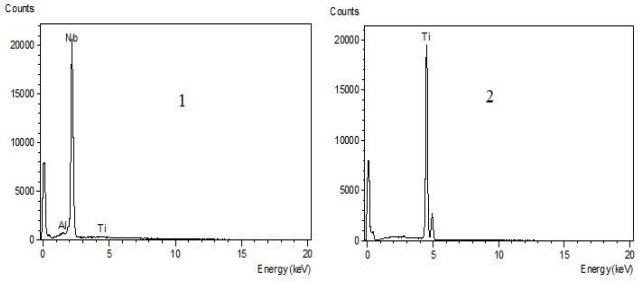

Fig. 5. EDS point analysis for points 1 and 2 in Figure 4a

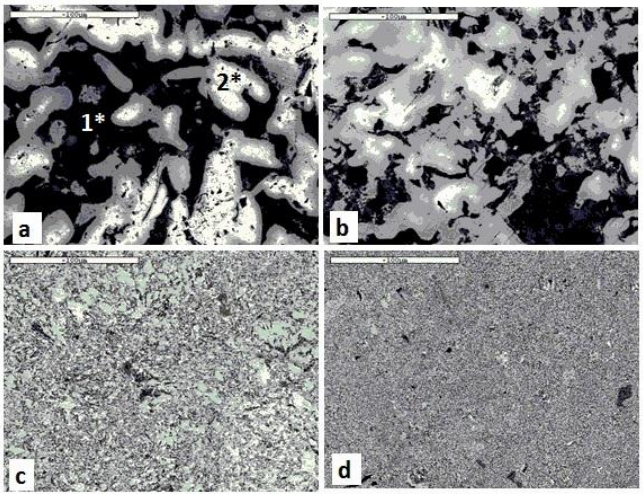

Fig. 6 Backscattered electron SEM micrographs of the bulk samples produced by CIP of different powders at 1000℃: (a) as-mixed powder (b) 1hr milling; (c) 2hrs milling (d) 4hrs milling.

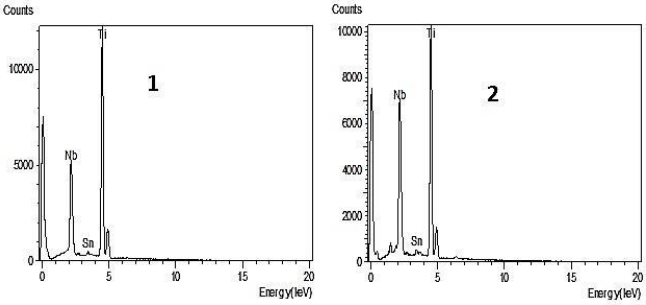

Fig. 7 EDS point analysis for point "1" and "2" in Figure 6(d).

3.3. Mechanical properties

3.3.1 Hardness

Vickers hardness values (Hv) of the bulk Ti–xNb–3.5Sn alloy with different milling time and sintering temperature using CIP under identical sintering conditions are shown in Fig.10. The results show that the hardness of the alloy increases as the sintering temperature increases at the same milling time. In addition, for the same sintering temperature, the hardness (Hv) of the bulk alloys also increased with increasing milling time, converging to a value of 390 Hv with milling time 4 hrs using high energy ball mill and 1050℃ sintering temperature. The lowest hardness of 350 Hv was reported for samples at as mix and sintering temperature 900℃. The increasing of hardness might be due to the increasing the milling time could be improving homogenization and densification in addition to the increase of sintering temperature might reduce the porosities and increase the making of solid solution that could be a reason

for increasing the hardness. Also The effect of Niobium on the Vickers hardness values (Hv) of the bulk Ti–xNb–3.5Sn alloy with different milling time at sintering temperature 1000oC using CIP are shown in Fig.11. The results indicated that slightly increasing of hardness as niobium contents increase. The increasing of Vickers hardness values with increasing niobium contents is attributed to the increasing the amount of solid solution leads to increase the homogeneity.

3.2 Young' Modulus

Fig. 12 shows the elastic modulus of the bulk Ti–xNb–3.5Sn alloy with different milling time and sintering temperature using CIP under identical sintering conditions.

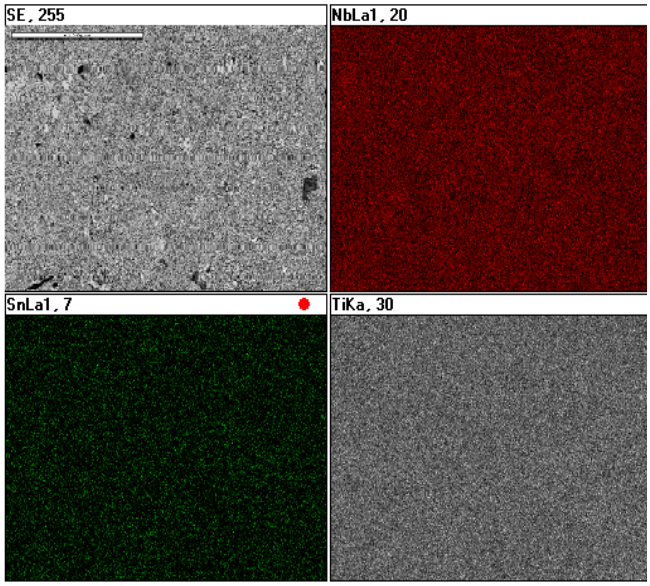

Fig. 8 X-ray mapping images for the distribution of Ti, Nb and Sn in the bulk sample produced by CIP of 4-hrs milled powder at 1000℃

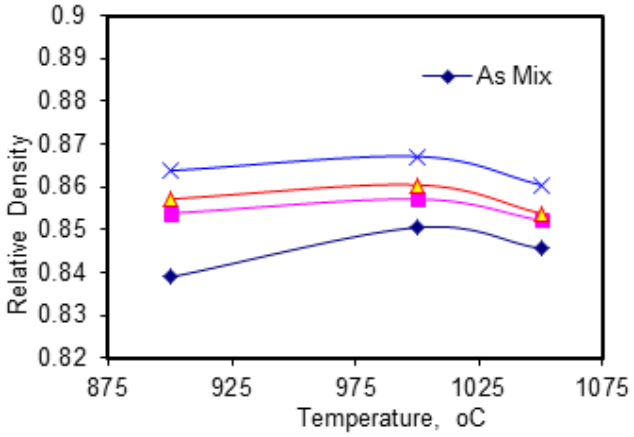

Fig. 9 Effect of temperature on the relative density in the produced Ti-36Nb-3.5Sn alloys by CIP at different milling time .

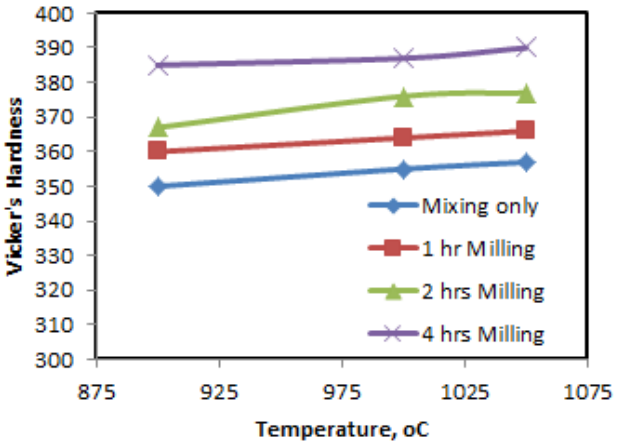

Fig.10 Effect of the temperature on the hardness of the sintered specimens at: as-mixed, 1hr, (3) 2 hrs-, 4hrs milled

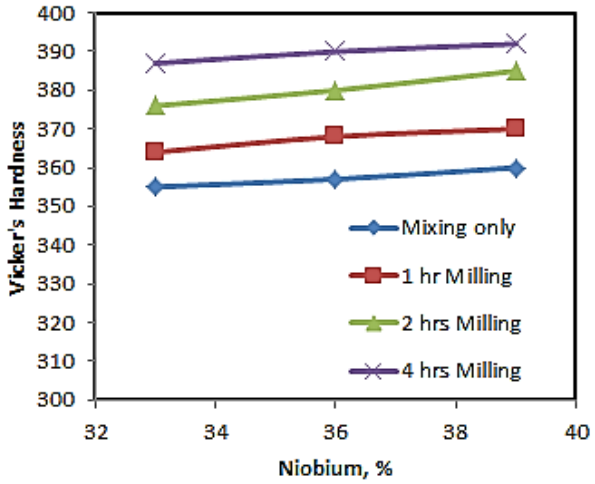

Fig.11 Effect of Niobium contents on the Vickers hardness of the sintered specimens at

(1) as-mixed, (2) 1hr-milled, (3) 2 hrs-milled, (4) 4hrs-milled -The results show that the Young's modulus of the alloy decreases as the sintering temperature increase up to 1000oC then the Young's modulus increases at the same milling time. In addition, at the same sintering temperature, the Young's modulus of the bulk alloys also increased with increasing milling time, converging to a value of 66.4 GPa with milling time 4 hrs using high energy ball mill and 1050℃ sintering temperature. The lowest value of Young's modulus was reported for samples at as mix and sintering temperature 1000℃. In spite of the hardness increases with increasing the milling time, the elastic modulus is almost constant at all milling time. This due to the increasing of □□□I phase in the sintered specimens with increasing milling time leads to the Young' modulus stability [24].

 ISBN: 978-81-932966-9-1

while the elastic modulus of Ti-6Al-4V Ingot is about 110 MPa. It can be conclude that the addition of Nb and Sn to the sintered Ti–xNb–2.5Sn alloys is reduced the elastic modulus to two third of the elastic modulus belongs to Ti-6Al-4V ingot. Also The effect of Niobium on the Young's modulus of the bulk Ti–xNb–3.5Sn alloy with different milling time at sintering temperature 1000oC using CIP are shown in Fig.13. The results indicated that linearly decreasing of Young's modulus as niobium contents increase. The decreasing of Young's modulus values with increasing niobium contents is attributed also to the increasing of solid solution amount leads to increase the homogeneity.

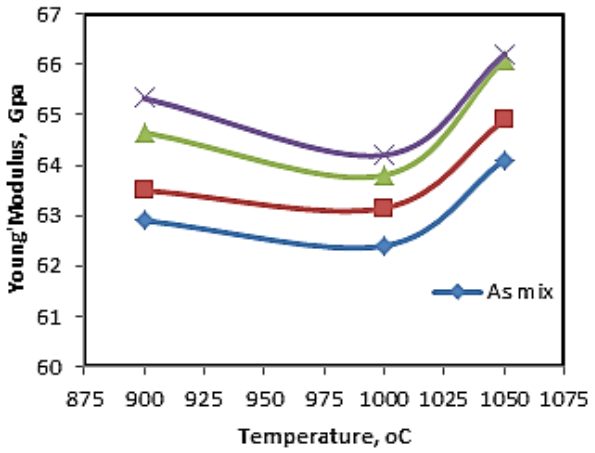

Fig. 12 The results of young's modulus of the sintered Ti–36Nb–3.5Sn specimens at different temperature : as-mixed, 1hr, (3) 2 hrs-, 4hrs milled

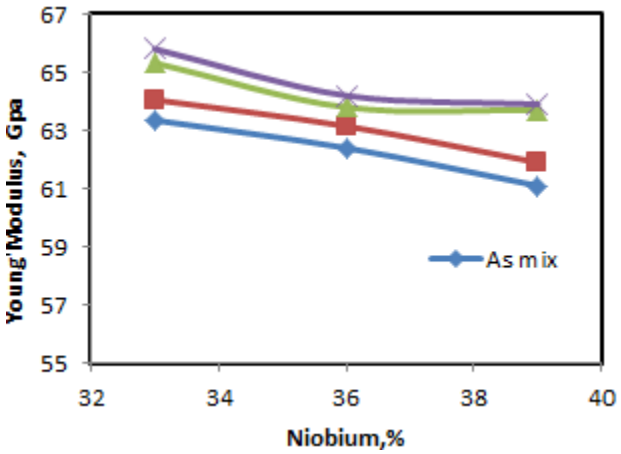

Fig.13 Effect of Niobium contents on the Vickers hardness of the sintered specimens at : as-mixed, 1hr, (3) 2 hrs-, 4hrs milled

IV. CONCLUSIONS

This study was conducted to observe the phase transformation of Ti-x%Nb-3.5%Sn during milling for various milling times using high-energy ball milling machine (HEBM). Also another objective are to observe microstructure, as well as mechanical for a new biomedical material of Ti-x%Nb-3.5%Sn sintered at different temperature and different particle sizes of milled powder.

The results are summarized as below.

1. The XRD analysis validated the complete transformation of the produced powder from □□Ti to □□Ti after 4 hrs milling time using HEBM in powder state and almost transformed to □□Ti after sintering at 1000 oC using CIP.

2. Decreasing particle size made a stabilizing of □□Ti by Nb and made high surface area between Ti and Nb encourage to create good homogeneity solid solution. and the sintered powder using CIP at 4hrs HEBM powder is almost the □□Ti.

4. The sintered temperature at 1000 oC to ensure that completely transformed from □□Ti to □□Ti.

5. The hardness of the sintered alloys is increased with increasing sintering temperature at the same milling time. Moreover, for the same sintering temperature, the hardness (Hv) of the bulk alloys also increased as the milling time and niobium contents increase, reached to a value of 395 Hv of the sintered alloys at 1050 oC using 4hrs HEBM powder. The lowest hardness of 348 Hv was reported for sintered samples at 900 oC using as mixed powder.

6. The Young' modulus of the sintered Ti–xNb–3.5Sn alloys is almost constant even if the hardness increased. The presence of Nb and Sn in the sintered Ti–Nb–3.5Sn alloys is reduced the elastic modulus comparing with the elastic modulus belongs to Ti-6Al-4V ingot.

REFERENCES

1. Xiaotian Liu, Shuyang Chen, James K.H. Tsoi, and Jukka Pekka Matinlinna, Regenerative Biomaterials, (2017) 315–323

2. W. Elshahawy , I. Watanabe, Tanta Dental Journal 11 (2014) 150-159.

3. Hamouda IM, Enan ET, Al-Wakeel EE, Int J Oral Maxillofac Implant 27 (2012)776–784.

4. Elias L.M., Schneider S.G., Schneider S., Silva H.M., and Malvisi F., Mater. Sci. Eng. A, 432:108 (2006).

5. Zhou Y.L., Niinomi M., Akahori T., Mater. Sci. Eng. A, 384: 92 (2004).

6. Gordin D.M., Gloriant T., Nemtoi Gh., Chelariu R., Aelenei N., Guillou A. and Ansel D., Mater. Lett. 59:2936 (2005).

7. Han-Sol Kim, Won-Yong Kim and Sung-Hwan Lim, Scr. Mater., 54: 887 (2006) .

8. Mantani Y., Tajima M., Mater.Sci. Eng. A, 438–440: 315 (2006).

9. Takahashi E., Sakurai T., Watanabe S., Masahashi N. and Hanada S., Mater. Trans. 43, No.12: 2978 (2002).

10. Kim H.Y., Kim J.I., Inamura T., Hosoda H. and Miyazaki S., Mater.Sci. Eng A 438–440: 839 (2006).

11. Nag S., Banerjee R., Fraser H.L., Acta Biomaterialia, 3: 369 (2007).

12. Rengen Ding, Ian P. Jones and Huisheng Jiao, Mater. Sci. Eng., A 458:126 (2007).

13. Seung Eon Kim, Jung Hyun Son, Yong Taek Hyun, Hi Won Jeong, Yong Tai Lee, Jae Sung Song, and Jun Hee Lee, Met. Mater.-Int., 13, No. 2: 151(2007).

14. Choubey A., Balasubramaniam R., Basu B., J. of Alloys and Compounds 381:288 (2004).

15. Hwan-Cheol Kim, In-Jin Shon, Jin-Kook Yoon, Jung-Mann Doh, Inter., J. of Refractory Metals & Hard Materials 25:46(2007).

16. A. Nouri, P.D. Hodgson, C.E. Wen, Acta Biomater. 6,1630–1639 (2010).

17. Alireza Nouri, et al., Mater. Sci. Eng., A 485, 562–570 (2008).

18. Yao Qiang, Sun Jian, Xing Hui, Guo Wen-yuan, Trans. Nonferrous Met. SOC. China 17, 1417-1421(2007).

19. H.Y. Kim et al., Mater. Sci. Eng., A 417, 120–128 (2006).

20. H.Y. Kim, J.I. Kim, T. Inamur, H. Hosod, S. Miyazaki; Mater. Sci. Eng., A 438–440, 839–843 (2006).

21. XU LI-juan, et al, Trans. Nonferrous Met. Soc. China, 19, 639-644 (2009).

22. A. M. Omran, K. D. Woo, D. K. Kim, S. W. Kim, M. S. Moon, N. A. Barakat, and D. L. Zhan, Metals and Materials International 14 -3 (2008) 321-325.

23. Abdel-Nasser Omran, Kee Do Woo, Eui Pyo Kwon, Nasser A. Barakat, Hyun Bom. Lee, Sug Won Kim, and Deliang Zhang, Sci. Adv. Mater. 1 (2009)205–211.

24. Eylon D., Properties and Selection: Nonferrous Alloys and Special-Purpose Materials, ASM International Handbook Committee, 2, 10 Ed. (1990).

Smart Trolley for a Smart Shopping

[1] Renjini Jose, [2] saleh Musallam Abdullah Al Harthi, [3] Ahmed Abdullah Awadh Koofan, [4] Aida Khamis Ahmed Al Raiisi
[1] Lecturer, [2, 3] Student, Department of Computing, Middle East College, Oman

Abstract: **-- Now world is in a digital era. In all the fields, education, medical, business, even in day-to-day life, prominence of technology is more. Millennial needs everything in one touch. So that in business filed, competitors are contesting harder in providing their services to people in the tranquil way. Especially this is very important in the retail shopping arena. As people are fond of shopping, day-by-day number goes on increasing. As a result the queue in front of cash counter is getting long, which the shopping lovers does not like. In this fast paced era, nobody want to wait for anything. In order to overcome these concerns, this paper propose the best possible solution - Smart trolley.**

Index Terms: - Smart trolley, easy shopping.

I. INTRODUCTION

Technology plays a key role in business filed. To enhance or expand upon the market, modern business world use highly innovative technologies. The changeover from traditional market to online shopping is one of the best epitomes for that. Everyday business field is finding new techniques to make customers life easier. One such new idea is smart trolley. Idea behind this smart trolley is that instead of using traditional trolley, a customer can use the smart trolley attached with tablet and can do the shopping by scanning each item.

II. INEVITABILITY OF SMART TROLLEY

The main aim of the smart trolley is to avoid the long queue in front of cash counter as customers can self-check out by using this smart system[2]. Other than it will also lessen the time of shopping and reduce the labor cost [3].

2.1 Survey on the requirement of smart trolley

In order to discern the opinion from communal, we conducted a survey in a shop and collected information from staff and customers regarding current shopping and about smart trolley. Everyone agreed on the difficulty of long queue in front of cashier counter especially on weekend. [3]In this paper there is detailed description regarding the difficulties of customers due to traditional way of shopping. [1]In this paper it is suggested that management is eager to modernize the traditional shopping system to attract customers by providing them with easy shopping and checkout options.

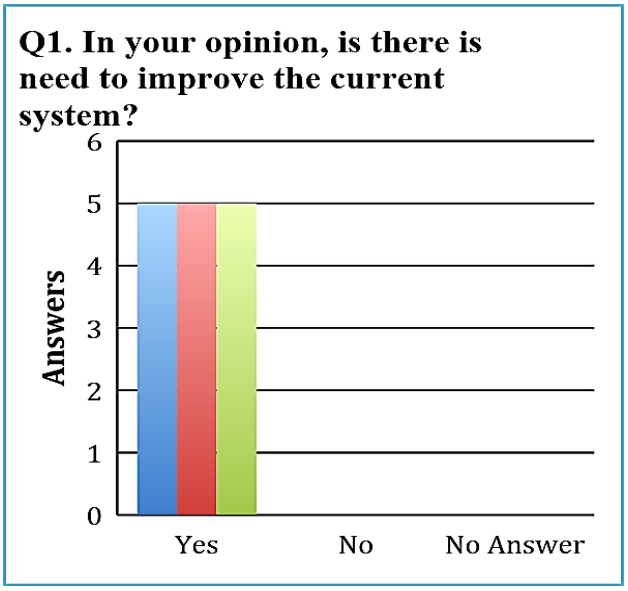

Fig: 1 Survey on current shopping system

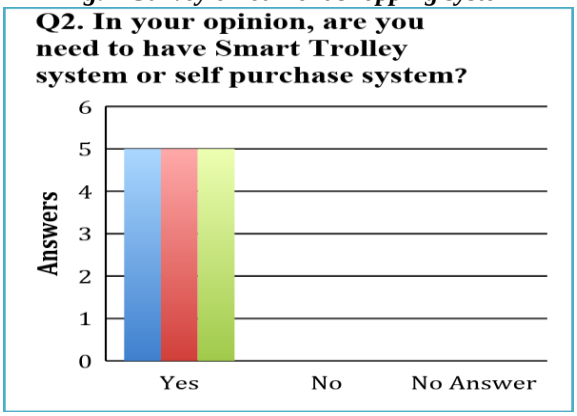

Fig: 2 Survey on smart trolley system

III. REQUIREMENTS:

- Hardware Requirements:

➢ Laptop with the below specifications along with screen, keyboard and mouse.

➢ Minimum 3 GB RAM

➢ Minimum 10 GB free space in Hard Drive.

➢ Minimum i5 processor.

➢ Trolley, Bar code reader, POS, RFID Sticker Tag, RFID reader, Tablet, Thermal Printer, Router.

- Software Requirements:

o Visual Studio to design the application

Microsoft SQL Server

IV. METHODOLOGY

Smart trolley consist of a scanner, card reader, a printer and a tablet in which the application is available. The customer will start Smart Trolley application by clicking on "Start Shopping Button" followed by scanning the products. The application keeps adding the items in the list and the total amount is updated accordingly. There is an option for customer to remove any product if not needed. Once the customer complete scanning, he/she can proceed with payment. For payment, application will provide two options for shopper; either self-checkout or proceed to counter.

4.1 Self-Check out

If customer prefers self-checkout, total amount to be paid will be displayed in the screen. Customer can pay using credit card or debit card by swiping the card in the card reader attached with the trolley. Once the payment is accepted, receipt will be printed through the printer. Automatically details will be stored in the database. This way customer can exit through the gateway.

4. 2 Counter Payment

If the customer prefers payment through counter, customer can select the option "Cash payment". Then the receipt will printed along with customer order id. With that order id, customer can proceed to the cash counter.

At the counter, cashier enter customer order id to check the order details and payment details. Cashier then enter payment amount and fill all the required information and then proceed for payment. Once the payment process is done, data will be updated in database and receipt will be print.

V. FLOWCHART

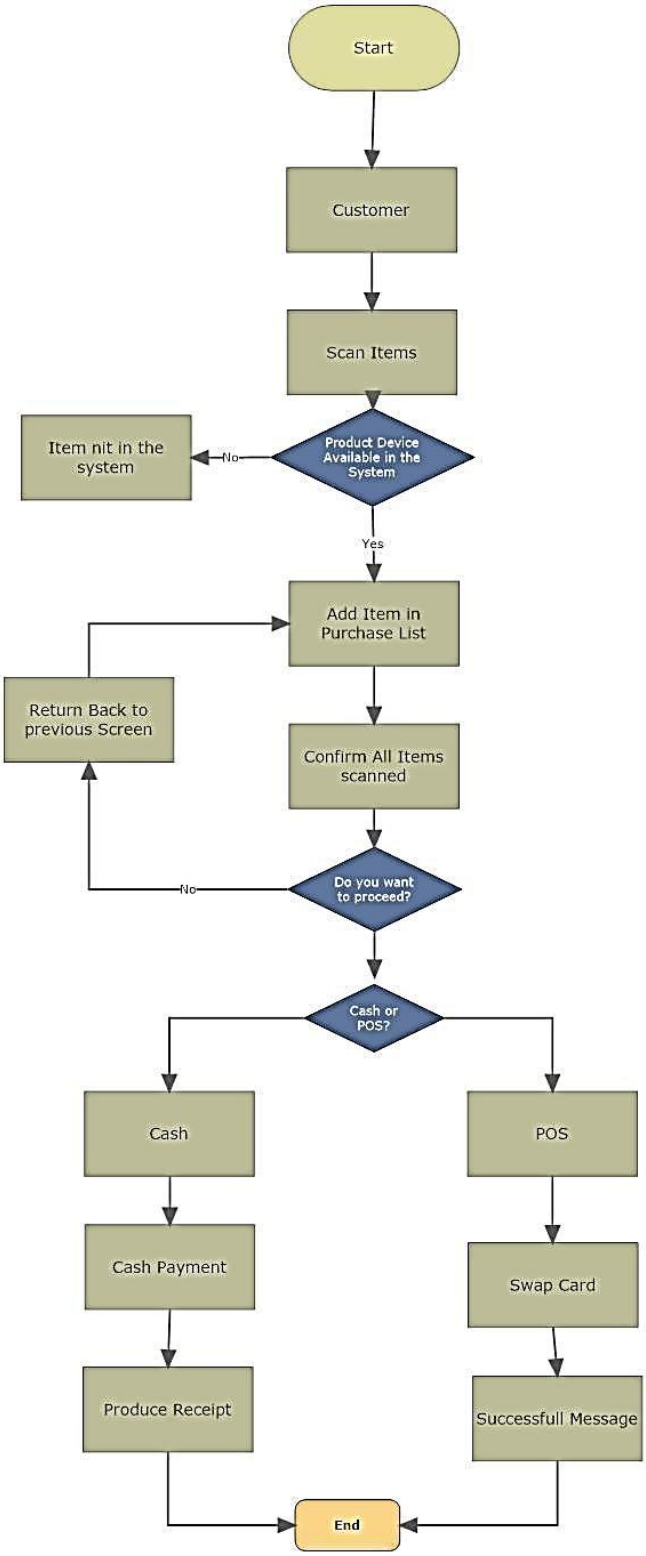

Fig: 3 Flowchart for customer

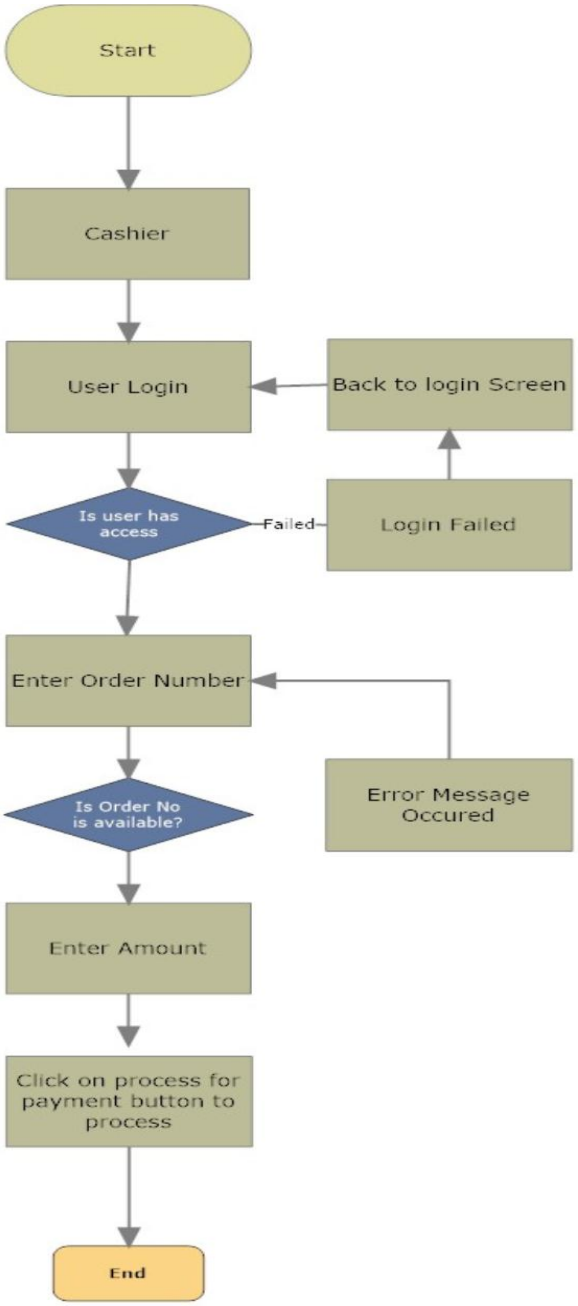

Fig: 4 Flow chart for cashier

VI. CONCLUSION

This paper discussed about the easiness of using a smart trolley for shopping. Instead of following the traditional way of shopping, if this smart system is implemented in hypermarkets, it will reduce the long waiting queue in front of the counter, thus saving the time of customers for a very enjoyable shopping experience.

VI. ACKNOWLEDGMENT

We would like to thank everyone who helped us to complete the project especially the peoples who cooperate with us to conduct the survey. Above all we thank GOD for all the blessings.

REFERENCES

1 S, Sainath; K,Surender; V,Vikram; and J, Thangakumar, "Automated Shopping Trolley for Super market billing System". International Journal of Computer Applications (0975 – 8887) 2014

2, Ankush Yewatkara , Faiz Inamdarb , Raj Singhc , Ayushyad , Amol Bandal, "Smart Cart with Automatic Billing, Product Information, Product Recommendation Using RFID & Zigbee with Anti-Theft". Procedia Computer Science 79, 793 – 800 2016

3. Vidya Palve, Arpita Mahale, Apurva Dandgaval, Unnati Deore, Prachi Jadhay, "Smart Trolley in MegaMall'.International Journal of Advanced Research in Science and Engineering" ,Vol No 6(2),408-415 2017.

4. Komal Ambekar, Vinayak Dhole, supriya sharma,Tushar Wadekar,"SMART SHOPPING TROLLEY USING RFID", International Journal of Advanced Research in Computer Engineering & Technology (IJARCET) Volume 4 no. 10.pp 3875-3877 2015.

Derivation of Probability Density Functions for Stress Concentration Factors In Uniplanar Tubular KT-Joints under In-Plane Bending Loads

[1] Hamid Ahmadi, [2] MirAmin MousaviNezhad Benam
[1] Faculty of Civil Engineering, University of Tabriz, [2] Faculty of Engineering, University of Maragheh

Abstract: **One of the crucial parameters in the fatigue reliability assessment of an offshore structure's tubular joints is the stress concentration factor (SCF). Depending on the joint geometry and loading type, the SCF exhibits considerable scatter which emphasizes the significance of deriving its governing probability distribution function. In the present paper, results of 144 finite element (FE) stress analyses, verified against experimental measurements, were used to develop a set of probability density functions (PDFs) for the SCFs in uniplanar tubular KT-joints under four types of in-plane bending (IPB) moment load cases. Based on a parametric FE investigation, a sample database was created for the chord-side SCFs of central and outer braces; and density histograms were generated for respective samples. Nine theoretical PDFs were fitted to the developed histograms and the maximum likelihood method was applied to evaluate the parameters of fitted PDFs. In each case, the Kolmogorov−Smirnov test was used to assess the goodness of fit. Finally, the Inverse Gaussian and Gamma models were proposed as the governing probability distribution functions for the central- and outer-brace SCFs, respectively. After substituting the values of estimated parameters, 10 fully defined PDFs were presented for the chord-side SCFs of central and outer braces in uniplanar tubular KT-joints under four types of IPB loading.**

Index Terms:- Uniplanar tubular KT-joint, Stress concentration factor (SCF), In-plane bending (IPB) load, Probability density function (PDF).

I. INTRODUCTION

Steel circular hollow sections (CHSs) are widely used in the offshore industry for the fabrication of jacket-type oil/gas production platforms. The welded connection among the main member (chord) and branch members (braces) in the space frame of a jacket structure is called a tubular joint (Fig. 1(a)). Tubular joints are subjected to cyclic stresses due to the wave loading; and consequently they are susceptible to fatigue damage. Hence, to ensure their safety and integrity, fatigue design is crucial. The stress-life (S–N) method, based on the hot-spot stress (HSS), i.e. extrapolated geometric stress at the weld toe, is widely used to estimate the fatigue life of the joints. The HSS can be calculated through the multiplication of nominal stress by the stress concentration factor (SCF).

The SCF is defined as the ratio of the local surface stress, at the brace/chord intersection, to the nominal stress in the brace. The value of SCF depends on the joint geometry, loading type, weld size and type, and the considered position for the SCF determination around the weld profile. Offshore structures are subjected to multi-axis loading; i.e. combined axial, in-plane bending (IPB) and out-of-plane bending (OPB) loads. The approach recommended by API RP2A [1] to calculate the HSS is to sum the products of the nominal stresses due to each load type and the corresponding SCFs. Under any specific loading condition, the SCF value along the weld toe of a tubular joint is mainly determined by the joint geometry (Fig. 1(b)). A set of dimensionless geometrical parameters including α, αB, β, γ, τ, and ζ are frequently used to relate the behavior of a tubular joint to its geometrical characteristics more easily. These parameters are defined in Fig. 1(c). Since limiting assumptions should be made on input parameters, a deterministic fatigue analysis usually results in conservative designs. Some of these parameters exhibit considerable scatter. This fact emphasizes the significance of running a reliability analysis in which the key parameters of the problem can be modeled as random variables. The fundamentals of reliability assessment, if properly applied, can provide immense insight into the performance and safety of the structural system. Regardless of the method used for the fatigue reliability analysis of steel offshore structures (i.e. either S–N or fracture mechanics (FM) approach), the probabilistic and statistical measures of the SCF are among the most important input parameters. The SCF shows considerable scatter highlighting the significance of deriving its governing probability distribution function.

In the present research, initially, available literature on deterministic and probabilistic analysis of SCFs was surveyed (Sec. 2). Afterwards, results from 144 finite element (FE) stress analyses, verified using experimental measurements, were used to derive a probability distribution model for chord-side SCFs in uniplanar tubular KT-joints under four different types of IPB loading (Fig. 1(d)). Based on the parametric FE study, a set of samples was generated for the central- and outer-brace SCFs (Sec. 3) and density histograms were created for respective samples (Sec. 4). Nine theoretical probability density functions (PDFs) were fitted to the developed histograms and the maximum likelihood (ML)

method was used to evaluate the parameters of fitted distributions (Sec. 5). In each case, the Kolmogorov−Smirnov test was applied to assess the goodness of fit (Sec. 6). Finally, the best-fitted distributions were detected and after substituting the values of estimated parameters, 10 fully defined PDFs were presented for the weld-toe central- and outer-brace SCFs in uniplanar tubular KT-joints under IPB loading (Sec. 7).

II. LITERATURE REVIEW

This section surveys the research works on the deterministic and probabilistic analysis of the SCF as a primary parameter in the fatigue design of tubular joints. For other aspects of the design, such as static strength, hysteretic behaviour, fire resistance, and crack considerations, the reader is referred to Yiyi and Wei [2], Choo [3], Lie et al. [4], Gao et al. [5], Liu et al. [6], Cui and Shao [7], Shao [8], and Nassiraei et al. [9], among others.

2.1. Deterministic studies on SCFs

The following three paragraphs summarize the literature available on unstiffened uniplanar joints, unstiffened multi-planar joints, and stiffened joints, respectively.

For uniplanar joints, the reader is referred for example to Efthymiou and Durkin [10], Efthymiou [11], Hellier et al. [12], Smedley and Fisher [13], HSE OTH 354 [14], and Karamanos et al. [15] (for the SCF calculation at the saddle and crown positions of simple uniplanar T-, Y-, X-, K-, and KT-joints), Gho and Gao [16], Gao [17], and Gao et al. [18] (for the SCF determination in uniplanar overlapped tubular joints), Morgan and Lee [19, 20], Chang and Dover [21, 22], Shao [23, 24], Shao et al. [25], and Lotfollahi-Yaghin and Ahmadi [26] (for the study of the SCF distribution along the weld toe of various uniplanar joints), and Pang and Zhao [27] (for the investigation of SCFs in dragline tubular joints).

For multi-planar joints, the reader is referred to Karamanos et al. [28] and Chiew et al. [29] [for the SCF calculation in XX-joints], Wingerde et al. [30] [for the SCF determination in KK-joints], Karamanos et al. [31] [for the study of SCFs in DT-joints], and Ahmadi et al. [32] [for the investigation of SCFs in three-planar tubular KT-joints], among others.

Ramachandra et al. [33] studied the effect of geometrical parameters on the SCFs in ring-stiffened tubular T- and Y-joints. Nwosu et al. [34] investigated the stress distribution along the brace/chord intersection of internally ring-stiffened tubular T-joints, under the action of axial, IPB, and OPB loads. Ramachandra et al. [35] studied the effect of internal ring stiffeners on the fatigue strength of tubular T- and Y-joints. Hoon et al. [36] investigated the SCF distributions along the intersections of a doubler-plate reinforced T-joint subjected to combined loadings. Myers et al. [37] studied the effect of three different longitudinal stiffeners on the SCFs in jack-up chords. Woghiren and Brennan [38] established a set of parametric formulas to calculate the SCFs in multi-planar tubular KK-joints stiffened by rack plates. Fatigue design equations for tubular KT-joints reinforced with internal ring stiffeners have been proposed by Ahmadi et al. [39] for axial loading and Ahmadi and Zavvar [40] for OPB loading.

2.2. Probabilistic studies on SCFs

In his comprehensive paper on the applications of probabilistic FM to offshore structures, Kirkemo [41] assumed that the SCFs follow a lognormal distribution with the CoV of 0.15 and the mean of 2.75 and 2.50 for axial and IPB loads, respectively.

Pillai and Prasad [42] performed a fatigue reliability analysis in time domain for the inspection strategy of fixed offshore structures. They assumed that the SCF has a lognormal distribution with the mean and CoV of 2.50 and 0.15, respectively. They investigated the sensitivity of the random variables that appear in the fatigue failure limit state equation and found that the SCF is one of the most sensitive variables and it accounts for considerable uncertainty in the probability of failure with respect to fatigue. This calls for greater emphasis in accurately determining the probability distribution of SCFs.

Mosayyebi and Aghakuchak [43] assumed a normal distribution for the SCFs with the mean of 2.56, 2.50, and 1.90 and the standard deviation of 0.26, 0.25, and 0.19 for axial, IPB, and OPB loads, respectively.

Rajasankar et al. [44] applying the reliability analysis to the structural integrity assessment of offshore tubular joints used the lognormal distribution for the SCF with the mean and standard deviation of 10.118 and 2.024, respectively.

Ahmadi and Lotfollahi-Yaghin [45] and Ahmadi et al. [46] performed fatigue reliability analyses, based on S−N and FM approaches, on two-planar tubular DKT-joints under axial loading. In these papers, a lognormal distribution was assumed for the SCF with the mean and standard deviation of 2.75 and 0.4125, respectively. Ahmadi and Lotfollahi-Yaghin [47] derived the PDFs for the weld-toe SCFs of the central brace in unstiffened multi-planar tubular DKT-joints under the axial loading. They suggested that the Birnbaum–Saunders distribution is the best probability model for the maximum value of the weld-toe SCF. Ahmadi et al. [48, 49] and Ahmadi [50] showed that the Inverse Gaussian, Gamma, and Generalized Extreme Value distributions are the best probability models for the maximum value of the weld-toe SCF in internally ring-stiffened tubular KT-joints subjected to axial, IPB, and OPB loads, respectively. They derived 15 fully defined PDFs for the maximum weld-toe SCFs of

central and outer braces, under nine different types of load cases.

III. DEVELOPMENT OF SCF SAMPLES FOR IPB-LOADED UNIPLANAR KT-JOINTS

A total of 36 FE models were generated using ANSYS and analyzed under four types of IPB loads, in order to develop a set of samples for the chord-side SCFs in uniplanar tubular KT-joints subjected to IPB loads. Altogether, 144 FE stress analyses were carried out; and to validate the FE results, experimental measurements were used. Details of FE modeling, parametric investigation, and samples organizing are given in the present section.

3.1. FE modeling and verification

3.1.1. Weld profile geometry

Accurate modeling of the weld profile is one of the most critical factors affecting the accuracy of SCF results. In the present research, the welding size along the brace/chord intersection satisfies the AWS D 1.1 [51] specifications. The dihedral angle (ψ) which is an important parameter in determining the weld thickness is defined as the angle between the chord and brace surface along the intersection curve. The dihedral angle at four typically important positions along the weld toe equals to: π / 2 (Crown), θ (Heel), π – cos–1θ (Saddle), and π – θ (Toe); where θ is the outer brace inclination angle (Fig. 1(b)). Details of weld profile modeling according to AWS D 1.1 [51] have been presented by Ahmadi et al. [32].

(a) Tubular KT-joints in a jacket structure during the fabrication

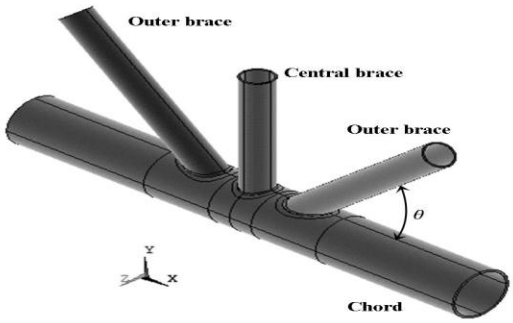

(b) Global geometry

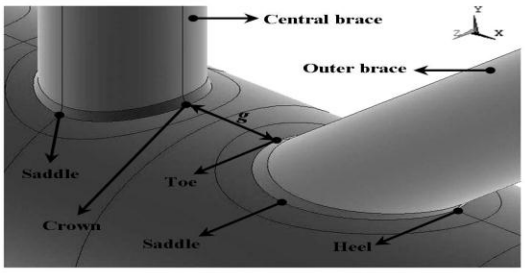

(c) Dimensionless parameters of the joint and critical positions along the weld toe

D: Chord diameter;
d: Brace diameter;
T: Chord wall thickness;
t: Brace wall thickness;
L: Chord length;
l: Brace length;
g: Gap

$\beta = d/D$
$\gamma = D/2T$
$\tau = t/T$
$\zeta = g/D$
$\alpha = 2L/D$
$\alpha_B = 2l/d$

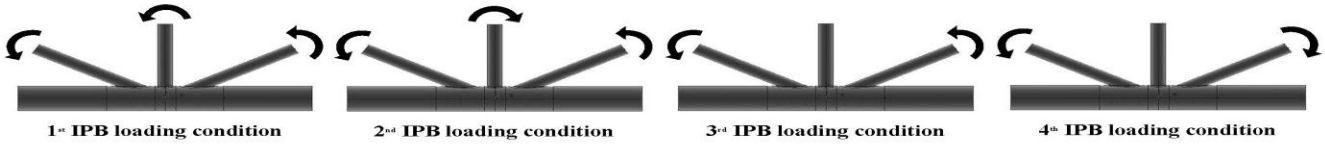

(d) Considered in-plane bending (IPB) loading conditions

Fig. 1. Geometrical notation and considered in-plane (IPB) moment load cases for studied uniplanar tubular KT-joints

3.1.2. Applied boundary conditions

The fixity condition of chord ends in tubular joints of offshore structures ranges from almost fixed to almost pinned with generally being closer to almost fixed [11]. Practically, the value of the parameter α in over 60% of tubular joints is in excess of 20 and is bigger than 40 in 35% of the joints [13]. Changing the end restraint from fixed to pinned leads to a maximum increase of 15% in the SCF at the crown position for joints with α = 6, and this increment reduces to only 8% for α = 8 [20]. In view of the fact that the effect of chord end restraints is only significant for joints with α < 8 and high β and γ values, which do not usually found in practice, both chord ends were assumed to be fixed, with the corresponding nodes restrained.

Symmetries and antisymmetries detected in IPB-loaded KT-joints of present study (Fig. 1(d)) are as follows:

The XY- and YZ-plane geometric symmetries

The XY-plane loading symmetry under all of four considered IPB loading conditions

The YZ-plane loading antisymmetry under the 1st, 2nd, and 3rd IPB loading conditions

The YZ-plane loading symmetry under the 4th IPB loading condition

Hence, in all cases, only one fourth of the entire joint is required to be modeled (Fig. 2(a)). Appropriate symmetric and antisymmetric boundary conditions were defined for the nodes located on the XY- and YZ-planes crossing the centroid of the chord.

3.1.3. Generated mesh

ANSYS element type SOLID95 was used to model the chord, braces, and the weld profiles. These elements have compatible displacements and are well-suited to model curved boundaries. The element is defined by 20 nodes having three degrees of freedom per node and may have any spatial orientation. Using this type of 3-D brick elements, the weld profile can be modeled as a sharp notch. This method will produce more accurate and detailed stress distribution near the intersection in comparison with a simple shell analysis.

To guarantee the mesh quality, a sub-zone mesh generation method was used during the FE modeling. In this method, the entire structure is divided into several different zones according to the computational requirements. The mesh of each zone is generated separately and then the mesh of entire structure is produced by merging the meshes of all the sub-zones. This method can easily control the mesh quantity and quality and avoid badly distorted elements.

As mentioned earlier, to calculate the SCF, the stress at the weld toe should be divided by the nominal stress of the loaded brace. The stresses perpendicular to the weld toe at the extrapolation points are required to be calculated in order to determine the stress at the weld toe position. To extract and extrapolate the stresses perpendicular to the weld toe, as shown in Fig. 2(b), the region between the weld toe and the second extrapolation point was meshed in such a way that each extrapolation point was placed between two nodes located in its immediate vicinity. These nodes are located on the element-generated lines which are perpendicular to the weld toe ($X_{\perp}$ direction in Fig. 2(d)).

To verify the convergence of FE results, convergence test with different mesh densities was conducted before generating the 36 FE models for the parametric investigation.

3.1.4. Analysis procedure and computation of SCFs

Static analysis of the linearly elastic type is recommended for the SCF determination in tubular joints [52]. The Young's modulus and Poisson's ratio were taken to be 207 GPa and 0.3, respectively.

The weld-toe SCF is defined as:

$$\text{SCF}=\sigma_{\perp W}/\sigma_n \quad (1)$$

In Eq. (1), σ_n is the nominal stress of the IPB-loaded brace which is calculated as follows:

$$\sigma_n=\frac{32dM_{IPB}}{\pi\left[d^4-\left(d-2t\right)^4\right]} \quad (2)$$

where MIPB is the in-plane bending moment; and d and t are the brace diameter and wall thickness, respectively.

To determine the SCF, the HSS should be calculated. The HSS is the stress at the weld toe position obtained through the extrapolation of the stresses from the outside of the region influenced by the local weld toe geometry. The location from which the stresses must be extrapolated, extrapolation region, depends on the dimensions of the joint and on the position along the intersection. According to the linear extrapolation method recommended by IIW-XV-E [53], the first extrapolation point have to be at a distance of 0.4T from the weld toe, and the second point should lie at 1.0T further from the first point (Fig. 2(c)).

In Eq. (1), $\sigma_{\perp W}$ is the extrapolated stress at the weld toe position which is perpendicular to the weld toe and is calculated by the following equation:

$$\sigma_{\perp W}=1.4\sigma_{\perp E1}-0.4\sigma_{\perp E2} \quad (3)$$

where $\sigma_{\perp E1}$ and $\sigma_{\perp E2}$ are the stresses at the first and second extrapolation points along the direction perpendicular to the weld toe, respectively (Fig. 2(c)).

The stress at an extrapolation point is obtained as follows:

$$\sigma_{\perp E} = \frac{\sigma_{\perp N1} - \sigma_{\perp N2}}{\delta_1 - \delta_2}\left(\Delta - \delta_2\right) + \sigma_{\perp N2} \quad (4)$$

where $\sigma_{\perp Ni}$ (i = 1 and 2) is the nodal stress at the immediate vicinity of the extrapolation point along the direction perpendicular to the weld toe (Eq. (5)); δ_i (i = 1 and 2) is the distance between the weld toe and the considered node inside the extrapolation region (Eq. (6)); and Δ equals to 0.4T and 1.4T for the first and second extrapolation points, respectively (Fig. 2(d)).

$$\sigma_{\perp N} = \sigma_x l_1^2 + \sigma_y m_1^2 + \sigma_z n_1^2 + 2\left(\tau_{xy} l_1 m_1 + \tau_{yz} m_1 n_1 + \tau_{zx} n_1 l_1\right) \quad (5)$$

where σ_a and τ_{ab} (a, b = x, y, z) are components of the stress tensor which can be extracted from ANSYS analysis results; and l_1, m_1, and n_1 are transformation components.

$$\delta = \sqrt{\left(x_w - x_n\right)^2 + \left(y_w - y_n\right)^2 + \left(z_w - z_n\right)^2} \quad (6)$$

In Eq. (6), (xn , yn , zn) and (xw , yw , zw) are the global coordinates of the considered node inside the extrapolation region and its corresponding node at the weld toe position, respectively.

At the crown, toe, and heel positions, Eq. (5) is simplified as:

$$\sigma_{\perp N} = \sigma_x \quad (7)$$

In the present research, the saddle position was not studied. The reason is that under the IPB loadings, the nominal stress at this position is zero and hence the determination of SCFs is not needed.

In order to facilitate the SCF calculation, above formulation was implemented in a macro developed by the ANSYS Parametric Design Language (APDL). The input data required to be provided by the user of the macro are the node number at the weld toe, the chord thickness, and the numbers of the nodes inside the extrapolation region. These nodes can be introduced using the Graphic user interface (GUI).

3.1.5. Verification of FE results based on experimental data

In order to verify the developed FE modeling procedure, a validating FE model was generated and its outputs were compared with the results of experimental tests conducted by Ahmadi et al. [54]. Details of test setup and program are not presented here for the sake of brevity.

The specimen fabricated by Ahmadi et al. [54] was tested under the axial loading. In order to verify the FE models using the data extracted from this experiment, the FE model of tested specimen was generated and analyzed under axial loading. The method of geometrical modeling (introducing the chord, braces, and weld profiles), the mesh generation procedure (including the selection of the element type and size), the analysis method, and the method of SCF computation are the same for the validating model and the IPB-loaded joints used here for the parametric study. Hence, the verification of SCFs derived from axially-loaded FE model with corresponding experimental values lends some support to the validity of SCFs derived from IPB-loaded FE models.

Moreover, in order to make sure that the IPB moment loading was correctly defined in ANSYS, nominal stresses obtained from the software were verified against the results of theoretical solid mechanics relations.

In Fig. 2(e), experimental data and FE results have been compared. In this figure, the SCF distribution along the central brace/chord intersection is presented. The polar angle (φ) along the 360˚ curve of the weld path is measured from the crown position. Hence, values of φ at the crown and saddle positions are 0˚ and 90˚, respectively. Due to the symmetry, only one fourth of the entire 360˚ SCF distribution is depicted.

The FE analysis predicts a stiffer structure than the actual one. This is expected, as the finite element model forces the structure into specific modes of displacement and effectively yields a stiffer model than the actual structure. This additional stiffness of the chord member yields to smaller deformation and consequently to lower SCFs of the chord member, compared to the experimental results. However, this does not mean that the results of FE models used for the parametric study are under-predicting. The reason is that weld sizes in FE models used for the parametric study satisfy the AWS D 1.1 [51] specifications and thus are smaller than weld sizes typically found in yard practice. Hence, as depicted in Fig. 2(e), the SCFs obtained from these models are higher than SCFs actually occurring in practice; and the FE results are even somewhat conservative.

As can be seen in Fig. 2(e), there is a good agreement between the test results and FE predictions. Hence, generated FE models can be considered to be accurate enough to provide valid results.

3.2. Details of parametric study

In order to prepare a sample database for the SCFs in uniplanar KT-joints subjected to four types of IPB loading (Fig. 1(d)), 36 models were generated and analyzed using ANSYS. The aim was to investigate the effects of dimensionless geometrical parameters on the chord-side SCFs at the crown, toe, and heel positions. As mentioned earlier, the saddle position was not studied. The reason is that under the IPB loading, the nominal stress at this position is zero and hence the determination of SCFs is not required.

Different values assigned to the parameters β, γ, τ, and θ are as follows: β = 0.4, 0.6; γ = 12, 24; τ = 0.4, 0.7, 1.0; and θ = 30˚, 45˚, 60˚. These values cover the practical ranges of

dimensionless parameters typically found in tubular joints of offshore jacket structures. Providing that the gap between the central and outer braces is not very large, the relative gap (ζ = g / D) has no considerable effect on the SCF values in a tubular KT-joint. The validity range for this conclusion is $0.2 \leq \zeta \leq 0.6$ [26]. Hence, a typical value of $\zeta = 0.3$ was designated for all joints. Sufficiently long chord greater than six chord diameters (i.e. $\alpha \geq 12$) should be used to ensure that the stresses at the brace/chord intersection are not affected by the chord's boundary conditions [11]. Hence, in this study, a realistic value of $\alpha = 16$ was designated for all the models. The brace length has no effect on SCFs when the parameter αB is greater than a critical value [21]. According to Chang and Dover [55], this critical value is about 6. In the present study, in order to avoid the effect of short brace length, a realistic value of $\alpha B = 8$ was assigned for all joints.

3.3. Organizing the SCF sample database

The SCFs extracted from the results of 144 FE stress analyses were organized as 10 samples for further statistical and probabilistic analyses. Samples 1−3 included the weld-toe SCFs under the 1st IPB loading condition at the crown position of the central (vertical) brace, heel position of the outer (inclined) brace, and toe position of the outer brace, respectively. Samples 4−6 included the SCFs at the same positions under the 2nd IPB loading condition. Samples 7 and 8 included the weld-toe SCFs under the 3rd IPB loading condition at the heel and toe positions of the outer brace, respectively; and finally Samples 9 and 10 included the SCFs at the same positions under the 4th IPB loading condition.

Values of the size (n), mean (μ), standard deviation (σ), coefficient of skewness ($\alpha 3$), and coefficient of kurtosis ($\alpha 4$) for these samples are listed in Table 1. The value of μ shows that the central-brace SCFs are generally higher than the corresponding outer-brace SCFs. The value of $\alpha 3$ for all samples is positive which means that the probability distribution for all samples is expected to have a longer tail on the right, which is toward increasing values, than on the left. Moreover, in Samples 3, 8, and 10, the value of $\alpha 4$ is greater than three meaning that the probability distribution is expected to be sharp-peak (leptokurtic) for these three

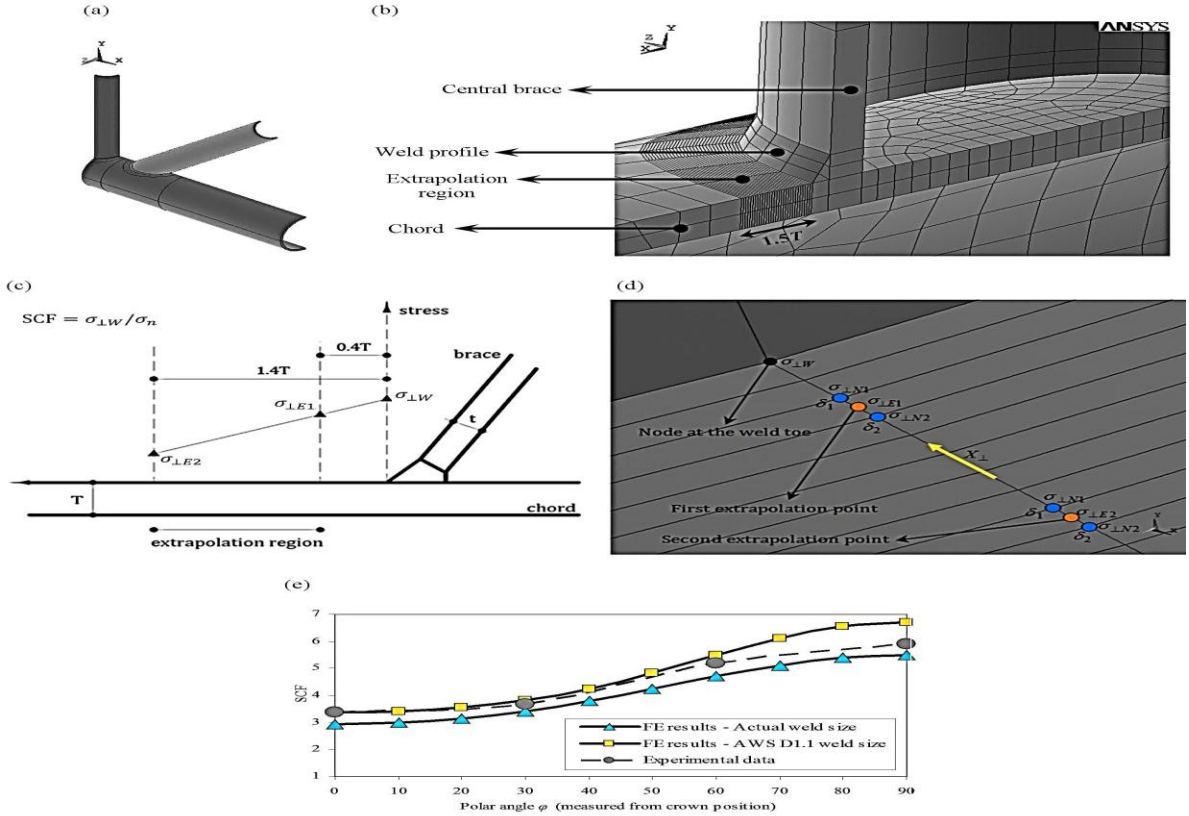

Fig. 2. (a) One fourth of the entire joint required to be modeled, (b) Mesh generated in the regions adjacent to the intersection, (c) Adapted linear extrapolation method, (d) Interpolations and extrapolations necessary to determine SCFs based on the stresses perpendicular to the weld toe, (e) Distribution of chord-side SCFs along the central brace/chord intersection of a uniplanar KT-joint: Comparison of the experimental measurements with the FE results

Table 1. Statistical measures of the generated samples

Statistical measure	SCF samples									
	Sample 1	Sample 2	Sample 3	Sample 4	Sample 5	Sample 6	Sample 7	Sample 8	Sample 9	Sample 10
	1st loading condition; central-brace crown SCFs	1st loading condition; outer-brace heel SCFs	1st loading condition; outer-brace toe SCFs	2nd loading condition; central-brace crown SCFs	2nd loading condition; outer-brace heel SCFs	2nd loading condition; outer-brace toe SCFs	3rd loading condition; outer-brace heel SCFs	3rd loading condition; outer-brace toe SCFs	4th loading condition; outer-brace heel SCFs	4th loading condition; outer-brace toe SCFs
n	36	36	36	36	36	36	36	36	36	36
μ	3.1583	2.483575	2.006375	3.2058	2.350050	2.174261	2.402727	2.084419	2.349544	2.217644
σ	1.2866	1.110180	1.226375	1.2648	1.177201	1.040296	1.129699	1.110468	1.118688	1.133185
α_3	0.5911	0.380664	0.865928	0.5643	0.534715	0.741863	0.499764	0.902267	0.460881	0.877139
α_4	2.2601	2.337246	3.043278	2.1843	2.536123	2.942387	2.518453	3.190353	2.524777	3.101219

samples which are all related to the SCFs at the toe position. In other SCF samples, the value of α_4 is smaller than three implying that the probability distribution is expected to be mild-peak (platykurtic) for these seven samples

IV. GENERATING THE DENSITY HISTOGRAMS BASED ON FREEDMAN−DIACONIS RULE

To generate a density histogram, the range (R) is divided into a number of classes and the number of occurrences in each class is counted and tabulated. These are called frequencies. Then, the relative frequency of each class can be obtained through dividing its frequency by the sample size. Afterwards, the density is calculated for each class through dividing the relative frequency by the class width. The width of classes is usually made equal to facilitate interpretation.

Care should be exercised in the choice of the number of classes (nc). Too few will cause an omission of some important features of the data; too many will not give a clear overall picture because there may be high frequency fluctuations. One of the widely accepted rules to determine the number of classes is Freedman−Diaconis rule expressed as [56]:

$$n_c = \frac{R\left(n^{1/3}\right)}{2\left(\mathrm{IQR}\right)} \tag{8}$$

where R is the range of sample data, n is the sample size, and IQR is the interquartile range calculated as:

$$\mathrm{IQR} = Q_3 - Q_1 \tag{9}$$

where Q1 is the lower quartile which is the median of lower half of the data; and likewise, Q3 is the upper quartile that is the median of upper half of the data.

5. PDF fitting using the maximum likelihood method

Nine different PDFs were fitted to the density histograms to assess the degree of fitting of various distributions to the SCF samples. Fig. 3 is presented as an example showing the fits for the 1st loading condition. In each case, distribution parameters were estimated using the maximum likelihood (ML) method. Results are given in Table 2. The ML procedure is an alternative to the method of moments. As a means of finding an estimator, statisticians often give it preference. For a random variable X with a known PDF, fX (x), and observed values x1, x2, . . . , xn, in a random sample of size n, the likelihood function of ω, where ω represents the vector of unknown parameters, is defined as:

$$L(\omega) = \prod_{i=1}^{n} f_X\left(x_i \mid \omega\right) \tag{10}$$

The objective is to maximize L(ω) for the given data set. It is done by taking m partial derivatives of L(ω), where m is the number of parameters, and equating them to zero. Then the maximum likelihood estimators (MLEs) of the parameter set ω can be found from the solutions of equations. In this way the greatest probability is given to the observed set of events, provided that the true form of the probability distribution is known.

6. Assessing of the goodness-of-fit based on the Kolmogorov−Smirnov test

The Kolmogorov−Smirnov goodness-of-fit test is a nonparametric test that relates to the cumulative distribution function (CDF) of a continuous variable. The test statistic, in a two-sided test, is the maximum absolute difference (which is usually the vertical distance) between the empirical and hypothetical CDFs. For a continuous variate X, let x(1), x(2), … , x(n) represent the order statistics of a sample of the size n, that is, the values arranged in increasing order. The empirical or sample distribution function Fn(x) is a step function. This gives the proportion of values not exceeding x and is defined as:

Fn (x) = 0,
For x < x(1) (11)
= k / n,

 ISBN: 978-81-932966-9-1

For $x(k) \le x < x(k+1)$ $k = 1, 2, \ldots, n-1$
$= 1,$
For $x \ge x(n)$

Let F0(x) denote a completely specified theoretical continuous CDF. The null hypothesis H0 is that the true CDF of X is the same as F0(x). That is, under the null hypothesis:

$$\lim_{n\to\infty} \Pr\left[F_n(x) = F_0(x)\right] = 1 \quad (12)$$

The test criterion is the maximum absolute difference between Fn(x) and F0(x), formally defined as:

$$d_n = \sup_x \left|F_n(x) - F_0(x)\right| \quad (13)$$

Theoretical continuous CDFs fitted to the empirical distribution functions of generated samples have been shown in Fig. 4 for the 1st loading condition. The fits of the other loading conditions are not presented here for the sake of brevity.

A large value of this statistic (dn) indicates a poor fit. Hence, acceptable values should be known. The critical values Dn,ξ for large samples, say n > 35, are $(1.3581 / \sqrt{n})$ and $(1.6276 / \sqrt{n})$ for ξ = 0.05 and 0.01, respectively [56] where ξ is the significance level.

Results of the Kolmogorov−Smirnov test for the 10 prepared samples were tabulated. As an example, results of the test for Sample 1 are given in Table 3. Outputs for the other samples are not presented here for the sake of brevity. Results of the Kolmogorov−Smirnov test indicated that the Generalized Extreme Value distribution has the smallest value of the test statistic (dn) for Samples 4, 7, and 9; while the Weibull distribution has the smallest dn value for Samples 2 and 3; and the Gamma distribution has the smallest dn for Samples 5 and 10. It was also observed that the Inverse Gaussian, Log-logistic, and Birnbaum−Saunders distributions have the smallest dn for Samples 1, 6, and 8, respectively. Hence, they are the best-fitted distributions for the corresponding SCF samples (Fig. 5).

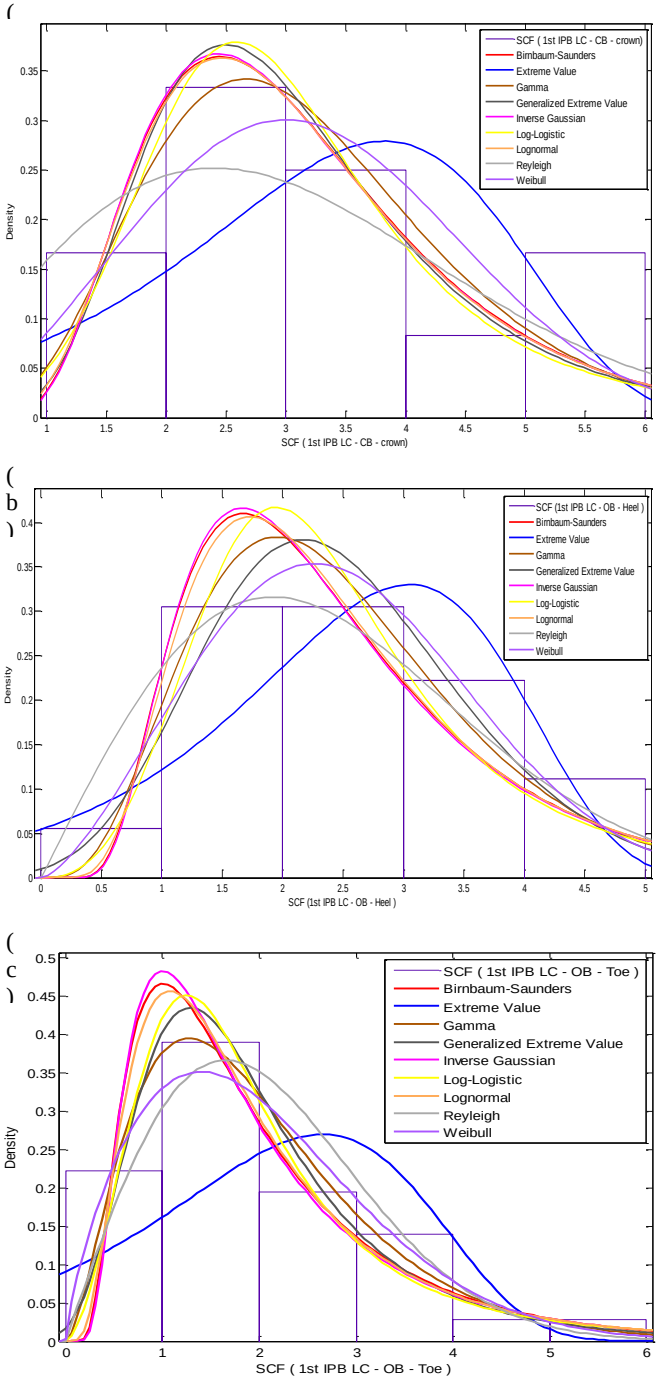

Fig. 3. Probability density functions fitted to the generated histograms: (a) Sample 1 (1st ILC, CB, C), (b) Sample 2 (1st ILC, OB, H), (c) Sample 3 (1st ILC, OB, T); [KEY: ILC: IPB loading condition; CB: Central brace; OB: Outer brace; C: Crown; H: Heel; T: Toe]

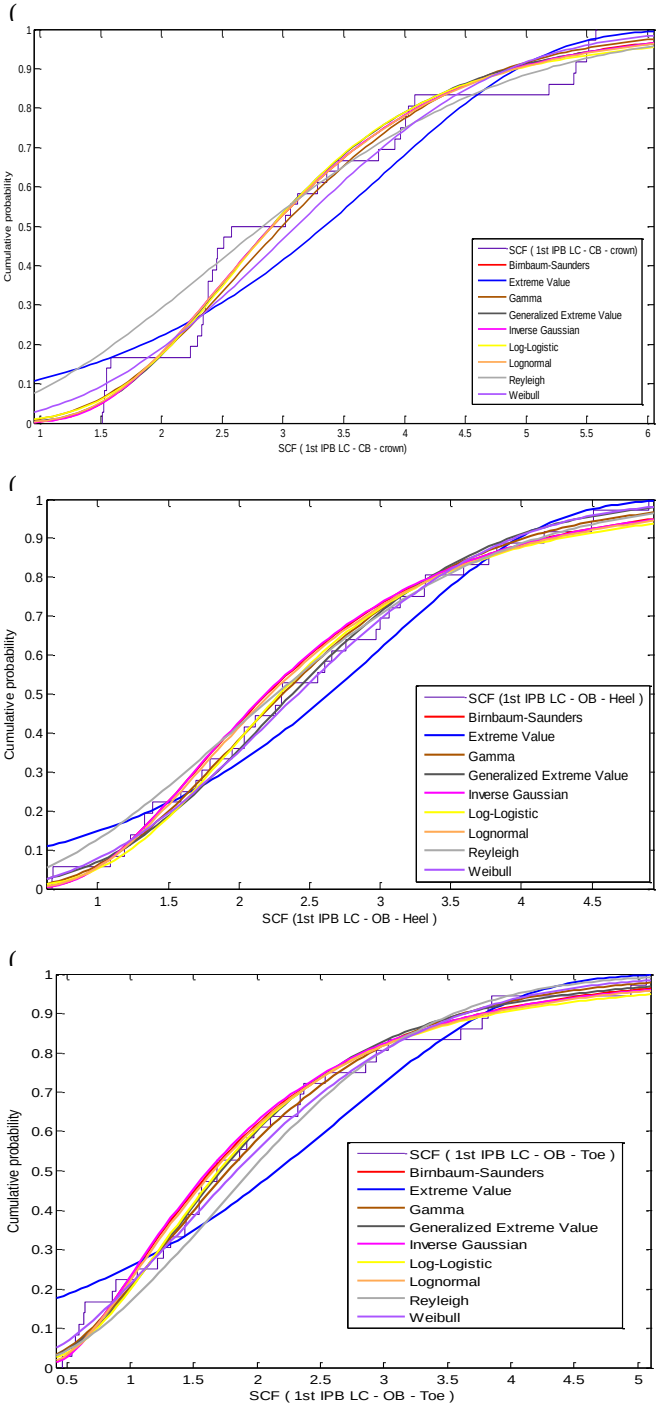

Fig. 4. Theoretical continuous CDFs fitted to the empirical CDFs of generated samples: (a) Sample 1 (1st ILC, CB, C), (b) Sample 2 (1st ILC, OB, H), (c) Sample 3 (1st ILC, OB, T); [KEY: ILC: IPB loading condition; CB: Central brace; OB: Outer brace; C: Crown; H: Heel; T: Toe]

Table 2. Estimated parameters for PDFs fitted to the density histograms of SCF samples

Fitted PDF	Parameters	Estimated values: Sample 1	Sample 2	Sample 3	Sample 4	Sample 5	Sample 6	Sample 7	Sample 8	Sample 9	Sample 10
		1st loading condition; central-brace crown SCFs	1st loading condition; outer-brace heel SCFs	1st loading condition; outer-brace toe SCFs	2nd loading condition; central-brace crown SCFs	2nd loading condition; outer-brace heel SCFs	2nd loading condition; outer-brace toe SCFs	3rd loading condition; outer-brace heel SCFs	3rd loading condition; outer-brace toe SCFs	4th loading condition; outer-brace heel SCFs	4th loading condition; outer-brace toe SCFs
Birnbaum-Saunders	β_0	2.913566	2.19859	1.635 86	2.973566	2.01255	1.92637	2.1013	1.80848	2.03462	1.95107
	γ_0	0.409872	0.507157	0.670526	0.395299	0.575938	0.5063	0.533229	0.551696	0.553259	0.522361
Extreme Value	μ	3.825266	3.04891	2.655 81	3.859888	2.95737	2.72021	2.984033	2.674 33	2.92326	2.81839
	σ	1.318177	1.11427	1.365 67	1.285 43	1.22555	1.13623	1.16728	1.248 71	1.15178	1.26591
Gamma	a	6.364866	4.69865	2.748 85	6.78978	3.77883	4.50136	4.30773	3.777 39	4.1021	4.13153
	b	0.496209	0.528572	0.729 895	0.472163	0.621899	0.48302	0.557771	0.551 815	0.572767	0.536761
Generalized Extreme Value	k	0.048522 8	-0.13979	0.133 884	0.055691 7	-0.06138 4	0.00912 559	-0.08857 75	0.102 537	-0.109344	0.103034
	σ	0.978184	0.976381	0.853 723	0.959277	0.974958	0.80661 2	0.955875	0.787 767	0.96315	0.805316
	μ	2.540556	2.02909	1.393 82	2.593355	1.83388	1.69681	1.9194	1.544 4	1.87949	1.66516
Inverse Gaussian	μ	3.1583	2.48358	2.006 37	3.20584	2.35005	2.17426	2.40273	2.084 42	2.34954	2.21764
	λ	1.286664	9.07255	4.011 64	19.7446	6.54231	7.97114	7.88962	6.364 09	7.1303	7.60838
Log-logistic	μ	1.067755	0.829664	0.528 206	1.086166	0.748525	0.67667 1	0.785843	0.606 876	0.763577	0.676465
	σ	0.240377	0.283776	0.378 692	0.233558	0.318281	0.28474 1	0.294587	0.312 846	0.303487	0.29805
Lognormal	μ	1.069433	0.799528	0.503 545	1.089533	0.716324	0.66151 8	0.756067	0.596 323	0.727409	0.670571
	σ	0.409992	0.499979	0.654 463	0.395875	0.562831	0.50018 9	0.523552	0.543 769	0.54136	0.51643
Rayleigh	b	2.406669	1.91917	1.656 47	2.432366	1.85338	1.69994	1.87268	1.664 89	1.83536	1.7559
Weibull	a	3.564277	2.80749	2.264 54	3.613177	2.66087	2.46314	2.71887	2.364 15	2.6581	2.51581
	b	2.689288	2.44854	1.758 68	2.781379	2.15894	2.26758	2.31158	2.036 56	2.27826	2.12555

Table 3. Results of the Kolmogorov-Smirnov goodness-of-fit test for SCF sample 1 (1st loading condition; central-brace crown SCFs)

Fitted distribution	Test statistic	Critical value: $\zeta = 0.05$	Critical value: $\zeta = 0.01$	Test result: $\zeta = 0.05$	Test result: $\zeta = 0.01$
Birnbaum-Saunders	0.117027	0.22635	0.27126	Accept	Accept
Extreme Value	0.178047			Accept	Accept
Gamma	0.140479			Accept	Accept
Generalized Extreme Value	0.117643			Accept	Accept
Inverse Gaussian	0.115216			Accept	Accept
Log-logistic	0.122583			Accept	Accept
Lognormal	0.116989			Accept	Accept
Rayleigh	0.184410			Accept	Accept
Weibull	0.157745			Accept	Accept

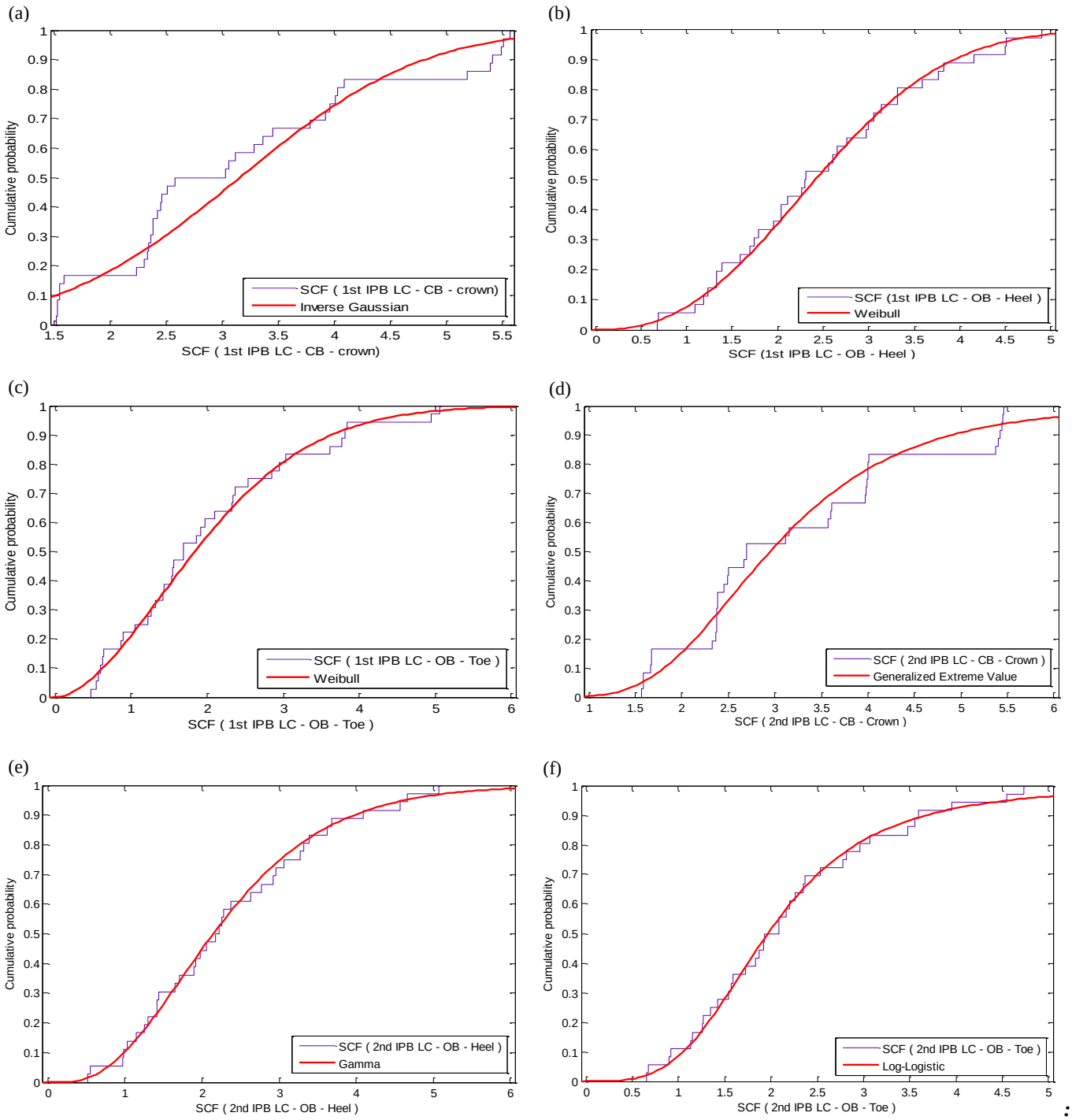

Fig. 5. The best-fitted distributions according to the Kolmogorov−Smirnov test: (a) Sample 1 (1st ILC, CB, C), (b) Sample 2 (1st ILC, OB, H), (c) Sample 3 (1st ILC, OB, T), (d) Sample 4 (2nd ILC, CB, C), (e) Sample 5 (2nd ILC, OB, H), (f) Sample 6 (2nd ILC, OB, T), (g) Sample 7 (3rd ILC, OB, H), (h) Sample 8 (3rd ILC, OB, T), (i) Sample 9 (4th ILC, OB, H), (j) Sample 10 (4th ILC, OB, T); [KEY: ILC

(g)

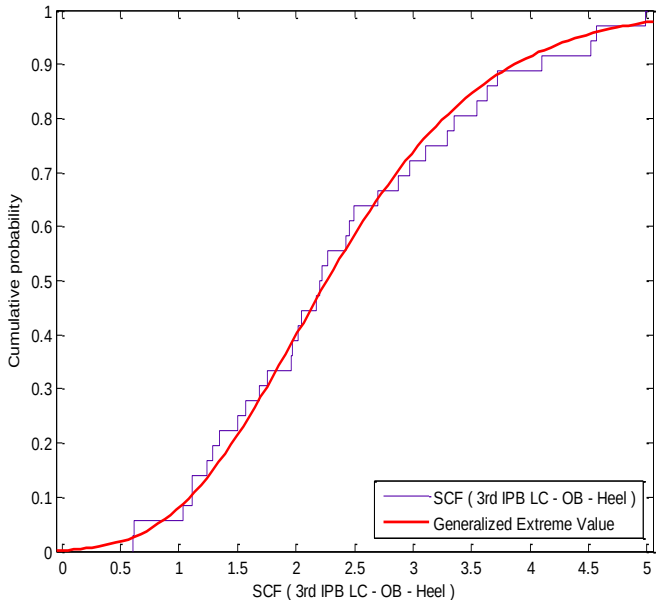
Cumulative probability
SCF (3rd IPB LC - OB - Heel)
SCF (3rd IPB LC - OB - Heel)
Generalized Extreme Value

(h)

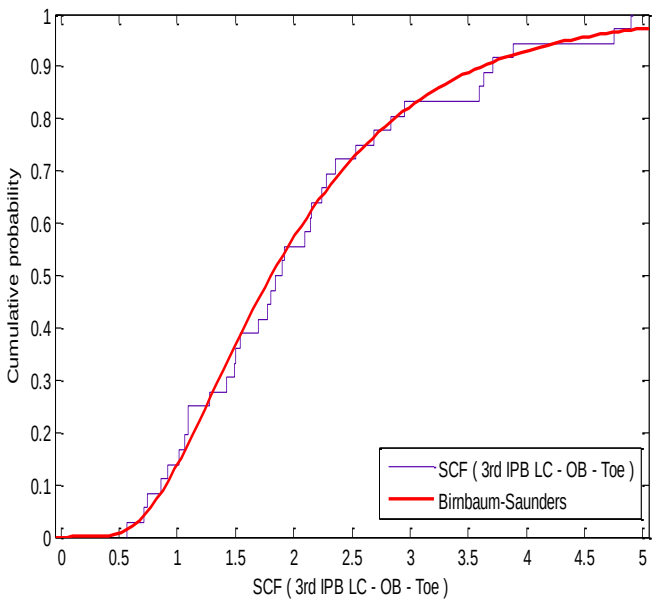
Cumulative probability
SCF (3rd IPB LC - OB - Toe)
SCF (3rd IPB LC - OB - Toe)
Birnbaum-Saunders

(i)

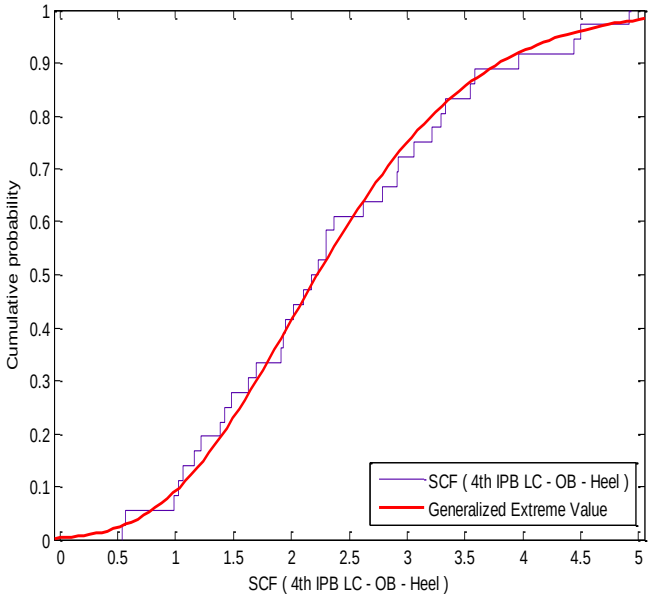
Cumulative probability
SCF (4th IPB LC - OB - Heel)
SCF (4th IPB LC - OB - Heel)
Generalized Extreme Value

(j)

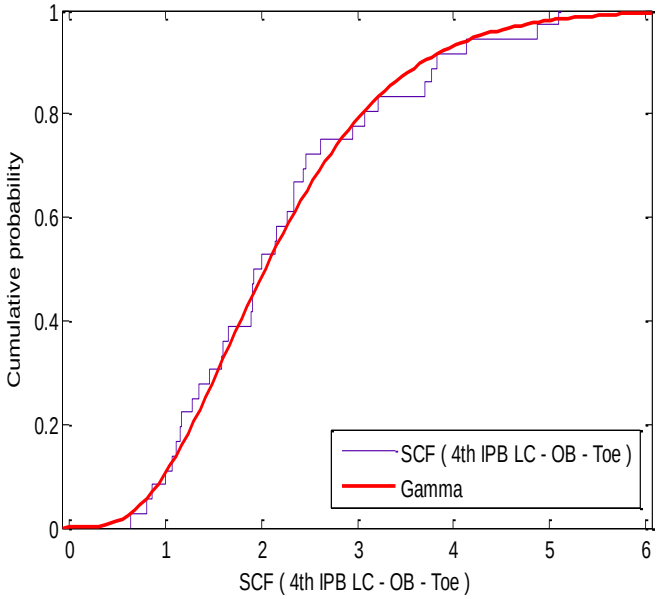
Cumulative probability
SCF (4th IPB LC - OB - Toe)
SCF (4th IPB LC - OB - Toe)
Gamma

VII. PROBABILITY DISTRIBUTION MODELS PROPOSED FOR THE SCFS IN IPB-LOADED KT-JOINTS

The best fitted distributions for the generated SCF samples were introduced in Sec. 6. It can be seen that the best fitted distributions for these 10 samples include six different models: Generalized Extreme Value, Weibull, Gamma, Inverse Gaussian, Log-logistic, and Birnbaum−Saunders distributions. The diversity of the best-fitted probability models derived for the studied SCFs may practically result in the confusion and difficulty of their application for the fatigue analysis and design. Hence, reducing the number of distribution types proposed for the SCFs might be a good idea. In order to do so, the top three distribution functions for each SCF sample were identified (Table 4). The aim was to propose only two probability models to cover all the central- and outer-brace SCFs. It should be noted that, for each sample, all of the three mentioned functions have acceptable fit according to the Kolmogorov−Smirnov test. After surveying the data presented in Table 4, the Inverse Gaussian and Gamma models are proposed as the governing probability distribution functions for the central- and outer-brace SCFs, respectively. The difference between the test statistic of the proposed distributions and the best-fitted ones for each sample are presented in Table 5. Using the information presented in Table 5, the analyst is able to make a choice, based on the engineering judgment, between the best-fitted and the proposed probability models for each of the 10 studied cases.

The PDF of the Inverse Gaussian and Gamma distributions are expressed as:

$$f_X(x) = \sqrt{\frac{\lambda}{2\pi x^3}} \exp\left\{-\frac{\lambda}{2\mu^2 x}(x-\mu)^2\right\} \quad \text{(Inv. Gauss.)} \quad (14)$$

$$f_X(x) = \frac{1}{b^a \Gamma(a)} x^{a-1} e^{-x/b} \quad \text{(Gamma)} \quad (15)$$

$$\Gamma(a) = \int_0^\infty e^{-r} r^{a-1} dr \quad (16)$$

where is the Gamma function defined as

Table 4. Best-fitted distributions for the SCF samples based on the results of the Kolmogorov-Smirnov test

	SCF samples									
	Sample 1	Sample 2	Sample 3	Sample 4	Sample 5	Sample 6	Sample 7	Sample 8	Sample 9	Sample 10
Best-fitted distributions	1st loading condition; central-brace crown SCFs	1st loading condition; outer-brace heel SCFs	1st loading condition; outer-brace toe SCFs	2nd loading condition; central-brace crown SCFs	2nd loading condition; outer-brace heel SCFs	2nd loading condition; outer-brace toe SCFs	3rd loading condition; outer-brace heel SCFs	3rd loading condition; outer-brace toe SCFs	4th loading condition; outer-brace heel SCFs	4th loading condition; outer-brace toe SCFs
# 1	Inverse Gaussian	Weibull	Weibull	Generalized Extreme Value	Gamma	Log-logistic	Generalized Extreme Value	Birnbaum-Saunders	Generalized Extreme Value	Gamma
# 2	Lognormal	Generalized Extreme Value	Gamma	Inverse Gaussian	Weibull	Generalized Extreme Value	Gamma	Inverse Gaussian	Log-logistic	Log-logistic
# 3	Birnbaum-Saunders	Gamma	Generalized Extreme Value	Lognormal	Rayleigh	Gamma	Log-logistic	Lognormal	Gamma	Generalized Extreme Value

Table 5. Comparison of the test statistics for the proposed and the best-fitted distributions based on the results of the Kolmogorov-Smirnov test

Test statistic	SCF samples									
	Sample 1	Sample 2	Sample 3	Sample 4	Sample 5	Sample 6	Sample 7	Sample 8	Sample 9	Sample 10
Best-fitted distribution	0.115216 (Inverse Gaussian)	0.065779 (Weibull)	0.079255 (Weibull)	0.119851 (Generalized Extreme Value)	0.063538 (Gamma)	0.051124 (Log-logistic)	0.057193 (Generalized Extreme Value)	0.072604 (Birnbaum-Saunders)	0.060320 (Generalized Extreme Value)	0.075240 (Gamma)
Proposed distribution	0.115216 (Inverse Gaussian)	0.070696 (Gamma)	0.082681 (Gamma)	0.123130 (Inverse Gaussian)	0.063538 (Gamma)	0.060784 (Gamma)	0.071462 (Gamma)	0.080282 (Gamma)	0.071798 (Gamma)	0.075240 (Gamma)
Difference	0%	7.5%	4.3%	2.7%	0%	19%	25%	10.5%	19%	0%

After substituting the values of estimated parameters from Table 2, following probability density functions are proposed for the weld-toe SCFs of the central and outer braces in uniplanar tubular KT-joints subjected to the four considered IPB load cases defined in Fig. 1(d):

- ***Weld-toe SCFs of the central brace:***

1st IPB loading condition − Crown position:

$$f_X(x) = \sqrt{\frac{0.64332}{\pi x^3}} \exp\left\{-\frac{0.064494145}{x}(x-3.1583)^2\right\} \quad (17)$$

2nd IPB loading condition − Crown position:

$$f_X(x) = \sqrt{\frac{9.8723}{\pi x^3}} \exp\left\{-\frac{0.960582472}{x}(x-3.20584)^2\right\} \quad (18)$$

- ***Weld-toe SCFs of the outer brace:***

1st IPB loading condition − Heel position:

$$f_X(x) = 1.298594855x^{3.69865}e^{-x/0.528572} \quad (19)$$

1st IPB loading condition − Toe position:

$$f_X(x) = 1.478776153x^{1.74885}e^{-x/0.729895} \quad (20)$$

2nd IPB loading condition − Heel position:

$$f_X(x) = 1.314984484x^{2.77883}e^{-x/0.621899} \quad (21)$$

2nd IPB loading condition − Toe position:

$$f_X(x) = 2.270439733x^{3.50136}e^{-x/0.483023} \quad (22)$$

3rd IPB loading condition − Heel position:

$$f_X(x) = 1.381972165x^{3.30773}e^{-x/0.557771} \quad (23)$$

3rd IPB loading condition − Toe position:

$$f_X(x) = 2.067828757x^{2.77739}e^{-x/0.551815} \quad (24)$$

4th IPB loading condition − Heel position:

$$f_X(x) = 1.439835091x^{3.1021}e^{-x/0.572767} \quad (25)$$

4th IPB loading condition − Toe position:

$$f_X(x) = 1.842725568x^{3.13153}e^{-x/0.536761} \quad (26)$$

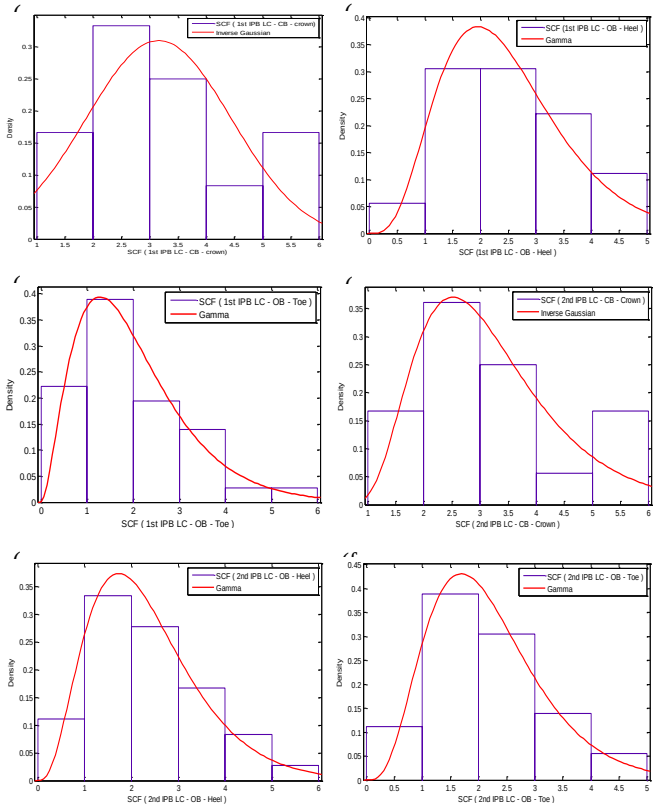

Figure 6. Proposed Inverse Gaussian and Gamma PDFs: (a) Sample 1 (1st ILC, CB, C), (b) Sample 2 (1st ILC, OB, H), (c) Sample 3 (1st ILC, OB, T), (d) Sample 4 (2nd ILC, CB, C), (e) Sample 5 (2nd ILC, OB, H), (f) Sample 6 (2nd ILC, OB, T), (g) Sample 7 (3rd ILC, OB, H), (h) Sample 8 (3rd ILC, OB, T), (i) Sample 9 (4th ILC, OB, H), (j) Sample 10 (4th ILC, OB, T); [KEY: ILC: IPB loading condition; CB: Central brace; OB: Outer brace; C: Crown; H: Heel; T: Toe]

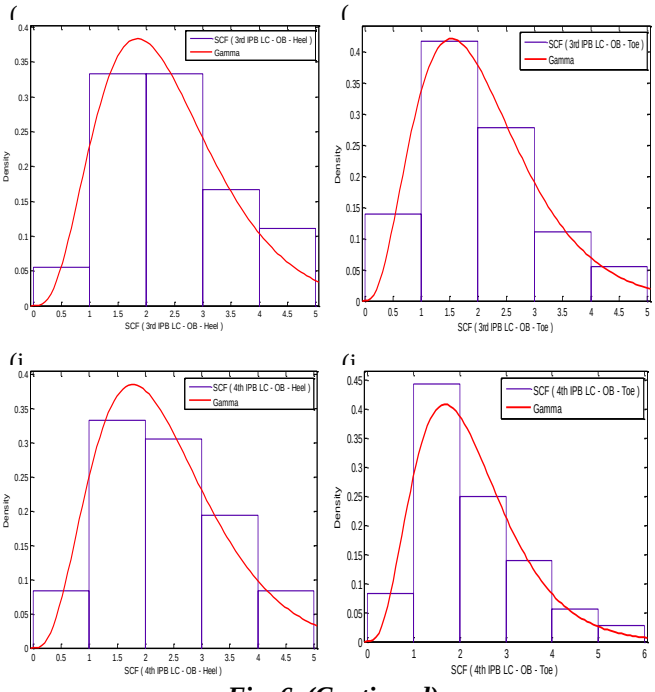

Fig. 6. (Continued)

VIII. CONCLUSIONS

In the present paper, results of 144 FE stress analyses, verified against experimental measurements, were used to develop a set of PDFs for the SCFs in uniplanar tubular KT-joints under four types of IPB moment load cases. Based on a parametric FE investigation, a sample database was created for the chord-side SCFs of central and outer braces; and density histograms were generated for respective samples. Nine theoretical PDFs were fitted to the developed histograms and the ML method was applied to evaluate the parameters of fitted PDFs. In each case, the Kolmogorov−Smirnov test was used to assess the goodness of fit. Finally, the Inverse Gaussian and Gamma models were proposed as the governing probability distribution functions for the central- and outer-brace SCFs, respectively. After substituting the values of estimated parameters, 10 fully defined PDFs were presented for the chord-side SCFs of central and outer braces in uniplanar tubular KT-joints under four types of IPB loading.

REFERENCES

[1] American Petroleum Institute (API) (2007) Recommended practice for planning, designing and constructing fixed offshore platforms: Working stress design: RP2A-WSD. 21st Edition, Errata and Supplement 3, Washington DC, US

[2] Yiyi C and Wei W (2003) Flexural behavior and resistance of uni-planar KK and X tubular joints. Steel and Composite Structures 3(2): 123−140.

[3] Choo YS (2005) Recent development and innovation in tubular structures. Advances in Structural Engineering 8(3): 217−230.

[4] Lie ST, Shao YB, Lee CK and Chiew SP (2006) Stress intensity factor solutions for semi-elliptical weld-toe cracks in tubular K-joints. Advances in Structural Engineering 9(1): 129−139.

[5] Gao F, Zhu HP and Liu XN (2013) Failure behavior of axially loaded tubular Y-joints under fire. Advances in Structural Engineering 16(9): 1523−1533.

[6] Liu H, Shao YB, Lu N and Wang Q (2015) Hysteresis of concrete-filled circular tubular (CFCT) T-joints under axial load. Steel and Composite Structures 18(3): 739−756.

[7] Cui MJ and Shao YB (2015) Residual static strength of cracked concrete-filled circular steel tubular (CFCST) T-joint. Steel and Composite Structures 18(4): 1045−1062.

[8] Shao YB (2016) Static strength of collar-plate reinforced tubular T-joints under axial loading. Steel and Composite Structures 21(2): 323–342.

[9] Nassiraei H, Lotfollahi-Yaghin MA and Ahmadi H (2016) Structural behavior of tubular T/Y-joints with collar plate under static in-plane bending. Journal of Constructional Steel Research 123(8): 121−134.

[10] Efthymiou M and Durkin S (1985) Stress concentrations in T/Y and gap/overlap K-joints. Proceedings of the Conference on Behavior of Offshore Structures, Delft, Netherlands.

[11] Efthymiou M (1988) Development of SCF formulae and generalized influence functions for use in fatigue analysis. OTJ 88, Surrey, UK.

[12] Hellier AK, Connolly M and Dover WD (1990) Stress concentration factors for tubular Y and T-joints. International Journal of Fatigue 12: 13–23.

[13] Smedley P and Fisher P (1991) Stress concentration factors for simple tubular joints. Proceedings of the International Offshore and Polar Engineering Conference (ISOPE), Edinburgh, UK.

[14] UK Health and Safety Executive (1997) OTH 354: stress concentration factors for simple tubular joints-assessment of existing and development of new parametric formulae. Prepared by Lloyd's Register of Shipping, London (UK): Health and Safety Executive.

[15] Karamanos SA, Romeijn A and Wardenier J (2000) Stress concentrations in tubular gap K-joints: mechanics and fatigue design. Engineering Structures 22: 4–14.

[16] Gho WM and Gao F (2004) Parametric equations for stress concentration factors in completely overlapped tubular K(N)-joints. Journal of Constructional Steel Research 60: 1761–1782.

[17] Gao F (2006) Stress and strain concentrations of completely overlapped tubular joints under lap brace OPB load. Thin-Walled Structures 44: 861–871.

[18] Gao F, Shao YB and Gho WM (2007) Stress and strain concentration factors of completely overlapped tubular joints

under lap brace IPB load. Journal of Constructional Steel Research 63: 305–316.

[19] Morgan MR and Lee MMK (1998a) Parametric equations for distributions of stress concentration factors in tubular K-joints under out-of-plane moment loading. International Journal of Fatigue 20: 449–461.

[20] Morgan MR and Lee MMK (1998b) Prediction of stress concentrations and degrees of bending in axially loaded tubular K-joints. Journal of Constructional Steel Research 45(1): 67–97.

[21] Chang E and Dover WD (1999a) Parametric equations to predict stress distributions along the intersection of tubular X and DT-joints. International Journal of Fatigue 21: 619–635.

[22] Chang E and Dover WD (1999b) Prediction of stress distributions along the intersection of tubular Y and T-joints. International Journal of Fatigue 21: 361–381.

[23] Shao YB (2004) Proposed equations of stress concentration factor (SCF) for gap tubular K-joints subjected to bending load. International Journal of Space Structures 19: 137–147.

[24] Shao YB (2007) Geometrical effect on the stress distribution along weld toe for tubular T- and K-joints under axial loading. Journal of Constructional Steel Research 63: 1351–1360.

[25] Shao YB, Du ZF and Lie ST (2009) Prediction of hot spot stress distribution for tubular K-joints under basic loadings. Journal of Constructional Steel Research 65: 2011–2026.

[26] Lotfollahi-Yaghin MA and Ahmadi H (2010) Effect of geometrical parameters on SCF distribution along the weld toe of tubular KT-joints under balanced axial loads. International Journal of Fatigue 32: 703–719.

[27] Pang NL and Zhao XL (2009) Finite element analysis to determine stress concentration factors of dragline tubular joints. Advances in Structural Engineering 12(4): 463−478.

[28] Karamanos SA, Romeijn A, and Wardenier J (1990) Stress concentrations in multi-planar welded CHS XX-connections. Journal of Constructional Steel Research 50: 259–282.

[29] Chiew SP, Soh CK and Wu NW (2000) General SCF design equations for steel multiplanar tubular XX-joints. International Journal of Fatigue 22: 283–293.

[30] Wingerde AM, Packer JA and Wardenier J (2001) Simplified SCF formulae and graphs for CHS and RHS K- and KK-connections. Journal of Constructional Steel Research 57: 221–252.

[31] Karamanos SA, Romeijn A and Wardenier J (2002) SCF equations in multi-planar welded tubular DT-joints including bending effects. Marine Structures 15: 157–173.

[32] Ahmadi H, Lotfollahi-Yaghin MA and Aminfar MH (2012a) The development of fatigue design formulas for the outer brace SCFs in offshore three-planar tubular KT-joints. Thin-Walled Structures 58: 67–78.

[33] Ramachandra Murthy DS, Madhava Rao AG, Ghandi P and Pant PK (1992) Structural efficiency of internally ring stiffened steel tubular joints. Journal of Structural Engineering: ASCE 118(11): 3016–3035.

[34] Nwosu DI, Swamidas ASJ and Munaswamy K (1995) Numerical stress analysis of internal ring-stiffened tubular T-joints. Journal of Offshore Mechanics and Arctic Engineering 117: 113–125.

[35] Ramachandra DS, Gandhi P, Raghava G and Madhava Rao AG (2000) Fatigue crack growth in stiffened steel tubular joints in seawater environment. Engineering Structures 22: 1390–1401.

[36] Hoon KH, Wong LK and Soh AK (2001) Experimental investigation of a doubler-plate reinforced tubular T-joint subjected to combined loadings. Journal of Constructional Steel Research 57: 1015–1039.

[37] Myers PT, Brennan FP and Dover WD (2001) The effect of rack/rib plate on the stress concentration factors in jack-up chords. Marine Structures 14: 485–505.

[38] Woghiren CO and Brennan FP (2009) Weld toe stress concentrations in multi planar stiffened tubular KK Joints. International Journal of Fatigue 31: 164–172.

[39] Ahmadi H, Lotfollahi-Yaghin MA, Shao YB and Aminfar MH (2012b) Parametric study and formulation of outer-brace geometric stress concentration factors in internally ring-stiffened tubular KT-joints of offshore structures. Applied Ocean Research 38: 74−91.

[40] Ahmadi H and Zavvar E (2015) Stress concentration factors induced by out-of-plane bending loads in ring-stiffened tubular KT-joints of jacket structures. Thin-Walled Structures 91: 82–95.

[41] Kirkemo F (1998) Applications of probabilistic fracture mechanics to offshore structures. Applied Mechanics Review 41: 61–84.

[42] Pillai TMM and Prasad AM (2000) Fatigue reliability analysis in time domain for inspection strategy of fixed offshore structures. Ocean Engineering 27: 167–186.

[43] Mosayyebi AR and Aghakuchak AA (2000) Fatigue reliability analysis of tubular joints of offshore structures using response surface method. Asian Journal of Civil Engineering 1: 75–87.

[44] Rajasankar J, Iyer NR and Appa Rao TVSR (2003) Structural integrity assessment of offshore tubular joints based on reliability analysis. International Journal of Fatigue 25: 609–619.

[45] Ahmadi H and Lotfollahi-Yaghin MA (2013) Effect of SCFs on S–N based fatigue reliability of multi-planar tubular DKT-joints of offshore jacket-type structures. Ships and Offshore Structures 8: 55−72.

[46] Ahmadi H, Lotfollahi-Yaghin MA and Aminfar MH (2011) Effect of stress concentration factors on the structural integrity assessment of multi-planar offshore tubular DKT-joints based on the fracture mechanics fatigue reliability approach. Ocean Engineering 38: 1883−1893.

[47] Ahmadi H, and Lotfollahi-Yaghin MA (2012) A probability distribution model for stress concentration factors in multi-planar tubular DKT-joints of steel offshore structures. Applied Ocean Research 34: 21−32.

[48] Ahmadi H, Mohammadi AH, and Yeganeh A (2015) Probability density functions of SCFs in internally ring-stiffened tubular KT-joints of offshore structures subjected to axial load. Thin-Walled Structures 94: 485–499.

[49] Ahmadi H, Mohammadi AH, Yeganeh A and Zavvar E (2016) Probabilistic analysis of stress concentration factors in tubular KT-joints reinforced with internal ring stiffeners under in-plane bending loads. Thin-Walled Structures 99: 58–75.

[50] Ahmadi H. (2016). A probability distribution model for SCFs in internally ring-stiffened tubular KT-joints of offshore structures subjected to out-of-plane bending loads. Ocean Engineering 116: 184–199.

[51] American Welding Society (AWS) (2002) Structural welding code: AWS D 1.1. Miami (FL), US.

[52] N'Diaye A, Hariri S, Pluvinage G and Azari Z (2007) Stress concentration factor analysis for notched welded tubular T-joints. International Journal of Fatigue 29: 1554–1570.

[53] IIW-XV-E (1999) Recommended fatigue design procedure for welded hollow section joints, IIW Docs, XV-1035-99/XIII-1804-99. Paris (France): International Institute of Welding.

[54] Ahmadi H and Lotfollahi-Yaghin MA (2013) Effect of SCFs on S–N based fatigue reliability of multi-planar tubular DKT-joints of offshore jacket-type structures. Ships and Offshore Structures 8: 55−72.

[55] Chang E, Dover WD (1996). Stress concentration factor parametric equations for tubular X and DT joints. International Journal of Fatigue 18(6): 363–387.

[56] Kottegoda NT and Rosso R (2008) Applied statistics for civil and environmental engineers. 2nd Edition, Blackwell Publishing Ltd, UK.

Molecular Ordering in Poly (Aniline) through Controlled Cross-linking

[1] Mohammad Changez, [2] Zainab Ibrahim Mohammad Al-Baushi, [3] Mohammad Faiyaz Anwar
[1][2] Department of Basic Sciences, College of Health and Applied Sciences, A' Sharqiyah University, Ibra, Oman.
[3] Department of Pathology, All India Institute of Medical Sciences, New Delhi, India

Abstract: -- **The design of molecular order at economically viable method is a challenging for materials science research. Here we report the one step process for molecular ordered in polyaniline through cross-linking with 1,4-dibromobutane. Resulting nanostructure show molecular ordering in polyaniline organic-organic frame work by transmission electron microscope and XRD with high conductivity in comparison to uncross-linked polyaniline.**

Index Terms: - Polyaniline, Molecular ordering, HRTEM, Semiconductor, Cross-linking.

I. INTRODUCTION

In an area of nanotechnology, long range molecular ordering is challenging expect in an area of materials science [1-3]. Molecular ordering enhanced the performance of organic molecules based devices devices. Self-assembly is an emerging, powerful, low-cost approach to generating nanostructured in materials. However, it faces challenge in controlling the molecules for formation of molecular level [4-5]. In materials science research, conducting polymers have recently received attention due to its simple synthesis procedure, less weight and their elasticity [6]. Therefore, sevearal efforts have been made to make devices based onconducting polymers for various electronic devices, such as organic photovoltaics, organic light-emitting diodes and organic field-effect transistors [7]. However, its face technqal difficulty maily due limitation chain entanglements and amorphous zone in film [8]. Thus, specific approach needed to get the long range order in conducting polymers system Several research groups have attempted to develop valuable methods such as chemical [9] and physical methods [10] to improve the ordered in conductive opolymer. Researcher tried to funtionalised polymer backbones or side chains to improve the interactions among the conducting polymer chains. However, in the study of crystalline conducting polymers, the difficulty is in controlling the precise arrangement of polymers at molecular scale. Cross-linked polymers genraly used in various devices for high mechanical strength or solvent resistance during device fabrication. Unlike typical research on cross-linked polymers, our group has used controlled crosslinking techniques for precisely ordering in polymers.

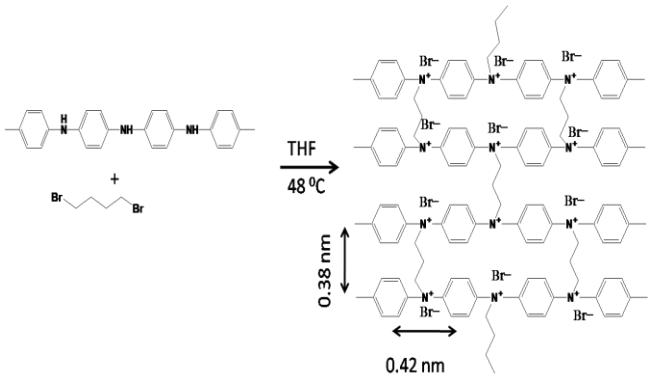

Fig.1. Scheme for molecular ordering in Polyaniline and reaction condition.

Recently, we reported molecular ordering in poly (2-vinylpyridine) (P2VP) through cosslinking [11]. Since the crosslinking of molecules under controlled conditions seectively suppress the directional freedom of polymers and decreased chain entanglements. Therefore, molecular ordering by crosslinking may be a solution to resolve the inherent morphological limitations of the conducting polymers. For this study, we had cross-linked polyaniline with 1,4-dibromo butane to induce molecular-scale ordering in cross-linked polyaniline using a simple solution process.

II. EXPERIMENTAL SECTION STARTING REAGENTS

Polyaniline EB (PANI) (Mw 20000), and 1,4 dibrobutane (DBB) and tetrahydrofuran were purchased from Sigma Aldrich. All materials were used as received without further

purification. Glass substrates were purchased from Marienfeld-Superior. Cross-linking of PANI with DBB ions was carried out in tetrahydrofuran (THF) for 48 h at 50 0C temperature (Aniline) repeating/ DBB mole ratio 1/1) and resulting sample were characterized by XRD, transmission electron microscope and conductivity of film was measured by four probe method after dialysis through membrane (cutoff MW =3000). Thin film XRD spectra was obtain using Reguka XRD instrument. Glass substrates were cut to a size of 15 × 15 mm2. Then, the cut glass pieces were ultra-sonicated with deionized water, acetone (Sigma-Aldrich) and isopropyl alcohol (Aldrich) for 15 min each. The washed glass pieces were dried in an oven at 60 °C, and their surfaces were exposed by means of UV-ozone to produce hydrophilic groups. The solution mixtures of PANI-DBB ions spin-coated or drop-cast on the glass substrates and coated films were then annealed at 150 °C for hours.

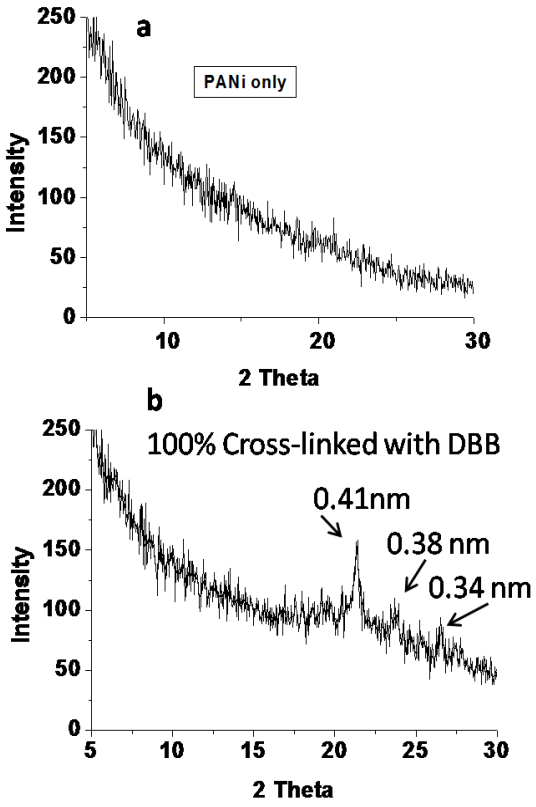

Fig. 2 Thin film XRD spectra of (a) pure PANI (b) cross-linked PANI .

For XRD spectra, films were prepared by drop casting the solution (150 µl) onto glass substrates (15 × 15 mm2), and XRD measurements were performed on a Rigaku D/max-2500 diffractometer with Cu–Kα radiation (λ = 1.54 Å) at 40 kV and 100 mA. A high-resolution electron microscope (JEOL Ltd, 200kV). The specimens were prepared by drop-casting the PANI-DBB ion cross-linked solution (15 µl) on carbon-coated copper grids (200 mesh, EM Science) and annealed at 150 0C for 12 hours. The sheet resistances of PANI-DBB cross-linked, PANI control solution films (~100 nm) were measured using a 4-point probe method from FPP-RS8 (Dasol Eng.). The mean value of the electrical conductivity of each film was calculated from the sheet resistances of 6 samples measured at room temperature. The film thickness of each film was measured using a surface profiler (NanoMap-LS).

III. RESULTS AND DISCUSSION

Organic–organic interactions generate hybrid organic frameworks (OOFs). For the growth of organic–organic prdered structures, in liquid state we select low molecular weight PANI and DBB (repeating unit of PANI: DBB mole ratio at 1) as a model for generation of molecular order in cross-linked PANI (Fig.1). The XRD spectra of PANI-DBB OOFs shows in presence of molecular level ordering (Fig.2). The X-ray diffraction spectrum was also used to investigate the d spacing, and peaks were observed at two theta value 21.34 (0.41 nm), 24.2 (0.38 nm), and 29.5 (0.30 nm), respectively, which is similar to reported work and shows cubic lattice. The d spacing 0.41 nm consider to be distance of reaping unit of the PANI and 0.38 nm is inter-chain distance of PANI in ordered structure [1].

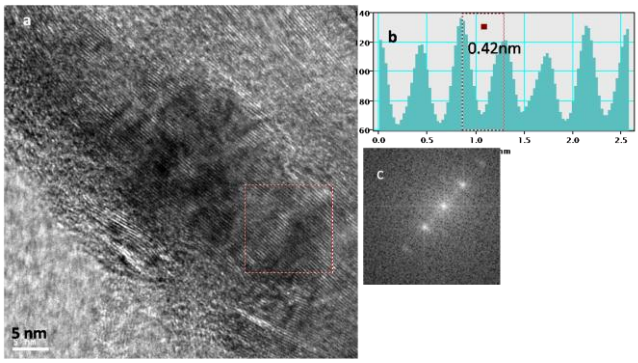

Fig. 3 High resolution transmission electron microscope micrograph of (a) cross-linked(PANI) at 5nm scale. (Unstained), (b) histogram showing ordering distance, and (c) fast Fourier transform age of figure a.

The morphologies of cross-linked sample characterized by high resolution transmission electrnn microscope (HRTEM electron microscope and it compared with X-rays data . For uncross-linked PANI molecular ordering was not observed in XRD Fig.1a (transmission electron micrograph also not show ordered structure in uncross-linked PANI sample). However, very clear molecular ordering was identified in

high resolution transmission electron micrograph of cross-linked PANI sample which are very similar to XRD data. Figure 3 shows high resolution transmission electron micrograph of cross-linked PANI. Figure 3a represent HRTEM image of the cross-linked PANI sample with and it DBB cross ponding fast Fourier transform image (IFFT) of selected area of 3a shown in Fig.3b, ordering at 0.41 nm clearly observed in Fig.3b (inside image shown histogram of size). Figure 3c shows fast Fourier transform (FFT) image of electron diffraction. The Gutan software were used to analyses the transmission electron microscope image at molecular level []. Fig.3b show lattice spacing of 0.41 nm which are generated from repeating unit distance of PANI after cross-linking and match with reported work. Electrical conductivity of the PANI cross-linked films (110 nm thickness) was measured by the van der Pauw method. The electrical conductivity of pure PANI observed at 0.004 S/cm as reported in Sigma Aldrich catalog (Cat No = 482552) and after cross-linking with DBB its conductivity increased to 7.28 S/cm which is higher by factor of approximately 1800.

IV. CONCLUSION

In this work, we reported the simple one step process for molecular ordering in polyaniline by cross-linking. The resulting molecularly ordered PANI shown 1800 time more conductivity than uncross-linked polypyrrole. This molecular ordering method can be applied to other functional polymer to get organic- organic frame work (OOF) with precise control over lattice spacing for multi applications such as electronics, photonic, magnetic and electrochemical devices.

V. ACKNOWLEDGMENT

Mohammad Changez thanks A'.Sharqiyah University Vice Chancellor for providing Internal grant for this nanomaterial research. Authors also thanks Korea Basic Science Institute for HRTEM analysis of samples.

References

[1] H.-J. Lee, H. Sang-Ook, A. Min-Kyoon, Changez M, and Jae-Suk L.,"In situ formation of molecular-scale ordered polyaniline films by zinc coordination". Nanoscale, vol 9, pp 6545-6550, April 2017.

[2] K. Haeng-Deog, M. Changez, M.S. Rahman. and J.- S. Lee. "Formation of Intermicellar-Chained and Cylindrical Micellar Networks From an Amphiphilic Rod-Coil Block Copolymer: Poly(n-hexyl isocyanate)-block-Poly(2-vinylpyridine". Langmuir, vol 25, pp 71887192, June 2009.

[3] M. Changez, K. Nam-Goo, and J.-S. Lee. "Uni-Molecular Hollow Micelles from Amphiphilic Homopolymer Poly(2-(4vinylphenyl)pyridine) Micelles to Vesicles" , Small, vol 8, pp 11731178, Feburary 2012.

[4] J. B. Jeremy "Breaking the mould: Casting on the nanometre scale" Nature Materials, vol 5, pp 2-5, January 2006.

[5] J. B. Johannes, Giovanni C., and Klaus K. "Engineering atomic and molecular nanostructures at surfaces: Nature, vol 437, 2005, pp 671679, September 2005.

[6] [R. F. Stephen. "The path to ubiquitous and low-cost organic electronic appliances on plastic,Nature vol 428, pp 911–918 , April 2004.

[7] C. C. Chen et al. " An efficient triple-junction polymer solar cell having a power conversion efficiency exceeding 11%.". Adv. Mater., 2014, vol 26, pp 5670-5677, July 2014. \

[8] S. Seongbeom, Y. Minyang, L.J. Guo and Y. Hongseok." Roll-to-Roll Cohesive, Coated, Flexible, High-Efficiency Polymer Light-Emitting Diodes Utilizing ITO-Free Polymer Anodes". Small, vol 9, pp 40364044, December 2013.

[9] M. T. Bohr, "Nanotechnology goals and challenges for electronics applications'. IEEE Trans. Nanotechnol. vol 99 (1), pp 56–62 , March 2002.

[10] F. Antonio. "Organic semiconductors: Made to order" ature Materials, vol 12, pp 598–600, June 2013.

[11] M. Changez., et al . "Molecular Level Ordering in Poly(2vinylpyridine". Adv. Mater., vol 24, pp 3253-3257, June 2012.

Employing Wind Energy as Aconveyance Mechanismfor India

[1] Yasin Yusuf Halai, [2] Naeesha Yusuf Halai
Department of Mechanical Engineering, Thakur Polytechnic College, Mumbai, India;
Department of Law, Pravin Gandhi College of Law, Mumbai, India

***Abstract*:-- "To truly transform our economy, protect our security, and save our planet from the ravages of climate change, we need to ultimately make clean, renewable energy the profitable kind of energy." -Barack Obama in an address to the Joint Session of Congress on February 24, 2009 Humans depend upon energy in all walks of life. Energy is pragmatic for the longevity of homo sapiens. Energy is the vitality derived from the convention of substantial or enzymatic means. Even energy is an indispensable element of a man`s life apart from food, clothing and shelter. Energy can be broadly classified into two types: Renewable energy and Non-renewable energy.Concepts for alternative energy are not new. They are as old as our civilization. Wind Energy is a form of renewable energy source which is also an alternate form of energy. Wind Energy is an energywhich is available everywhere and in abundance. It is employed using the latest scientific know-how. Wind energy generates electricity which helps a mortal being to provide a source of clean and low cost renewable energy. There are cars that run on wind energy. These cars are also called air cars. These type of cars will work on compressed air.These cars are also known as Zero pollution cars. These cars cause hardly any pollution. It`s important for the human race to utilize these forms of alternative energies. The Research Paper discusses about the forms of energy and emphasizes on the concept of Wind energy powered cars or Zero pollution cars and it`s need in the near future. "When the wind of change blows, some build walls while others build windmills."**

Indexterms: **Alternative energy, Renewable energy, Wind, Zero pollution**

I. INTRODUCTION

"The use of alternative energy is inevitable as fossil fuels are finite." -Gawdat Bahgat "We need to bring sustainable energy to every corner of the globe with technologies like solar energy mini-grids, solar powered lights, and wind turbines." -Ban Kimoon Energy is pragmatic for the longevity of homo sapiens. They require energy in all walks of life. Energy is the vivacity resulting from the usage of physical or chemical means. It is one of the most significant inputs for growth of all sectors including automobiles, engineering, agricultural, industrial service and transport sectors. Energy is being used at the national and global level for the development of society since several decades. The demand for energy all around the world is increasing. Concepts for alternative energy are not new. Theyareasoldasour civilization.There is a constant tussle as to what is "alternative energy" andwhat are it's advantages and disadvantages.It includessolar power, hydroelectric power, and even things like natural gas and "clean coal" whichdonotincreasecarbonfootprints.It also includesnon-traditional methods of energylikesolarenergy, windenergy, geothermal energy,biomass etc. [Refer fig(b)] Alternativeenergyisclean.Itshould be considered in order to improve man`s life.They do not produce harmful intoxicants which can adversely affect the environment. Nuclear energy is not alternative energy. This is because it emits radioactive waste which are highly
toxic and harmful to the personage. They adversely affect human survival.
So, alternative energy, in simple terms, can be called as an energy which will replace fossil fuels and will be commodious for mankind.Energy is broadly classified into two types: Renewable and Non-Renewable sources of energy.[Refer fig(a)]

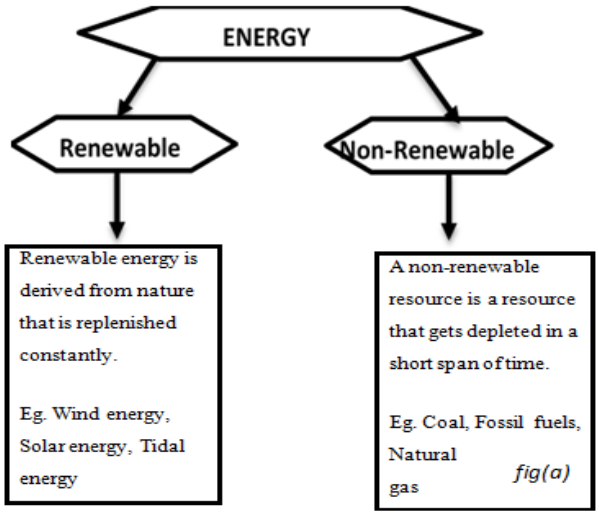

fig(a)

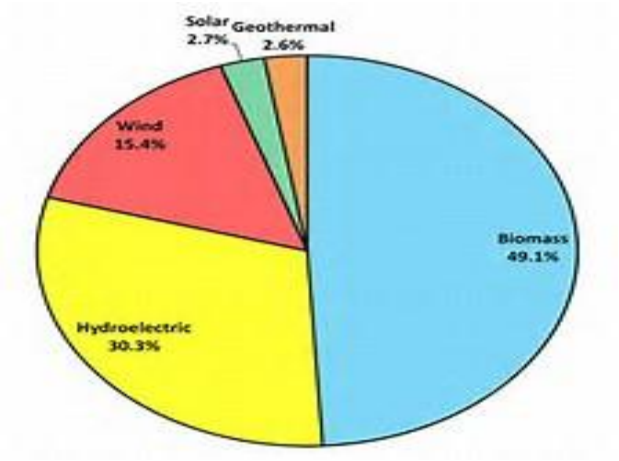

II. MEANING AND DEFINITION OF ALTERNATIVE ENERGY

"It is time for a sustainable energy policy which puts consumers, the environment, human health, and peace first."-Dennis Kucinich Alternative energy is an interesting concept.Tidal energy, Solar energy, Wind energy, Marine energy, Hydroelectric energy, Geothermal energy are all alternative sources of energy.

All these alternative sources of energy are basically a substitute for some other form of energy. Oxford dictionaries define Alternative energy as "Energy fuelled in ways that do not use up the earth's natural resources or otherwise harm the environment, especially by avoiding the use of fossil fuels or nuclear power." Merriam Webster defines it as "Usable power (such as heat or electricity) that comes from a renewable or green resource." As per Dictionary.com it is definedin the following terms, "Energy, as solar, wind, or nuclear energy, that can replace or supplement

traditional fossil-fuel sources, as coal, oil, and natural gas." Natural resources Defense Council defines it as, "Energy that is not popularly used and is usually environmentally sound, such as solar or wind energy (as opposed to fossil fuels)."

III. MEANING AND DEFINITION OFRENEWABLE SOURCES OF ENERGY

"I think that the world is in the middle of a huge transition that we have to make to renewable energy. We have to transition away from fossil fuels very, very quickly."
-Josh Fox
Environmentally, sustainable energy can diminish air pollution which is the initial cause of asthma among youngsters. It disinfects the air which can diminish respiratory diseases and even prevent early ageing amongst the people of all age. Economically, it will aid to safeguard fossils for the forthcoming convention.
Renewable energy can be defined as "an energy from a source that is not depleted when used, such as wind or solar power."
According to Dictionary.com, "Renewable energy is any naturally occurring, theoreticallyinexhaustible source of energy, as biomass, solar, wind, tidal, wave, and hydroelectric power, that is not derived from fossil or nuclear fuel."

"Unless the sun dies, winds stop, plants die and rivers stop running, there will always be green energy to be had. Some of these energy sources are completely free and we have them no matter what. Why not take advantage of them?"
-Edgar Cervantes Wind is simply air in motion. Wind energy is a free and a renewable resource. Oxford dictionary defines wind energy as "electrical energy obtained from harnessing the wind with windmills or wind turbines." Dictionary.com defines wind energy as "power derived from wind: used to generate electricity or mechanical power." Wind energy is abundant. The terms "wind energy" or"wind power" can be described as the process by which the wind is used to generate electricity or mechanical power.

 ISBN: 978-81-932966-9-1

Wind turbines convert the kinetic energy in the wind into mechanical power. Wind is caused by huge convection currents in the Earth's atmosphere, driven by heat energy from the Sun. This means as long as the sun shines, there will be wind. Wind power offers a sustainable option of renewable energy. Wind is the movement of air from an area of high pressure to an area of low pressure. Wind exists because of the sun which unevenly heats the surface of the Earth. As hot air rises, cooler air moves in to fill the void. Till the time the sun shines, the wind continues to blow.

Today, more and more wind turbines are generating electricity from the breeze.

In ancient times, mariners used sails to capture the wind. Farmersused windmills to grind their grains and pump water.Wind energy produces no air or water pollution.

V. USES OF WIND ENERGY

"Studies show that investments to spur renewable energy and boost energy efficiency generate far more jobs than oil and coal." -Jeff Goodell India is probably the only country in the world with a well-developed ministry dedicated to the production of energy from renewable energy sources.In 1950's wind energy was being used in India to pump water for domiciliaryuse as an alternative to diesel pump-sets. Wind energy is the generation of electricity from wind, commonly by using turbines.Wind Energy is used for the production of electricity

Wind energy is the atmospheric kinetic energy determined by the mass and motion speed of air. The kinetic energy K for an air mass m with a wind speed V can be expressed as: $K=1/2mV2$

In the 6th National Five-Year Plan (NFYP) the Government of India introduced the National Windmill Demonstration Program, which, continued throughout the 7th NFYP (1985-1990), and saw the installation of hundreds of units of 12 PU-500 wind pumps for shallow water pumping.

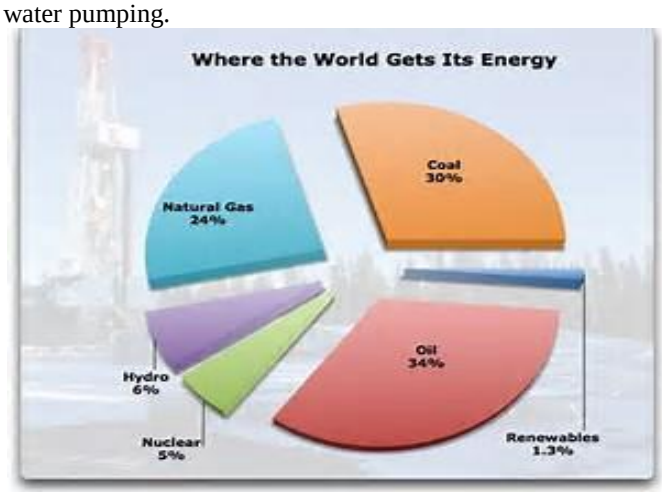

VI. WIND POWERED CAR

"Green energy is the way of the future." -Edgar Cervantes "Of all the forces of nature, I should think the wind contains the largest amount of motive power—that is, power to move things. As yet, the wind is an untamed, and unharnessed force; and quite possibly one of the greatest discoveries hereafter to be made, will be the taming, and harnessing of it."-Abraham Lincoln There are cars that run on wind energy. These cars are also called as air cars. These type of cars will work on compressed air instead of gasoline.

These carsare powered by two cylinders. They have a compressed air engine.These air powered carscause low pollution. So they are even known as ‘zero pollution cars’. These cars are environment friendly. They run on compressed air.

It has various parts. It includes:

(i) Compressed air tanks:It is a tank in a car where heat is exchanged of some kind in order to maintain the temperature of the vehicle

(ii) The body:The entire physical structure avehicle like a car

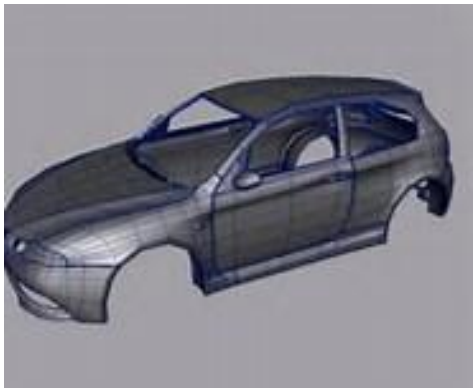

(iii) The Air Filter:An air filter is an important part of a car's intake system. It allows the car to "breathe."

AIR FILTER

(iv) The chassis: A chassis is a frame of a car that supports an artificial object. It is used in car construction. It can provide protection for some internal parts.

Eg. The underpart of a motor vehicle, consisting of the frame usually on which the body is mounted.

(v) Brake power recovery: It is an energy recovery mechanism. It helps in slowing a vehicle or object by converting the kinetic energy present to a form of energy which can be either used immediately or stored until needed.

Zero pollution cars run on compressed air instead of gasoline. It consists of two cylinders, compressed air engines which powers the car. These cars cause hardly any pollution.These enginesrun either on compressed air or act as an internal combustion engine. The air is inserted in a car through an air injector to the engine and flows into a small chamber which later expands the air. These cars are very beneficial for the environment. They are eco-friendly in nature. They help to maintain a sustainable environment. They utilize wind energy in the best possible way.

VII. CONCLUSION

“Alternative energy is a future idea whose time is past. Renewable energy is a future idea whose time has come.”

- Bill Penden

“I've been very passionate about renewable energy for many years, particularly solar energy and its capacity to bring abundant clean, sustainable energy to millions around the globe.”

-Richard Branson

Wind powered cars are the most viable option in order to prevent fosil fuels for the future generation. They help us in maintaining a sustainable and a clean environment. It reduces pressure on non-renewable sources of energy. It makes human survival on this planet possible. Let us take the initiative to use wind powered cars which are beneficial for the human environment and bring about a change because **CHANGE BEGINS WITH US.**

“I feel more confident than ever that the power to save the planet rests with me.”

 ISBN: 978-81-932966-9-1

VIII. REFERENCES

[1] Gipe, P. (2004), Wind Power—Renewable Energy for Home, Farm, and Business, Chelsea Green Publishing, White River Junction, VT.
[2]http://onlinelibrary.wiley.com/doi/10.1002/2013EF000206/ful
[3] https://www.nrdc.org/how-we-work
[4] windeis.anl.gov/guide/basics
[5]www.eschooltoday.com/energy/renewable-energy/wind-energy.html
[6] warming/wind-power/google.co.in
[7]http://onlinelibrary.wiley.com/doi/10.1002/2013EF000206/full

The Microstructures of Hydroxyapatite/Collagen Thin Films Coating on Ti6Al4V TitaniumAlloy Using Electrodeposit Method

[1] Supachai Surapunt, [2] Thanyalak Chumsud
Department of Industrial Engineering, Faculty of Engineering, Thammasat University,
Klong Nuang, Klong Luang,Pathumtani12120

Abstract:-- **Composite coating of hydroxyapatite/collagen (HAP/collagen) was prepared on the Ti6Al4V, titanium alloy platefor implant materials of orthopedic and dental applicationsby using electrodeposit method.The aim of this research was to study the coating process of hydroxyapatite/collagen and investigate the effect of electrical voltage on structure of coating surface. In this research, Ca(NO3)2. 4H2OandNH4H2PO4 were used to prepare HAP, and collagen type I was from SIGMA-ALDRICH. The electrical-voltage coating parameters were usedbetween of 2-10 voltage for 50 minute at room temperature. The result of X-ray diffraction (XRD) test found that at 5 voltageof electrodeposit showed theclearest peaks of hydroxyapatite, which were accordance to thecharacteristic of coating surface and its components which were analyzed by SEM-EDS method, while collagen on coating surface was analyzed by FT-IR method.**

Index Terms-**surface coating,hydroxyapatite,collagen,electrodeposit method.**

I. INTRODUCTION

Hydroxyapatite (HAP) is a bioactive ceramic that is composed mainlyof calcium and phosphorus which are the components of mineral bone [1].It has been coated on metallic implants to promote osseointegration [1]. Most techniques to coat HAP on an implant material, such as plasma spray, electrophoretic deposition and hot isostatic pressing, require high sintering temperature which leads to crack formation due to mismatch of thermal expansion [2]. Furthermore, these techniques are expensive and consume high energy power to operate the instruments [4].

The biomimetic technique is one of the methods to coat HAP on a metallic implant [5]. It does not require high energy power and high processing temperature, preventing the formation of crack and coating instability [3]. Recently, a polydopamine film was utilized to form the biomimetic HAP on medical grade stainless steel (SS316L) through a functionalization process [6]. The application of polydopamine as an intermediate layer to functionalize biomolecules is adopted from the work of Lee et al. [7]. The functionalization mechanism is based on the existence of amine and thiol/catechol functional groups which will participate in the binding process [8]. This mechanism produces strong and stable anchorage properties [9]. Besides, the biomimetic HAP grafted on the polydopamine film mimics the natural properties of bone. Those properties cause the polydopamine film to become a favorable way to optimize the surface of metallic implants [10].

Collagen fibers are another type of component, existing as the main organic composition of bone extracellular matrix [11]. It is commonly used to improve the biocompatibility of implant surfaces [12,13]. These fibers act as a building template for bone formation and provide mechanical strength to bone [14]. The immobilization of collagen on material surfaces through a physical absorption technique shows simplicity and flexibility, but generally this method produces instability of the coating film [15]. Meanwhile, a covalent immobilization technique compromises better control of coating parameters such as coating thickness, ligand density and molecular orientation [16]. There are various strategies to covalently immobilize the collagen onto metallic surfaces that usually involve complex chemistry and regularly induce additional toxic factors [17,18]. Therefore, the exploration of a simple and versatile covalent immobilization technique is crucial to immobilize the collagen fibers to promote osseointegration without producing toxic residues. The aim of this study was to coat collagen type I and HAP on a Ti6Al4V, titanium alloy plate using electrodeposit method.The crystal structure of HAP was investigated by X-ray diffractometer. The morphology of HAP was characterized using scanning electron microscope, and the chemical composition was analyzed by energy dispersive X-ray spectroscopy (EDX).Finally, Fouriertransform infrared

spectroscopy (FT-IR) was used to analyze the molecular structures of HAP and collagen.

II.EXPERIMENT PROCEDURE

A.Material Preparation

Material for electrolytic coating in this study, the Ti6Al4Vtitanium alloy plate with the size of 10 x 20 mm2 and 1.5 mm of thickness was grinded with 600 and 1000 of grid number of abrasive papers and polished with 0.3 micron of alumina powder

B.Solution Preparation

Hydroxyapatite(HPA) solution was prepared with Ca/P ratio at 1.67 by using NH4H2PO4 0.143 mg and Ca(NO3)2.4H2O 0.248 mg dissolved in deionized water 50 ml and stirred by magnetic stirrer at 240 rpm for 30 minus. The concentrations of NH4H2PO4 andCa(NO3)2.4H2O were 0.025 and 0.042 molar, respectively.

HAP/collagen compound solution was prepared by using HAP solution mixed with Collagen Type I at the concentration of 0.1% and was stirred by magnetic stirrer at 240 rpmfor 30 minus.

C.Experimental method

The first step of this study, hydroxyapatite electrolytic coating was carried out at 2, 5 and 10 voltage for 50 minus by usingthe TI6Al4Vtitanium alloy plate as cathode and the stainless steel plate as an anode in HAP solution. Then, the specimen was rinsed by deionized water and dried at room temperature. The HAP coated specimens were analyzed by X-ray diffraction, scanning electron microscope and FT-IR spectrometer. The best condition of HAP coating was selected and coated in the second step of HAP/collagen electrolytic coating. The specimen was analyzed by Fourier Transform Infrared (FT-IR) spectrometer

III. RESULTS AND DISCUSSION

A.XRD Analysis

The standard peaks of the hydroxyapatite crystal structure analyzed by using XRD spectrometer were found at the 2θ angles of 25.89, 28.68, 32.05 and 39.66 [19]. Fig. 1 shows the analysis peaks of the hydroxyapatite crystal structure of the specimens which were coated at 2, 5, 6, 8 and 10 voltage.It was found that the clearest peaks are at 5 voltage coating. The specimens of 5, 6, 8 and 10 voltage were analyzed by scanning electron microscope (SEM) and energy dispersive x-ray spectroscopy (EDX).

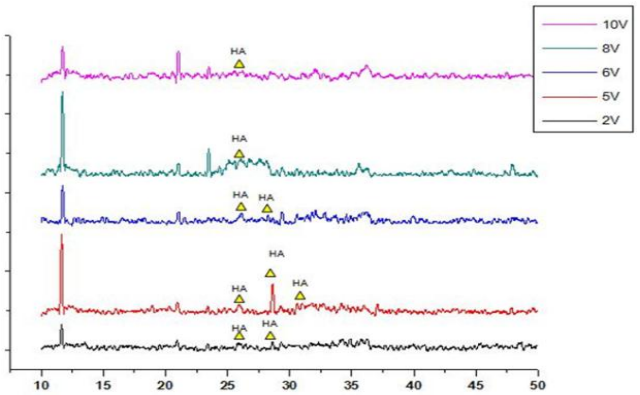

B.SEM/EDXAnalysis

The results of the surface structures of coated hydroxyapatite at 5, 6, 8 and 10 voltage analyzed by SEM were shown in Fig. 2.The plate structure of hydroxyapatite was found. From EDX analysis, the CA/P ratio of 5 voltage coated specimen is at 1.44 which is the nearest ratio of 1.67 in the human bone [20]. The specimen coated at 5 voltage was selected to coat collagen and analyze by Fourier Transform Infrared (FT-IR) spectrometer.

C. FT-IR Spectrometer Analysis

The result of HAP/collagen surface structure of 5 voltage coated specimen analysis by using FT-IR spectrometer shows the relationship between wave range of infrared between 650-4000 cm-1 and transmittance in Fig. 3. The wave numbers of collagen and HAP were found at 1646.31 and 3257.41 cm-1, respectively. The HAP/collagen surface was analyzed by SEM and shown in Fig. 4.

IV. CONCLUSION

The result of HAP coating on the TI6Al4V titanium alloy plate by using electrodeposit method was found that the coating at 5 voltage can be obtained Ca/P ratio of 1.44 which is nearest number of human bone ratio of 1.67. The crystal plate of HAP was found. The coating of HAP/collagen was analyzed by FT-IR spectrometer and found that collagen and HAP were at the wave numbers of 1646.31 cm-1 and 3257.41 cm-1, respectively.

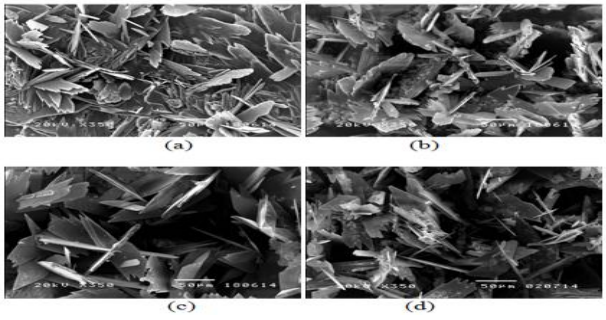

Fig. 2 SEM photographs of hydroxyapatite surfaces coated at (a) 5V, (b) 6V, (c) 8V and (d) 10V

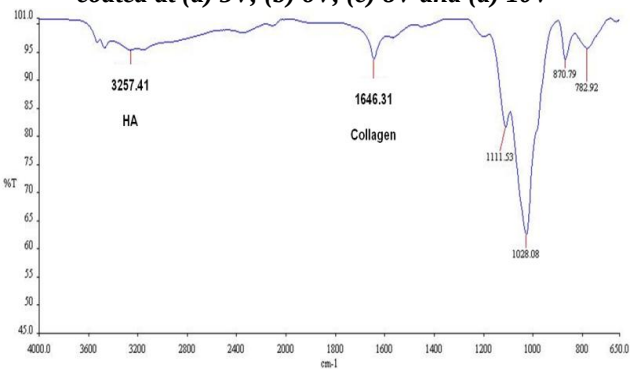

Fig.3 FT-IR spectrum HAP/collagen

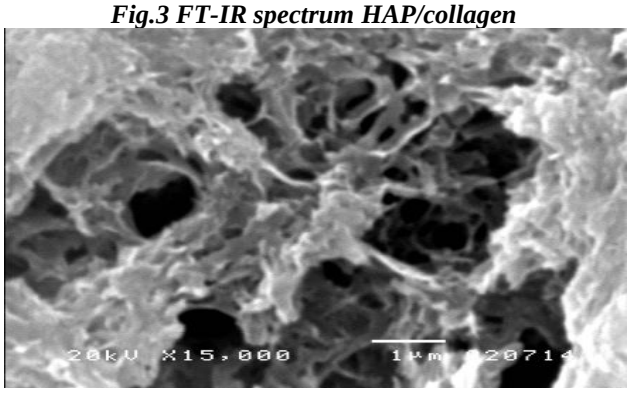

Fig. 4SEM photograph ofHAP/collagen

V. ACKNOWLEDGEMENT

This research was financial supported by Faculty of Engineering, and X-ray diffraction and SEM/EDX analyses were investigated at Department of Physics, Faculty of Science and Technology, Thammasat University, Thailand. The investigation of FT-IR spectrometer was performed at The Science and Technology Research Tool Center, Rungsit University, Thailand.

REFERENCES

[1] J. Faig-Martí, F.J. Gil-Mur, Hydroxyapatite coatings in prosthetic joints, Rev. Esp. Cir. Ortop. Traumatol. (English ed.) 52 (2008) 113–120.

[2] O.S. Yildirim, B. Aksakal, H. Celik, Y. Vangolu, A. Okur, An investigation of the effects of hydroxyapatite coatings on the fixation strength of cortical screws, Med. Eng. Phys. 27 (2005) 221–228.

[3] M. Kamitakahara, C. Ohtsuki, T. Miyazaki, Coating of bone-like apatite for development of bioactive materials for bone reconstruction, Biomed. Mater. 2 (2007) R17–R23.

[4] X. Liu, Coating titanium implant surface comprises gelling hydroxyapatite powder, atomizing and drying into powder, spraying on surface of titanium implant ground blasted with phosphate calcium particles, dry-type dipping, and sintering, in, JIN X (JINX-Individual), p. 12.

[5] G.M. Vidigal,M. Groisman, L.A. de Sena, G.D. Soares, Surface characterization of dental implants coated with hydroxyapatite by plasma spray and biomimetic process, Implant. Dent. 18 (2009) 353–361.

[6] J. Ryu, S.H. Ku, H. Lee, C.B. Park, Mussel-inspired polydopamine coating as a universal route to hydroxyapatite crystallization, Adv. Funct.Mater. 20 (2010) 2132–2139.

[7] H. Lee, S.M. Dellatore,W.M. Miller, P.B.Messersmith,Mussel-inspired surface chemistry for multifunctional coatings, Science 318 (2007) 426–430.

[8] H. Lee, Y. Lee, A.R. Statz, J. Rho, T.G. Park, P.B. Messersmith, Substrate-independent layer-by-layer assembly by using mussel-adhesive-inspired polymers, Adv. Mater. 20 (2008) 1619–1623.

[9] Z.G. Liu, S.X. Qu, J. Weng, Application of polydopamine in surface modification of biomaterials, Prog. Chem. 27 (2015) 212–219.

[10] X. Yu, J. Walsh, M. Wei, Covalent immobilization of collagen on titanium through polydopamine coating to improve cellular performances of MC3T3-E1 cells, Royal Sci. Chem. Adv. 4 (2014) 7185–7192.

[11] P. Sasmal, H. Begam, Extraction of type-I collagen from sea fish and synthesis of Hap/collagen composite, Procedia Mater. Sci. 5 (2014) 1136–1140.

[12] L. Cen,W. Liu, L. Cui,W. Zhang, Y. Cao, Collagen tissue engineering: development of novel biomaterials and applications, Pediatr. Res. 63 (2008) 492–496.

[13] L.C. Abraham, E. Zuena, B. Perez-Ramirez, D.L. Kaplan, Guide to collagen characterization for biomaterial studies, J. Biomed. Mater. Res. Part B Appl. Biomater. 87B (2008) 264–285.

[14] K.-L. Ou, R.-J. Chung, F.-Y. Tsai, P.-Y. Liang, S.-W. Huang, S.-Y. Chang, Effect of collagen on the mechanical properties of hydroxyapatite coatings, J. Mech. Behav. Biomed. Mater. 4 (2011) 618–624.

[15] H. Ao, Y. Xie, H. Tan, X. Wu, G. Liu, A. Qin, X. Zheng, T. Tang, Improved hMSC functions on titanium coatings by type I collagen immobilization, J. Biomed. Mater. Res. Part A 102 (2014) 204–214.

[16] S. VandeVondele, J. Vörös, J.A. Hubbell, RGD-grafted poly-l-lysine-graft (polyethylene glycol) copolymers block non-specific protein adsorption while promoting cell adhesion, Biotechnol. Bioeng. 82 (2003) 784–790.

[17] R. Müller, J. Abke, E. Schnell, F. Macionczyk, U. Gbureck, R. Mehrl, Z. Ruszczak, R. Kujat, C. Englert, M. Nerlich, P. Angele, Surface engineering of stainless steel

materials by covalent collagen immobilization to improve implant biocompatibility, Biomaterials 26 (2005) 6962–6972.
[18] T. Yan, R. Sun, C. Li, B. Tan, X.Mao, N. Ao,Immobilization of type-I collagen and basic fibroblast growth factor (bFGF) onto poly (HEMA-co-MMA) hydrogel surface and its cytotoxicity study, J. Mater. Sci. Mater. Med. 21 (2010) 2425–2433.
[19] M. Haïdopoulos, S. Turgeon, C. Sarra-Bournet, G. Laroche, D. Mantovani, Development of an optimized electrochemical process for subsequent coating of 316 stainless steel for stent applications, J. Mater. Sci. Mater. Med. 17 (2006) 647–657.
[20] Y. Liao, Y. Wang, X. Feng, W. Wang, F. Xu, L. Zhang, Antibacterial surfaces through dopamine functionalization and silver nanoparticle immobilization, Mater. Chem. Phys. 121 (2010) 534–540.

Potential of Soya Beans Seasoning With Garlic and Ginger for Sustainable Health

[1] Aishatu Ibrahim,, [2] Eldah Ephraim Buba
Department Of Leisure And Tourism Management Federal Polytechnic Bauchi

Abstract:-- **This study assessed the use of soya bean in enhancing ginger and garlic seasoning in food production for healthy eating. The objectives of the research was to; produce soya bean seasoning enhanced with ginger and garlic, to produce dishes using enhanced soya bean seasonings for sensory evaluation to taste for acceptability and to review the health benefits of soya bean seasoning with ginger and garlic. The study adopted both survey and experimental research using a purposive random sampling in getting the data. The population of the study was made of the sensory evaluators drawn from among the staff and students of Federal Polytechnic Bauchi, and chefs from selected hotels in Bauchi, Bauchi State. A stratified random sampling was used where fifty (50) sensory evaluators were selected, comprising 25 persons from the polytechnic community and 25 men and women from the hotels as respondents. The study used dried soya beans, ginger, and garlic as sample A, B, and C respectively. Both descriptive statistics and One – Way Analysis of Variance (ANOVA) were used to analyze the data. The result of the study indicated that soya bean – ginger seasoning differs from soya bean – garlic and soya bean – ginger – garlic seasonings at P = 0.717 and 0.148 > 0.05 but soya bean – garlic seasoning shows no significant difference from soya bean – ginger – garlic seasoning at P = 0.024 < 0.05. The study has opened up more avenues for exploiting the numerous health benefits of soy bean, ginger and garlic therefore recommend that; families and commercial hospitality enterprises should adopt and incorporate soya bean enhanced seasonings into their exquisite cuisine and processing of these seasonings should be done under good hygienic condition to avoid contamination because they easily attract germs.**

Index Terms— Soya Beans Potential Ginger Sustainable Health

I. INTRODUCTION

Seasoning is the process of adding herbs, salt, or spices to food, seasoning include herbs and spices which are themselves frequently referred to as seasoning soya beans is widely cultivated all over the world. Garlic grows in many parts of the world and is popular ingredients in cooing due to its strong smell and delicious taste. Leech (2015) explains that ginger is among the healthiest (and most delicious) spices on the planet. Soya beans are traditional part of diet in china, Japan, Korea, Nigeria countries etc. and are currently grown in countries across the world including brazil, Argentina, India unit states and Nigeria. Barnes (2010) discovered that small and unique peptides in soya beans include defacing glycines, Conglycinins and lanansin and all are known to provide us with health benefits, including benefits in the area of improved blood pressure regulation, better control of sugar levels and improved immune function. Fermented soya beans powder or mold have been used in various houses in the Northern Nigeria as local seasoning which gives taste and flavor to food. Likewise the herb and spices garlic and ginger has served as flavoring since earliest time of mankind history. Despite the way garlic and ginger are widely used in Nigeria and it's proved nutritional value to man, it is observed that it has not gained general acceptance by the public. The limited evidence of soya beans seasoning enhanced with ginger and garlic or with other spices is part of the reasons that prompted this study. Personal observation has shown chemical contents in most of the seasoning used for cooking. Numerous studies have shown the negative effect of consuming chemicals to one's health. The advocating for the consumption of natural food substances is a pressing need for healthy eating and living, It is of this reasons the study seek to carry out this research work in order to promote the healthy eating of local women and low income earner, and to gain general acceptability by the public. Bolla (2015), explain that Soya beans foods have become more familiar to consume worldwide and have become a popular choice of many health conscious valued for their Versatility, Taste, Nutritional Content, Environmental Advantages and Health Benefits. Soya available in Boiled Soybeans, Soy Flour, Soy Oil, Soy Sauce, Soy Milk, Soy Tofu, Soy Curd, Fried Soy Curd, Fortified Soy Products for Infants & Women, Fermented Soybeans and other. Soy is used for High Cholesterol, High Blood Pressure. When the pressing needs to alleviate poverty and malnutrition and to improve the welfare of poor people are considered, issues relating to high quality protein food, greater income opportunities for male and female are of paramount importance. Protein content is approximately 40% and fat

20% (Glami, 2002) with considerable variations depending on the cultivars.

II. SOYA BEAN

Morton (2015) observed that heart attack, cancer and stroke are leading sicknesses worldwide. While it is impossible to avoid risk factors such as age, sex and family history, there is plenty we can do to protect our bodies against their life threatening diseases. Science has shown that more of healthy foods is the way to keep the body health and happy. Soya bean is regarded as equal in protein to animal foods. It has been found to be excellent for a number of different conditions such as high blood pressure, diabetes – related diseases and many others (WHF, 2004). Osho and Dashiell (1998) reported that soyabean which has less purchase cost has about 40% protein,30% carbohydrates, 20% oil and 10% mineral. It is very useful in improving the menu of malnourished children and revitalizing heart and breast cancer patients and has no cholesterol.

Studies by Faryna (1987) and Enwere (1998) soyabean can be as a nutritional supplement for pregnant women, lactating mothers and children. The household use of soyabean is targeted to suit local dishes for Nigerians and communities all over the country. About 140 soyabean products are now available (Enwere, 1998; Osho and Dashiell, 1998; Okoruwa, 2002).

A key problem associated with soyabean is that it contains some anti-nutritional factors, which inhibit the availability of the desirable elements such as protein (Lewis, 2015). Fortunately most of these anti-nutritional factors can be destroyed through processing and boiling (Loo, 1978; NAERLS, 1989; Enwere, 1998; Osho and Dashiell, 1998). Major processing of these products includes cleaning, soaking, dehusking, milling, sieving, boiling, roasting and fermentation. Further processing depends on the type of products to be produced, Owolabi and Iita (1995).

However, soya bean is said to cause allergy, trigger such symptoms as vomiting and diarrhea in children, causePhytoestrogen in men, cause tumour or breast cancer in women, cause pancreatic cancer and prostate cancer (Mitchell, Cawood, Kinniburgh, Provan, Collins, Irvine 2001).

A. Nutritional Benefits

Soybeans contain all the three macronutrients required for good nutrition, as well as fiber, vitamins, minerals. Soybean protein provides all the essential amino acids in the amounts needed for human health. Almost 40 per cent of the calories from soybeans are derived from protein, making soybeans higher in protein than any other legumes and many animal products. Protein in just 250

B. Garlic

Food beverage venture (2015) states that garlic has been used to treat a wide variety of illness. Garlic has been used to treat seizure, joint pain, parasite infection, for wood dressing etc. Other health benefits of garlic include lowering cholesterol, athletic performance, building strong bones, detoxing heavy metals, and building strong bone and building immunity. Garlic is anti-fugal, antibacterial it has shown that garlic can build immunity, and speed recovery from the cold and flu (Lewis, 2015).

C. Ginger

Food beverage ventures (2015) identified the benefits of ginger as an antibiotic with anti-inflammatory, antibiotic and anti-viral properties. It protects the kidney and liner from damage, with its array of anti-oxidants and other therapeutic actions. It promotes blood circulation, a condition necessary for efficient for kidney function, ginger also contains an enzyme which helps you digest animal protein that many build up area and weaken the kidneys.

Ginger contains volatile oil, resins and protein digesting enzymes, which neutralize acid and toxins in the digestives tract that harm the kidney. Adel and Prakash (2010) further buttresses this point by describing that Ginger root is the main part of the spice of ginger which contains a number of essential minerals that kills bacteria and small micro-organisms. Yamahara *et al.,* (2011), if there is any patient who is treated with cytotoxic compounds, ginger is recommended basically for the reduction of vomiting, in Related to this, Kraft and Hobbs, (2004) and Adame & Adame, (2001) wrote that ginger root in a suitable recipe form can enhance and stimulate appetite and accelerate digestion and act as ant flatulent for the reduction of bloating and gas.

Ahmed and Sherma (1997) and Surh *et al.,* (1998) find out that, the vitro and animal trials with ginger and ginger root have emphasized that it possesses powerful antioxidant ability and thereby empower with sufficient protective effect against free radical damage. In addition to this, ginger root by products release anti-tumor effects in vitro on particular cells under Epstein-Barr virus stage of infection as well as antioxidant effects that prevent the human body not to be affected in certain types of cancer. Finally, this scientific experiment has shown how ginger root has applicable principles to protect human nerve system and even it may have bright hope in the treatment of Alzheimer's disease. The crude aqueous extract of ginger had been used commonly in tenderizing the tough meats

III.METHODOLOGY

This paper explains the methodology for the study, the research design, target population, sample and sampling technique, data collection instrument, validation of research,

procedure for data collection and the method of data analysis.

The study is a mixed design. It is the combination of survey and experimental research, likewise secondary and primary study. The study is survey because it entails using survey questionnaire to collect some amount of data (Saunders, Lewis &Thornhill, 2012), Survey study is explained by Veal (2012) as a research that collects sample opinions, attitudes of feeling in order to estimate the total or overall situation. Survey researches could be used to test the acceptability of certain educational innovations. An experimental research uses apparatus and materials, and follows a basic procedure for establishing a position from the results obtained. Secondary data are data used for a study that was originally collected for different purpose (Saunders *et al.,* 2009), while primary data are data collected from direct involvement of the researcher or someone assigned by the researcher for the study (Finnegan, 1996). Secondary data is economical; secondary data reduces cost and time for the researcher. (Bryman, 2012, Saunders *et al.,* 2009), in contrast, Saunders *et al.,* (2009) observed that primary data collection can take time and resource of the researcher. Secondary data is extensive; it can be used for longitudinal design allowing researchers to examine the changes (Hammersley, 2004).

A survey questionnaire was used for the study to assess the sensory evaluation of the three products produced from suya beans, ginger and garlic. The practical production in this research was conducted in the hospitality laboratory kitchen and restaurant,

The population for this study which was made of the sensory evaluators was drawn from among hospitality professionals, nutritionist, and chefs from selected hotels in Bauchi, Bauchi State. This is to enable them give a better judgment on the products used for the sensory evaluation. Sample is the segment of a population that is selected in a research; it is the subset of the population (Saunders *et al.,* 2009; Bryman, 2009). The non-probability sampling was chosen based on the researcher's judgment regarding the population characteristics (Johnson and Clark, 2006). The population characteristics are those features used in identifying the population (Travers, 2001). Purposive sampling is a form of non-probability sampling which a researcher samples cases in a tactical way so that they units are relevant to the research questions. Fifty (50) sensory evaluators, comprising 25 persons from the polytechnic community and 25 men and women from the hotels and general public formed the body of respondents. The taste panelists evaluated the dishes produced from the soya bean enhanced seasoning on the basis of taste, colour, aroma and texture using a likert scale.

A.Data Collection Procedures

The first stage was the production of the soya seasoning which was used in producing local delicacies to determine the level of acceptability of the products. Nine different dishes were produced using the three different seasonings produced on fish pepper soup, Joll of rice and mixed vegetable and pounded yam. The panelists tasted the dishes produced with soya beans seasoning enhanced with garlic and ginger and then rated them based on their judgment. The sensory evaluation was carried out by the respondents in the Federal Polytechnic Bauchi demonstration restaurant. This is because of the facilities available for production and service of the dishes to the group of panelists. All samples produced were documented on a CD.

The method of data analysis employed by the researchers includes descriptive statistics and One – Way Analysis of Variance (ANOVA). A brief analytical description was included for each statistical presentation in order to aid clarification and to justify findings from the respondents about the variables based on the taste, flavor and appearance of dishes prepared. For the third objective of the study which entails secondary data; data analysis of secondary data analysis is the analysis of data by researchers who will probably not have been involved in the collection of those data, for purposes that in all likelihood were not envisage by those responsible for the data collection.

IV. DATA PRESENTATION, DATA ANALYSIS AND DISCUSSION

This paper consists of the data collected for the study which includes data presentation, data analysis, data interpretation and discussions. A total of forty-five respondents randomly selected from among the hospitality lecturers, students and industry practitioners participated in the taste panel for this research. Three sampled dishes prepared with Soya bean - ginger seasoning, soya bean – garlic seasoning and Soya bean – ginger- garlic seasoning were produced and served to the panelists respectively. The products were evaluated against taste, aroma, appearance and general acceptability on a 5-point scale ranging from very poor to very good. The cumulative mean rating on taste, aroma, appearance and general acceptability of the panelists was determined as follows: 5= Very good, 4= Good, 3= Fair, 2= poor and 1= very poor. The data collected are analyzed below:

Table 1: Sample A1 Pepper Soup seasoned with soya beans and ginger

Variables	Average mean	Total Response
Taste	4.35	45
Aroma	4.33	45
Appearance	4.47	45
General acceptability	4.44	45

Source: Sensory Evaluation (2016)

The table above shows data from the taste of the fish pepper soup seasoned with soya bean and ginger. The result shows the taste is considered very good with average mean score

of responses of 4.53.Aroma has an average mean score of 4.33 which is good while appearance and general acceptability have mean score of 4.33, and 4.44. The data above shows that the seasoning of soya beans and ginger is generally accepted.

Table 2: Sample A2, Pepper Soup Seasoned with Soya Beans and Garlic

Variables	Average mean	Total Response
Taste	3.27	45
Aroma	4.33	45
Appearance	4.47	45
General acceptability	4.01	45

Source: Sensory Evaluation (2016)

Data shown on the above table on the taste of the pepper soup using soya beans and garlic has average mean score of 3.27 which rates as poor. The aroma has 4.33 which is good. The appearance of the meal has a mean of 4.47 which is good. General acceptability is good with average mean score of 4.01.

Table 11: ANOVA (LIKENESS)

	Sum of Squares	Df	Mean Square	F	Sig.
Between Groups	1.234	2	.617	3.736	.026
Within Groups	21.806	132	.165		
Total	23.040	134			

Source: Sensory Evaluation 2016

Table 8 above shows the results of One-Way ANOVA performed to test the relative acceptability of the three products from Soya Bean Composite seasonings. At **α** = 0.05, F (3.736) P=0.026<0.05. Hence, the null hypothesis is rejected and the alternate is accepted. There is statistically significant difference among the three products from soya bean composite seasonings. The detailed explanation for this result is seen in the Multiple Comparisons in table .K..

Table 12: Multiple Comparisons

(I) Samples	(J) Samples	Mean Difference (I-J)	Std. Error	Sig.	95% Confidence Interval	
					Lower Bound	Upper Bound
Soya bean + ginger Pepper soup	Soya bean + ginger pepper soup	-.06667	.08569	.717	-.2698	.1364
	Soya bean + ginger + garlic pepper soup	.16111	.08569	.148	-.0420	.3642
Soya bean + garlic jollof rice	Soya bean + ginger jollof rice	.06667	.08569	.717	-.1364	.2698
	Soya bean + ginger + garlic jollof rice	.22778*	.08569	.024	.0247	.4309
Soya bean+ ginger + garlic mixed vegetables	Soya bean + ginger mixed vegetables	-.16111	.08569	.148	-.3642	.0420
	Soya bean + garlic mixed vegetables	-.22778*	.08569	.024	-.4309	-.0247

***. The mean difference is significant at the 0.05 level.**

From this table, it is noticed that the seasoning used in Soya bean + ginger Pepper soup differs from Soya bean + ginger pepper soup. Likewise suya beans + ginger pepper soup differs with Soya bean + ginger + garlic pepper soup at P = 0.717 and 0.148 > 0.05. Soya bean + garlic jollof rice

differs with Soya bean + ginger jollof rice with P= 717>0.05. However soya beans + ginger jollof rice and Soya bean + ginger + garlic jollof rice seasoning shows no significant difference from soya bean – ginger – garlic

seasoning at P = 0.024 < 0.05. Soya bean+ ginger + garlic mixed vegetables and Soya bean + ginger mixed vegetables differs at P=0.148 while Soya bean+ ginger + garlic mixed vegetables and Soya bean + garlic mixed vegetables has no significant difference with P = 0.024 < 0.05.

Table 13, Uses and benefits of Suya beans, Ginger and Garlic to health

Suya Beans	Ginger	Garlic
Cancer prevention, and	Antibiotic and anti-viral properties	Wound dressing etc.
Cholesterol reduction,	It promotes blood circulation,	Flavour in meals
Combating osteoporosis	Efficient for kidney function,	Lowering high blood pressure (BP)
Menopause regulation	Neutralize acid and toxins in the digestives tract that harm the kidney.	lowering cholesterol
Useful for treating menstrual symptoms in females.	Treatment of nausea, common cold, anemia, toothaches, and hemorrhages.	treatment for the common cold and flu
Nutritional supplement for pregnant women	Treatment blood pressure,	treat seizure, joint pain, parasite infection
Supplement for lactating mothers and children.	Treatment of Alzheimer's disease.	Anti-fugal and antibacterial
Lowers high blood pressure	Stimulate appetite and accelerate digestion.	Increases athletic performance,
Lowers cholesterol	Act as flatulent for the reduction of bloating and gas	building strong bones,
	Tenderizing the tough meats.	it has shown that garlic can build immunity,

Source: Abdeldaiem, Hoda& Ali, 2014; Hammami and El-May, 2012; Adel and Prakash, 2010; Lewis, 2015; Rakasi, 2011; Ahmed and Sherma, 1997; Surh, Kim, Liem, Lee, Miller, 1998.

The table above has the various uses and benefits of suya beans, ginger and garlic. The study identified findings of different authors on this. Suya beans, garlic and ginger are used for treatment and control of diseases, cooking of meals, dressing of wounds, nutritional supplements, menopause regulation and flavor in meals.

V. DISCUSSIONS

Findings of the study show favourable results on the three products produced. The study produced nine dishes seasoned by the products. Findings on the fish pepper soup which has three dishes made from suya beans and garlic, suya beans and ginger and suya beans, ginger and garlic gained acceptability. The taste of the meal with suya beans and ginger, likewise that of suya beans, ginger and garlic were rated high which shows the product is accepted. The second meal which is jollofrice cooked by the same products shows the taste of all the three samples accepted. The third meal which was mixed vegetable soup with pounded yam has the seasoning of suya beans and ginger, suya beans, ginger and garlic all rated very good and good respectively, however the seasoning with suya beans and garlic has a fair acceptance of taste. Though the taste of the meal with suya beans and garlic season shows fair rating, the result still shows acceptability.

Many have feeling of food being fresh due to its smell and they discovered it was fresher (Kivela and Crotts, 2006). The aroma derived from food is a motivation for eating of the particular food. Seasoning tends to contribute to food aroma and adds to choice of some certain types of seasoning used for cooking. The aroma of the pepper soup, jollof rice and the mixed vegetable soup were all accepted. Though the aroma for suya beans seasoning and garlic on the vegetable soup was rated fair. On the appearance of the dishes, the fish pepper soup, jollof rice and the mixed vegetable soup with pounded yam all have good appearances. The general acceptability of the three types of seasoning on the three dishes shows that all dishes cooked with the soya bean enhanced seasoning were generally good and accepted. The taste, aroma and appearance of the dishes compare favorably as can be seen from tables 1 to 9. Considering the composition of the sensory evaluation panel drawn from the industry and institution, the implication of this finding is that soya bean seasoning enhanced with ginger and garlic could offer an excellent choice among the condiments in Nigerian cuisine.

This supports the findings by Furst *et al*. (1996) which identified that sensory perceptions can play a crucial physiological and psychological part in appreciation of food. They further mentioned that sensory perceptions represent the considerations that people develop related to their taste in eating and drinking. In addition, taste can be a key consideration for most people in nearly all food and

drinking settings. Furthermore, Kivela and Crotts (2006) emphasized that tasting local food and beverages are a kind of pleasurable sensory experience.

The relative acceptability of the three products from Soya Bean Composite seasonings are at $\alpha = 0.05$, F (3.736) P=0.026<0.05. Hence, the null hypothesis is rejected and the alternate is accepted. There is statistically significant difference among the three products from soya bean composite seasonings. Comparison of the three products on nine different dishes shows seasoning used in Soya bean + ginger Pepper soup differs from Soya bean + ginger pepper soup. Likewise suya beans + ginger pepper soup differs with Soya bean + ginger + garlic pepper soup at P = 0.717 and 0.148 > 0.05. Soya bean + garlic jollof rice differs with Soya bean + ginger jollof rice with P= 717>0.05. However soya beans + ginger jollof rice and Soya bean + ginger + garlic jollof rice seasoning shows no significant difference from soya bean – ginger – garlic seasoning at P = 0.024 < 0.05. Soya bean+ ginger + garlic mixed vegetables and Soya bean + ginger mixed vegetables differs at P=0.148 while Soya bean+ ginger + garlic mixed vegetables and Soya bean + garlic mixed vegetables has no significant difference with P = 0.024 < 0.05. Lewis, 2015; Rakasi, 2011)

VI. CONCLUSION AND RECOMMENDATION

The purpose of this study is to determine the acceptability of enhanced seasonings produced from soya bean, using ginger and garlic as the composites. The results of the sensory evaluation reveal that the seasonings were rated good and accepted as seasonings that could be used in the commercial hospitality industry. The outcome of this study and its significance coincide with many other previous researches conducted to determine the uses of ginger and garlic both for nutritional and medicinal purposes.

Soya bean, ginger and garlic can be used in various forms in cookery. They can be used as spices, condiments or seasonings. In this study they were processed and used as seasonings enhanced with ginger and garlic.

A.Recommendation

The acceptability of the ginger and garlic used in enhancing suya beans seasoning is a finding that is of benefit to numerous individuals and organizations. The study therefore recommends that:

- Families and hospitality enterprises should adopt and incorporate soya bean enhanced seasonings into their exquisite cuisine.
- Those into healthy or natural dieting can replace the different seasonings used which contain chemicals with this natural and healthy product.

B.Recommendation for Further Research

This study recommends the following areas for further studies:

- Further research should be conducted to determine the shelf life of soya bean seasoning enhanced with ginger and garlic.

REFERENCE

[1] Abdeldaiem, M., Hoda , H., & Ali , G. (2014). Tenderization of camel meat by using fresh ginger (Zingiberofficinale) extract. *Food Science and Quality Management 23*, 25-38.

[2] Ahmed, R., & Sharma, S. (1997). Biochemical studies on combined effect of garlic(Allium sativum Linn) and ginger (Zingiberofficinale Rosc) in albino rats. *Indian journal of experimental biology 35*, 841-843.

[3] Ajayi, G., & Arvind, B. (2009). Genistein: A multipurpose flavone. *International Journal of Green Pharmacy Year: 2009 Vol: 3 Issue: 3*, 176-183.

[4] Barnes, S. (2010). The Biochemistry, Chemistry and Physiology of the Isoflavones in Soybeans and their Food Products. *Lymphat Res Biol. 2010 March; 8(1)* , 89—98.

[5] Bollak, N. (2015). *International Journal of Scientific & Technology Research Volume 4, Issue 07, July Issn 2277*.

[6] Cerella, C., Dicato , M., Jacob , C., & Diederich , M. (2011). Chemical properties and mechanisms determining the anti-cancer action of garlic-derived organic sulfur compounds. *Anticancer Agents Medicinal Chemistry 11*, 267–271.

[7] Enwere, N. J., Ukaegbu, K. O., & Nwokolo, E. (1992). Development of Soyabean [Glycine max (L.) Merr.]. In: high fibre breakfast cereal product with by product Legume and Oilseeds in Nutrition. S E.

[8] Faryna, P. J. (1987). Soybean in Nigerian Diet, Extension . *Conference of the institute of Food Science and Home Economics Series No.1, Agric Technology, Enugu October*, 26-30.

[9] Glami, S. Y. (2002). Chemical composition and nutritional . *Workshop on Small-scale and Industrial Level attributes of selected newly developed lines of Processing of Soya bean, July, 1993, Ibadan*.

[10] Hammami, I., & El-May, M. (2012). Impact of garlic feeding(allium sativum) on male fertility,Andrologia.

Identifying and Maintaining Overleaded Servers Through Dynamic Placement of Virtual Machines in Cloud

[1] Dr. Md. Mahbubul Alam Joarder, [2] Asif Imran, [3] Lamisha Rawshan
Institute of Information Technology, University of Dhaka, Ramna, Dhaka 1000, Bangladesh

***Abstract*:-- The cloud has become a widespread and commonly used service due to its improved resource utilization. The little maintenance expense and on demand characteristics of cloud has made it one of the most popular commercial infrastructure. However, cloud computing possesses many kinds of technical challenges such as fault tolerance, reliability, availability, integrity etc. But the main problem related to all those is overload incurred by Virtual Machines (VM). This research proposes an approach to identify and manage overloaded servers with dynamic placing of its VMs. It monitors and stores resource usage data. The algorithm checks server resource usage status by calculating the value of skew after a predefined time interval. Next skewness is used to identify the over-loaded and under-loaded vm-instances. Positive skewness indicates overloading and negative skewness indicates under-loading. For experimental purposes, -0.75 is considered as the lower threshold and 1.50 is considered to be the upper threshold. Experimental evaluation show that out of the 40 vm-instances, on average 17 vm's were found to be under-loaded and 10 vm's were found to be over-loaded. The analysis shows that using skewness to aid in migration reduces migration time by about 21% for user processes ranging from 1500 to 3000 users.**

***Keywords*: Cloud Computing, Resource management, Skewness, Virtual machine migration, Overload Detection**

I. INTRODUCTION

Cloud is a group of physical machines pretending to be one computing environment [1]. User see the cloud as an illusion of unlimited computing resources [2]. But the main challenge is to manage the variability and heterogeneity of application requirement [3]. VMs shares the resources of PMs among several users to maximize the use of resources. The mapping of these PMs to VMs is very important to gain better performance of cloud computing [4]. This mapping is completely unknown to the users. They have no knowledge about the location of the PMs from where their VM is running. It is one of the main responsibilities of the cloud provider to meet the resource demand of users. The capability of PM must satisfy the resource demand of VMs running in it. Otherwise, the PMs will degrade its performance due to overloaded VMs [5]. From this the need to a framework that detect load of a PMs and dynamically place VMs in a way to maximize the resource utilization is needed.

This paper will present a framework to detect overloaded PMs and manage VMs re- sponsible for overload. To improve performance of the existing scheme, skewness detection mechanism has been used. Skewness can be of two types. One is positive skewness and the second is negative skewness. Any type of skewness will indicate that the server is either heavily loaded (positive skewness) or under-loaded (negative skewness). As a result, it is an important indicator of the current load distribution of servers. Since load distribution is an important aspect of cloud computing, it can be effectively managed with skewness.

This paper proposes an algorithm to detect the current load on cloud servers. At the same time, it presents a mechanism which shows the Effective X-factor based mechanism has been described for the detection of load on servers in the cloud. Next algorithms for the detection of skewness in the load of the servers are provided. Afterwards an algorithm for Reallocation of resources to solve the issue of overload and under-load has been described. Effective framework to detect the migration of the jobs in the cloud to reduce the overload or under- load condition has been provided. Results have been tabulated which shows the number of migration jobs which are performance affecting can be reduced if skewness is determined and based on skewness the decision are taken. Also, the performance improvement of skewness based reallocation of jobs is seen when results indicate that time taken to re-allocate resources significantly decreases when the output of detected skewness if followed.

The rest of the paper are as follows. Section 2 represents the concise discussion on the existing research in our field of interest. Section 3 showcases the proposed methodology and algorithms and provides justification on the effectiveness of using skewness. Section 4 highlights the experimental test-bed (i.e. environment) which was set up and used for this research. Section 5 shows the obtained

results and presents a discussion on these results. Finally, Section 6 draws a conclusion to the paper and identifies some scope of future research in this field.

II. LITERATURE REVIEW

An inaccurate resource allocation can cause insufficient use of resources, higher cost and low performance [6]. Because of the importance and effectiveness of performance increasing in recent years, researchers have discussed different methods of load detection and dynamic placement of VMs. This section highlights recent works that are performed to identify overloaded servers and managing those VMs of cloud computing. Vijayakumar et al. [7] have presented a model to allocate resources dynamically for data streaming applications. The main objective of their research is to ensure careful allocation of resources to avoid both over provision and the under provision. They detect buffer overflow by comparing time interval between receiving two blocks of streaming data and processing of one block of that data. When any overflow occurs their model increase a fixed amount of CPU based on requirement. They define a fixed amount of CPU percentage for multiplicative increase and additive decrease of CPU. They evaluate their model in both static and dynamic environments. In their research, they used fixed amount of CPU addition which is costly.

Multi-Attribute Utility Theory is used for VM allocation and migration. VM allocation and migration decision is affected by many attribute like resource availability, network band- width, network cost and Service Level Objectives (SLO) violation. In this scheme, nodes are organized using unstructured Peer-to-Peer (P2P) architecture to avoid single point of fail- ure threat. Every physical machine collects information from its neighbored with a constant distance.

III. PROPOSED METHODOLOGY

This section describes the algorithm for detecting overloaded servers and necessary self- healing to recover from failed condition. The algorithm maintains a timer, SpareT ime after which it becomes alive to collect data. It collects I nputRate, OutputRate, M axM emV ector, and ResourceU tilizationV ector over a specified interval.

The LoadDetection algorithm detects overloaded server by calculating the value of skew. The SkewDetection algorithm detects the percentage of unevenness of resource utilization among the PMs. So, it computes resource utilization skew of the cloud by combining re- sources utilization of its PMs. This skew is compared with a threshold. If skewness crosses the threshold, it means uneven resource utilization exists in the cloud. Therefore, perfor- mance of some PMs can be degraded. In this situation VM redistribution is needed to equalize load. Next, it computes X factor values to fix the destination of the overloaded PMs. ResourceM apGenerator uses the X factor values and generate a resource map to reallocate VMs to PMs.

Detection of the skew is a way to understand that all resources occupied load distribution symmetrically. This section contains an algorithm to detect uneven resource utilization (Skew) between PMs.

3.1. Skew Detection Algorithm

Skewness is an important aspect of statistics which will ensure that whether the system is over-loaded, under-loaded or the load is evenly distributed. As a result, if the graph has positive skewness then it is overloaded, on the opposite if it is under-loaded then the graph will have negative skewness. Our load is to use the skewness graph to detect which servers are overloaded and under-loaded and finally evenly distribute the load across the system to ensure evenness. the reason for using skewness is to ensure that the load can be distributed to a greater level of accuracy using less time which will ensure that the system is optimized in performance. The more the number of physical machines, the power of skewness is likely to be even more clear in terms. also skewness will enable lesser number of migrations.

One common property of cloud computing that can cause low performance or failure is uneven distribution of resources. So it is necessary to distribute resources in such a way that all nodes of a system will consume approximately similar amount of memory (uniform load distribution) . In order to prevent unevenness of resource distribution, detection of skew is necessary. Node with enough space will be chosen for migrating an overloaded VMs. Equation 1 contains formulas for detecting resource utilization skew of overall cloud. Skew,

$$S = \frac{m_3}{m_2^{\frac{3}{2}}} \tag{1}$$

Here

$$m_2 = \sum_{i=1}^{i=N} \frac{(U_i - U_{avg})^2}{N} \tag{2}$$

$$m_3 = \sum_{i=1}^{i=N} \frac{(U_i - U_{avg})^3}{N} \tag{3}$$

In equations 2 and 3, Ui indicates memory uses of ith server in the time, t. N is the total number of PMs running in the cloud. At last, skew is generated using the values of m2 and m3. From the value of S, resource redistribution decision will be made. The value of S will help to decide if further resource reallocation is needed or not. When the resource distribution is approximately symmetric, migrations of VMs will be stopped.

Algorithm 1 Find Skew of the Cloud

Input: $N, ResourceUtilizationVector, ResourceRequirement$
Output: $Skew$
1: procedure SKEW DETECTION
2: for $i \leftarrow 1$ to N do
3: $m \leftarrow Number\ of\ VMs\ running\ on\ i^{th}\ PMs$
4: for $j \leftarrow 1$ to m do
5: $m_2 \leftarrow \sum_{j=1}^{j=N} \frac{(U_j - U_{avg})^2}{N}$
6: $m_3 \leftarrow \sum_{j=1}^{j=N} \frac{(U_j - U_{avg})^3}{N}$
7: end for
8: end for
9: $S \leftarrow \frac{m_3}{m_2^{\frac{3}{2}}}$
10: $Skew \leftarrow S$
11: Return $Skew$
12: end procedure

This algorithm is presented in 1. The Skew Detection algorithm takes 2 inputs- Num-ber of physical machines and Resource utilization metrics. By using equation 2 and 3, it determines the deviation from average usage for every server. It calculates Skew for the cloud.

Algorithm 2 Reallocate Overloaded VMs

Input: $Skew, ResourceUtilizationVector, OverloadedPMsIDVector$
Output: $ResourceReAllocationMap$
1: procedure RESOURCE ALLOCATION
2: for $i \leftarrow 1$ to N do
3: $X_i \leftarrow \frac{(U_i - U_{avg})}{D}$
4: $m \leftarrow Number\ of\ VMs\ running\ on\ i^{th}\ PMs$
5: for $j \leftarrow 1$ to m do
6: $ServerID \leftarrow AllocateResource(X_i, ResourceUtilization[i][j], OverloadedPMsIDVector)$
7: $ResourceReAllocationMap \leftarrow ResourceMap[ServerID][j]$
8: end for
9: end for
10: Return $ResourceReAllocationMap$
11: end procedure

3.2. Placement of Overloaded VMs

In the above section we discussed about the skew detection mechanism. When skewness is not in the range of the threshold value, VM migration will be done using the value of X factor. X factor is the value which de

$$D = \sqrt{\sum_{i=1}^{i=N} \frac{(U_i - U_{avg})^2}{N}} \quad (4)$$

X-factor,

$$X = \frac{(U_i - U_{avg})}{D} \quad (5)$$

ResourceMapGenerator algorithm determines which PM can continue normal work ow of overloaded servers. The input of this algorithm is -Skew, overloaded servers and resource utilization details. It outputs ResourceReAllocationMap from overloaded PMs to VMs. The procedure is depicted in algorithm 2. It sorts the X values list in decreasing order. Add overloaded VMs resource requirement with the low valued PMs. The main purpose is to choose a PM with low valued and enough space for migrating overloaded server. If the PM with low X value have enough space to continue the normal work of overloaded VMs, map the VM with the PM. If the PM with low x value not satisfy the resource requirement, choose the second low valued PM.

IV. EXPERIMENTAL TESTBED (I.E. ENVIRONMENT)

For experimental purpose, BSD Unix systems have been used. More specifically, in BSD Unix system, the researchers installed OpenStack Cloud which had kernel virtual machine (kvm) enabled. as a result of this the virtualization methodology can be used to lauch vm instances and migrate workload into the new vm-instances whenever a machine is overloaded. In the case of under-loading, the vm-instances were reduced in number after migration of the jobs running in under-loaded servers into other vm-instances. As a result, cloud virtualization was used.

Apart from the physical sertup of cloud computing environment, the researchers im- plemented the algorithms in those cloud server to detect the number of U nusedmachines, skewness, mean of the machine load, Standard Deviation, m1, m2 and Z − scores. Based on a series of calculations, the under-loaded and overloaded machines were determined. It was seen that for experimental purposes, 1.5 was considered to be the upper threshold whereas -0.75 was considered to be the lower threshold. Based on this, the overloaded and under-loaded servers were identified as shown in Figure. Skewness was determined for a range of +.5 to -.5 which is normal. Above this range all are asymmetrical. Range is +1.0 to -1.0 is normal also. Hence, above this range all numbers are considered to be asymmetrical as well. Based on the above

determinations, the experiment was repeated for 6 times using the same set of vm-instances in the cloud using various workloads and based on that the under- loaded and overloaded servers were marked. More specifically, 40 vm-instances were tested for this purpose. Hence, the algorithms automatically identified the overloaded and under- loaded vm-instances and the migration algorithm conducted migration more effectively using the skewness. The results of this proposed experimental setup is highlighted in the later sections of this paper.

V.ANALYSIS OF OBTAINED RESULT

This section focuses on the results of proposed algorithms. It shows performance of proposed algorithms by graphical representation. Resource utilization vs. load graph shows the performance of skew detection algorithm. A comparison is given between the traditional approach and our algorithm which shows that the proposed algorithm needs less number of migration to equalize loads between physical machines. As seen in Figure 1, the purple line are showing which machines are under-loaded. On the other hand, the red colored Z-scores represent which marks are over-loaded. As a result, the skew detection algorithm can be effectively used to detect the under-loaded and overloaded vm-instances. For the 40 vm-instances covered in our test case, 21 are shown in Figure 1. The output of all Z-scores for the 40 vm-instances used in our experiment are shown in Figure 2. As we considered 1.5 to be the upper threshold of the Z-scores, it was found that 7 vm-instances are over-loaded. On the other hand -0.75 was considered to be the lower threshold as per out experimentation assumptions. Hence, 9 vm-instances were found to be under-loaded. This shows that number of overloaded machines are lesser than number of under-loaded machines, which is caused mainly due to the type of workload.

Machine Name	Unused Resource, x	Mean, A	STD. DEV	Skewness	Deviation x-A	m2 987.95	m3 34878.3	Z-scores
1	5				-25	625	-15625	-0.79537608
2	6				-24	576	-13824	-0.76356104
3	9				-21	441	-9261	-0.66811591
4	12				-18	324	-5832	1.940717635
5	13				-17	289	-4913	-0.54085573
6	4				-26	676	-17576	-0.82719112
7	11				-19	361	-6859	1.527122073
8	3				-27	729	-19683	-0.85900617
9	1				-29	841	-24389	-0.92263625
10	13	30	31.43167192	1.123189049	-17	289	-4913	-0.54085573
11	4				-26	676	-17576	-0.82719112
12	16				-14	196	-2744	-0.4454106
13	10				-20	400	-8000	-0.63630086
14	17				-13	169	-2197	-0.41359556
15	18				-12	144	-1728	-0.38178052
16	2				-28	784	-21952	-0.89082121
17	5				-25	625	-15625	-0.79537608
18	7				-23	529	-12167	-0.73174599
19	23				-7	49	-343	-0.2227053
20	29				-1	1	-1	-0.03181504
21	45				15	225	3375	0.477225648

Figure 1: Sample test vm-machines with load detection

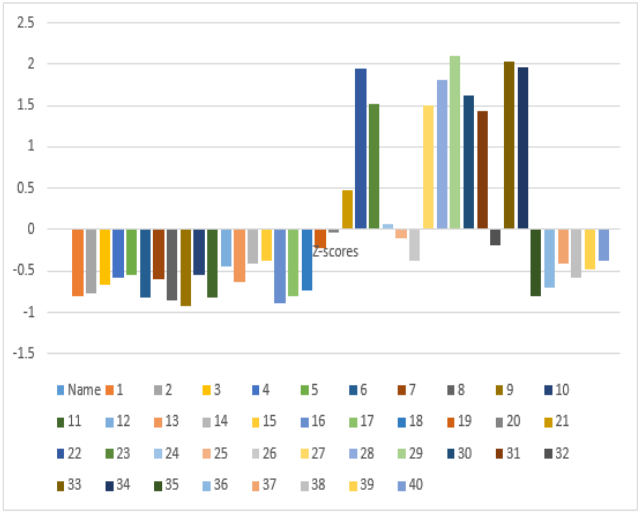

Figure 2: Machine wise identification of vm overloading and vm-under-loading

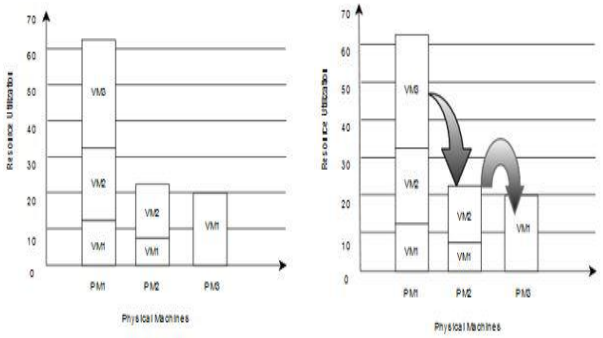

(a) Figure 1(a) ***(b) Figure 1(b)***

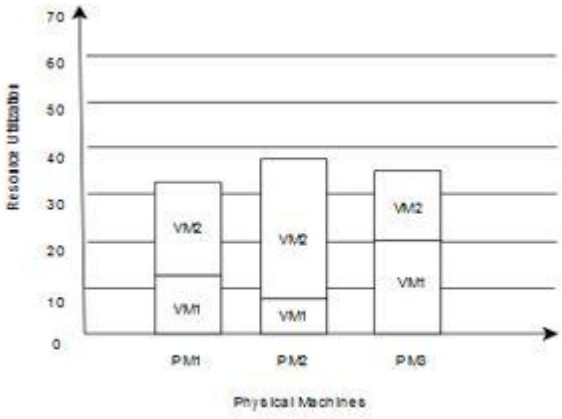

(c) Figure 1(c)

Figure 3: Resource utilization in the physical machines

5.1. Resource Utilization vs Load The main goal of proposed algorithm is to equalize resource utilization among PMs. Because uneven utilization of resources reduce overall performance of cloud as well as service expectation of users. Figure 3 shows a graph containing three physical machines. The Y-axis indicates resource utilization of

respected machines. It indicates resource consumption of three machines. Here, resource utilization of machine 1 is more than average. On the other hand, 2nd and 3rd machines resource utilization is little. Using the skew Ndetection algorithm a resource reallocation map is generated. Figure 3(b) indicates where to allocate the extra load of machine 1. Figure 3(c) presents the utilization of machines after implementing map.

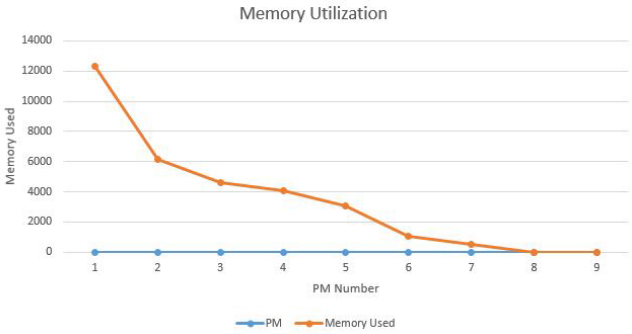

Figure 4: Memory Utilization Before Migration

5.2. Skew detection of cloud

Table 1: Skewness

Memory Uses of PMs	Skew Before Migration	Skew After Migration
12288	9*1.12	9*0.19
6144		
4608		
4096		
3072		
1024		
512		
0		
0		

Table 1 represent values of PMS memory utilization in the cloud. For this simulation two thresholds are selected to compare with the skewness. When skewness is greater than 1 or less than - 1, the resource distribution is considered as highly asymmetry otherwise it is moderately symmetry. Before migration of VMs the skew value of cloud is 1.1278. Which means the resource distribution is highly asymmetry in compared to the threshold. Figure 4 shows a chart with positive skewness. The graph is spotted in respect to memory utilization of all the PMs. So, a long tail is shown in positive side. It indicates that the cloud contains uneven resource distribution. So there exists a possibility of low performance as some of the PMs are highly loaded by its VMs. Figure ?? shows the result of resource distribution after implementing our algorithm. Now the skewness is 0.19. The resource distribution is now symmetric.

Table 2: Skew Detection execution Time

User	Average Execution Time (with skew millisec)	Average Execution Time(millisec)
500	2.9	2.9
1000	5.8	6.1
1500	11.5	13.6
2000	15.5	19.4
2500	24.89	28.7
3000	31.5	39.7

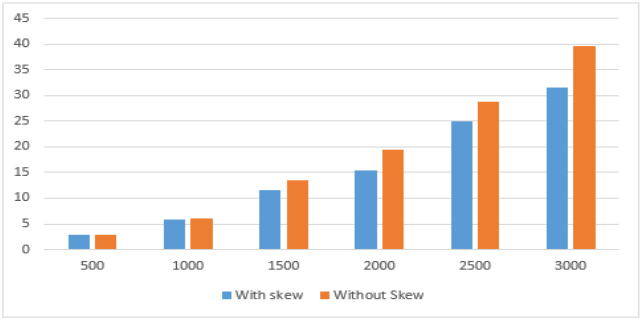

Figure 5: Comparison of execution times when migration is done with skewness and without using skewness

Table 3: Migration Number

User Number	Migration Number(with skew)	Migration Number
500	0	0
1000	2	3
1500	6	10
2000	8	15
2500	11	16
3000	18	25

5.3. Comparison with Traditional Approaches

5.3.1. Migration Number

As shown in Figure 5, the comparison of time taken for migration using the skewness and without skewness technique is highlighted. It is seen that for a variety of number of user processes ranging from 500 to 3000 processes, in all cases of higher number of user processes, the time taken for migrating vm-instances is significantly lower when skewness is used compared to that when skewness is not used. The performance of using skewness is justified when it is seen that for a higher number of users, the time difference for migration of all overloaded and under-loaded instances is almost 21% lower when skewness is deployed compared to when skewness is not deployed.

The performance of using skewness is personified when larger number of user processes are involved similar to real life cloud scenarios. The justification for this is that if

skewness is not used, then brute-force technique is needed to detect overloaded and under-loaded vm's and migrate those. On the other hand, when skewness is used, the vm-instances who are under-loaded and overloaded are first pinpointed which makes the job of the migration algorithm easier since it has a specific cluster of vm-instances to migrate. As it has a lesser number of vm-instances under consideration compared to brute-force, it can complete migration procedures much faster compared to when skew is not used.

Figure 5 shows that our algorithm significantly decrease the average number of over- loaded servers in the system. It presents that our algorithm is highly effective to proactively preventing overload of servers. Without load detection the algorithm tries to migrate VMs of PM as soon as the load of PM is below the threshold. Figure shows the migration num- bers of traditional approach and proposed approach for a certain amount of given load. It is clear that our approach significantly reduces the migration number of VMs. Table 3 shows the migration number in traditional approach and proposed approach. First column of the table contains VM numbers against a certain load. Second and third column contains migration numbers with and without load detection.

5.3.2. Average Execution Time

Table 2 shows average execution time against user load of the skew detection algorithm. First column shows user number. Second column shows average execution time of the pro- posed approach and the third column shows average execution time in traditional approach. From this table it is clear that the proposed approach needs less migrations to equalize the load in all PMS.

VI. CONCLUSION

This paper have proposed a methodology to detect overloaded servers which are running in multiple PMs. When any overloaded server is found, it dynamically maps VMs to PMs. The main goal of this work is to avoid failures due to overload by users, which implies to increase performance of a hybrid cloud computing infrastructure. To achieve this goal, three algorithms are developed- Failure Detection, Skew Detection and Resource Allocation. These algorithms give overloaded servers enough resources to continue their running task without any interruption. Resource are distributed in a way that resource utilization skew of every physical machine will be minimized. Which improves overall working efficiency of the cloud.

REFERENCES

[1] D. Barrett, Security architecture and forensic awareness in virtualized environments, Cybercrime and Cloud Forensics: Applications for Investigation Processes: Applications for Investigation Processes (2012) 129.

[2] A. M. Sampaio, J. G. Barbosa, Dynamic power-and failure-aware cloud resources allocation for sets of independent tasks, in: Cloud Engineering (IC2E), 2013 IEEE International Conference on, IEEE, 2013, pp. 1–10.

[3] Z. Gong, P. Ramaswamy, X. Gu, X. Ma, Siglm: Signature-driven load management for cloud computing infrastructures, in: Quality of Service, 2009. IWQoS. 17th International Workshop on, IEEE, 2009, pp.

1–9.

[4] H. Kim, M. Kang, S. Kang, S. Oh, A novel adaptive virtual machine deployment algorithm for cloud com- puting, in: proceedings of International Conference on Information Science and Industrial Applications (ISI 2012), Philippines, 2012.

[5] S. Prathima, S. S. Ali, Dynamic resource allocation using virtual machines for cloud computing envi- ronment.

[6] M. Arias, E. Rojas, J. Munoz-Gama, M. Sepu´lveda, A framework for recommending resource allocation based on process mining, in: 3th International Workshop on Decision Mining and Modeling for Business Processes (DeMiMoPˆa AZ15), 2015.

[7] S. Vijayakumar, Q. Zhu, G. Agrawal, Dynamic resource provisioning for data streaming applications in a cloud environment, in: Cloud Computing Technology and Science (CloudCom), 2010 IEEE Second International Conference on, IEEE, 2010, pp. 441–448.

Online Shop: Influences of Online Shopping

LARKAI JONATHAN
Vitebsk State University

Abstract: -- **Many are the factors that influences online shopping decision process. The objective of this study is to provide an overview of online shopping decision process by comparing the offline and online decision making and identifying the factors that motivate online customers to decide or not to decide to buy online.**

***Keywords*: Online shopping, online shopper behavior.**

I. INTRODUCTION

The internet has played a very important role in our everyday life. We can send emails, make international calls and even buy things online. Meanwhile, Internet shopping has been widely accepted as a way of purchasing products and services. It also provides consumer more information and choices to compare products and it makes it easier to find anything online. Online shopping has shown to provide more satisfaction. On the other hand, some consumers still feel uncomfortable to buy online. Lack of trust, for instance, seems to be the major reason that prevents consumers to buy online. Also, consumers may have a need to exam and feel the products and to meet friends and get some more comments about the products before purchasing. Such factors may have negative influence on consumer decision to shop online. This study identifies some basic factors that drive consumers to decide to buy or not to buy through online channel. Finally, we identify how online sellers can use this knowledge to improve their online stores to be more attractive and get more online shoppers.

Reasons why people shop online

Easy Availability of items:
Consumers can buy anything at anytime without going to the store. They can find the same product at a lower price by comparing different websites at the same time. Online shopping is available for customers around the clock comparing to local stores as it is open 24 hours a day. Most people shop online because they want to avoid crowds and wailing lines, especially during holidays . Consumers not only look for products, but also for online services. Some companies have online customer services available 24 hours therefore, even after business hours customers can ask questions and get necessary support or assistance.

Availability of Adequate Information:
Data accessing has been made easier thanks to the internet. Given customers rarely have a chance to touch and feel product and service online before they make decision, online sellers normally provide more product information that customers can use when making a purchase. Customers put the weight on the information that meets their information needs. In addition to getting information from its website, consumers can also benefit from products' reviews by other customers. They can read those reviews before they make a decision.

Cost and time efficiency:
Because online shopping customers are often offered a better deal, they can get the same product as they buy at store at a lower price. Since online stores offer customers with variety of products and services. it gives customers more chances to compare price from different websites and find the products with lower prices than buying from local retailing stores. Some websites, Ali Express for example, offer customers auction or best offer option, so they can make a good deal for their product. Again, since online shopping can be anywhere and anytime, it make consumers' life easier because they do not have to get stuck in the traffic, look for parking spot, wait in checkout lines or be in a crowd at a store. As such, customers often find shop from the website that is offering convenience to reduce cost.

Factors that prevents Consumers from online Shopping:
Concerns about security:
Since the payment modes in online shopping are most likely made with credit card, customers sometime pay attention to seller's information in order to protect themselves . Customers tend to buy product and service from the seller who they trust, or brand that they are familiar with. Online trust is one of the most critical issues that affect the success or failure of online retailers. Security seems to be

a big concern that prevent customers from shopping online because they worried that the online store will cheat them or misuse their personal information, especially their credit card.

Online shopping dissatisfaction:
In online shopping, for example, they may get unwanted product or low quality products, products which does not match what is described or expected. The product may be fragile, wrong or not working. Some online sellers may not agree to refund those products even though it is not what the customer wanted. Delivery is another thing that affects online purchasing decision. Slow or late shipping, for instance, makes customer walk away from online shopping.

Inability to try or examine actual product online:
Customers are less likely to buy clothes through online channel because they have no chance to try or examine actual product. Customers viewing a product on a computer screen can show a different effect than actually feeling it. Customers cannot see, hear, feel, touch, smell, or try the product that they want when using online channel. In many cases, customers prefer to examine the product first and then decide whether or not they want to buy . Some people think the product information provided in website is not enough to make a decision. Online shoppers will be disappointed if the product information does not meet their expectation.

Lack of salesperson's professional assistance:
Many online shopper's would find it difficult to make a choice and thus get frustrated if there is no experienced salesperson's professional assistance. Moreover, some customers are highly socially connected and rely on other peoples' opinions when making purchase decision. There are also consumers who sometimes shop at local store because they want to fulfill their social needs which are limited by online stores.

How online shop owners can improve their online stores:
Making of a more secured and trustworthy website:
Customer's are concerned about transaction security and data safety when purchasing product's online Getting approved certificate from an organization is one of the ways to make a website more trustable so, a website will be more secured and it will increase customer confidence and lead to sale increase. When the companies have thiscertificate, the address bar of their website will change t green color and the Web address will begin with https:// so customers know that the website is secure and trustable.

Using a more user Friendly Website:
Customers can be influenced by the image of the web site when they decide what website or buyer they want to buy from. Websites should have enough information about the product's being advertised. Moreover, if online stores want to convert visitor into buyer, they should improve their website by offering customer a comfortable, logical, interesting and hassle-free process and easy language by creating fast website with functional design as smooth as possible. Online payment process is another issue that should be taken care of because it affects the willingness to pay. Online stores should make their payment process to be easy and secure.

Offering customers more affordable prices and additional options:
Offering customers more affordable prices and promotions is one of the ways online stores can use to make their business succeed. Sellers might consider to offer money-back guarantee policy including shipping expenses refund to reduce purchasing risk. In addition, to avoid shipping delay and product lost, online store may cooperate with other companies with expertise in logistic to improve their distribution channels. This may help sellers to gain more sales from those who want to buy online products.

REFERENCES

1. Amin, S., (2009),Why do so many people shop online?http://www.articlesbase.com/print/1335596 Articlebase.com.

2. Anonymous, (2009),"How to shop online more safely," http://www.microsoft.com/ protect/fraud/finances/shopping_us.aspx, Microsoft.com.

3. Butler, P. and Peppard, J, (1998), "Consumer purchasing on the internet: Processes and prospects", European Management Journal, vol. 16, no. 5, pp.600-610.

4. Hofacker, C.R., (2001), Internet Marketing, 3rd ed., Wiley, New York.

5. Seock, Y.K. and Norton, M., (2007), "Attitude toward internet web sites, online information search, and channel choices for purchasing", Journal of Fashion Marketing and Management, vol. 11, no. 4, pp.571-586.

6. Liang, T.P. and Lai. H.J., (2002), "Effect of store design on consumer purchases: An empirical study of on-line bookstores", Information & Management, vol. 39, no. 6, pp.431-444.

7. Lim, H. and Dubinsky, A.J., (2004), "Consumers' perceptions of e-shopping characteristics: An

expectancy-value approach", The Journal of Services Marketing, vol. 18, no. 6, pp. 500-513.

8. Liu, C. and Guo, Y., (2008), "Validating the end-user computing satisfaction instrument for online shopping systems", Journal of Organizational and End User Computing, vol. 20, no. 4, pp.7496.

9. Maignan, I. and Lukas, B., (1997), "The nature and social uses of the internet: A qualitative Investigation", The Journal of Consumer Affairs, vol. 31, no. 2, pp. 346-371.

10. Parks, S., (2008), "7 Reasons why people shop online," http://www.articlesbase.com/ home-business-articles/7-reasons-why-people-shop-online-554620.html, Articlebase.c